



ELSEVIER

Physica D 74 (1994) 301–352

**PHYSICA** D

# Towards a universal theory for natural patterns

T. Passot<sup>a</sup>, A.C. Newell<sup>b</sup>

<sup>a</sup> *Observatoire de la Côte d'Azur, BP 229, Nice cedex 4, 06304, France*

<sup>b</sup> *Department of Mathematics, University of Arizona, Tucson, AZ 85721, USA*

Received 29 March 1993; revised 21 December 1993; accepted 1 March 1994

Communicated by H. Flaschka

## Abstract

Our goal is to find a macroscopic description of patterns that both unifies and simplifies classes of externally stressed, dissipative, pattern forming systems, such as convecting fluids, liquid crystals, wideband lasers, that are seemingly unrelated at the microscopic level. We construct an order parameter equation which provides a controlled approximation of the original microscopic field in the limit of large aspect ratios. It is built from, and is a regularization of, the Cross–Newell phase diffusion equation obtained by averaging over the local periodicity of the pattern. Unlike the latter, it is valid for all wavenumbers and can correctly capture the nucleation, shape and nontrivial properties of the far fields of disclinations, dislocations and grain boundaries. It reduces to the Cross–Newell equation away from pattern singularities and to the Newell–Whitehead–Segel equation near onset. As a consequence, it correctly determines all the long wave instability boundaries (zig-zag, Eckhaus-skew-varicose) of the Busse balloon. Far from onset, the order parameter is a real variable but its equation involves a functional corresponding to its local amplitude. The local amplitude and phase, required for the order parameter equation and the reconstruction of the approximation to the original field respectively, are extracted from the order parameter field by wavelet analysis. Numerical comparisons between solutions of the original equation and the regularized equation are carried out. We also explore a new class of singular and weak solutions of the Cross–Newell equation which take account of the energetics of defects as well as their topologies. These solutions correspond to convex and concave disclinations and their composites, including saddles, vortices, targets, dislocations and two new objects, handles and bridges. Finally, we show that phase grain boundaries, lines across which the wavevector is discontinuous but the phase is continuous are captured by shock solutions of the phase diffusion equation.

## 1. Introduction and general discussion

### 1.1. Preamble. What has been done

A fundamental goal of theory is to provide a macroscopic description of almost periodic patterns that both simplifies and unifies one's understanding of classes of pattern forming systems which are seemingly unrelated at the mi-

croscopic levels. For example, much attention in recent years has been given to finding such descriptions of Rayleigh–Bénard convection patterns in pure fluids. There are several classes of such models which differ in their domains of validity and/or their qualitative/quantitative characters. Some, like the Swift–Hohenberg (SH) equation [1, 2], or its extension including a coupling with a mean-drift term [3, 4], are

obtained by averaging all fields over the vertical direction and making certain assumptions on their vertical structures. In some parameter ranges, these models give a good qualitative agreement with observations, but they do not allow for precise predictions. Other macroscopic descriptions are derived semi-rigorously from the primitive microscopic governing equations after averaging over the horizontal as well as the vertical direction, but are restricted in their applicability. Such is the case for the Newell-Whitehead-Segel (NWS) equation [5, 6] which is valid near onset and if the rolls in the pattern are everywhere almost parallel. Its modification to include mean drift effects at finite Prandtl numbers was given by Zippelius and Siggia [7]. The rotational invariance of the Oberbeck-Boussinesq equations imposes a major restriction on the validity of such a description since natural patterns rarely exhibit parallel sets of rolls. Rather, rolls tend to be aligned perpendicular to the boundaries and therefore the bulk is likely to contain rolls with all orientations. Unlike the case of nematic liquid crystals [8], for normal fluids there is no restoring force which obliges the rolls to stay parallel to a fixed direction. The problem of rotational degeneracy has been successfully addressed by Cross and Newell [9] and these authors derive a phase-diffusion equation which generalizes the equation of Pomeau and Manneville [10] for fluctuations about a fixed orientation. A complete determination of the phase diffusion-mean drift equations for the Oberbeck-Boussinesq system of equations has recently been done [11, 12] which gives for the first time a complete quantitative agreement with the Busse balloon at all finite Rayleigh and Prandtl numbers.

However, the phase diffusion equation has one glaring weakness. It is a partial differential equation for the phase, first order in time and second order in the two spatial variables. The latter part is quasilinear and can be elliptic negative definite, elliptic positive definite or hyperbolic depending on wavenumber. Only

when the wavenumber lies in the elliptic, negative definite band (the Busse balloon [13]) is the equation well-posed. It is ill-posed in all of the other regions. Moreover, a combination of boundary conditions, topology and instabilities can force the local wavenumber outside of the Busse balloon. It is therefore necessary to make sense of the equation over a wavenumber band much wider than that stable band. The goal of the present work is to develop a regularized version of the phase diffusion equation, hereafter known as the OPE, which has the properties that it (i) describes the behavior of the pattern when the local wavenumber is forced out of the Busse balloon, (ii) reduces via the Cross-Newell formalism to the same phase diffusion equation derived from the original microscopic equations (iii) is simpler than the latter. It should also allow us to make sense of (regularize) the weak and singular solutions of the phase diffusion equation which describe point and line defects. This paper will describe the extent of our success to date in addressing these challenges.

We begin by discussing the philosophy and shortcomings of various macroscopic descriptions. The basic idea is to use certain properties of the pattern to reduce the dimension of the original microscopic system and to define an order parameter (or order parameters) which successfully captures its macroscopic behavior. Near onset, linear stability theory determines all the active modes of the system, namely those modes that are either amplified, remain neutral or are only weakly damped as the stress parameter  $R$ , e.g. the Rayleigh number, exceeds a critical value  $R_c$ . In systems possessing translational and rotational symmetry, this set of active modes can be characterized in Fourier space and consists of all modes with wavevectors  $\mathbf{k}$  lying in an annulus about the circle  $|\mathbf{k}| = k_c$  determined by linear stability theory. The order parameters are the complex Fourier amplitudes  $\hat{A}(\mathbf{k}, t)$  of these modes and Bestehorn and Haken [14] have shown that for small amplitudes they obey the set of integro-differential equations:

$$\begin{aligned} \frac{d\hat{A}}{dt} = & -\lambda(k^2, R)\hat{A} \\ & + \int dk_1 dk_2 dk_3 \Gamma(k_1, k_2, k_3) \hat{A}(k_1) \hat{A}(k_2) \\ & \times \hat{A}^*(k_3) \delta(k - k_1 - k_2 + k_3) + \text{h.o.t.}, \end{aligned} \quad (1.1)$$

where h.o.t. refers to higher order terms in amplitude. Unfortunately, without further simplification, these equations are impossible to handle. The first simplification involves the choice of planform and is found by testing the relative stabilities of the finite amplitude solutions associated with (a) rolls,  $\hat{A}(\mathbf{k}, t) = A_1(t)\delta(\mathbf{k} - \mathbf{k}_1)$ ,  $|\mathbf{k}_1| = k_c$ , (b) rhombi,  $\hat{A}(\mathbf{k}, t) = A_1(t)\delta(\mathbf{k} - \mathbf{k}_1) + A_2(t)\delta(\mathbf{k} - \mathbf{k}_2)$ ,  $|\mathbf{k}_1| = |\mathbf{k}_2| = k_c$ ,  $\mathbf{k}_1 \cdot \mathbf{k}_2$  arbitrary, (c) hexagons  $\hat{A}(\mathbf{k}, t) = \sum_{j=1}^3 A_j(t)\delta(\mathbf{k} - \mathbf{k}_j)$ ,  $\mathbf{k}_2 = \mathbf{k}_2 \cdot \mathbf{k}_3 = \mathbf{k}_3 \cdot \mathbf{k}_1 = -1/2k_c^2$ , (d) quasicrystals  $\hat{A}(\mathbf{k}, t) = \sum_{i=1}^N A_i(t)\delta(\mathbf{k} - \mathbf{k}_i)$ ,  $N \geq 3$ ,  $|\mathbf{k}_j| = k_c$ ,  $\mathbf{k}_j \cdot \mathbf{k}_l$  arbitrary and (e) turbulent crystals  $\hat{A}(\mathbf{k}, t) = \sum_{i=1}^N A_i(t)\delta(\mathbf{k} - \mathbf{k}_i)$ ,  $N$  large,  $|\mathbf{k}_j| = k_c$ , some of which ((a), (b), (c)) tile the plane in a periodic lattice. Assuming that rolls are indeed the preferred planform, one can then go on to ask about the finite amplitude evolutions of a state containing modes  $(k_c + (R - R_c)^{1/2}K_x, (R - R_c)^{1/4}K_y)$  within a neighborhood of a fixed wavevector  $(k_c, 0)$  and obtain from (1.1) by Fourier transform the NWS equation, or in systems supporting travelling waves, the appropriate coupled complex Ginzburg Landau (CGL) equations [15]. These equations are restricted in their domains of validity. They assume rolls are almost parallel and that the amplitude is small, so that they obtain only near onset. They contain within them solutions which correspond to dislocations, grain boundaries and, in travelling wave systems, defects acting as sources or sinks for right and left travelling waves. They fail, however, to contain solutions corresponding to disclinations. Another simplification of (1.1) seeks to retain the rotational symmetry by representing the linear term  $\lambda(k^2, R)\hat{A}(k, t)$  as  $\lambda(-\nabla^2, R)A(\mathbf{x}, t)$

and then by approximating the nonlinear convolution in (1.1) as certain combinations of  $A^3$ ,  $|A|^2A$ ,  $|\nabla A|^2A$ , choices which lead to the SH equation and variations thereof. One obtains in this way an equation which again has small scales but which may nevertheless be simpler than the original microscopic system. However, it represents an uncontrolled approximation of the latter and, in all likelihood, will fail far from onset.

### 1.2. Discussion of goals and results

In this Section, we discuss the goals of the present work in detail, delineate the successes and the shortcomings, the main results, and point out several remaining challenges yet to be overcome.

#### 1.2.1. When is the phase diffusion relevant and in what circumstances does our theory apply?

In contrast with the amplitude equation theories which are relevant near onset and for which the small parameter is  $R - R_c$ , the amount by which the stress parameter exceeds critical, the Cross–Newell (CN) approach takes as its starting point an exact finite amplitude solution  $w_0(\theta = \mathbf{k} \cdot \mathbf{x})$  corresponding to the preferred local planform. Although applicable to patterns whose local planform contains several phases (stationary rolls, squares, hexagons, multidirectional travelling waves), here we focus our attention on the case in which quasistationary rolls or stripes are the only locally stable planform, and for which coupling with some mean drift field can be ignored. The small parameter in the theory is  $\epsilon$ , the inverse of the aspect ratio  $\Gamma = l/\lambda$ , the ratio of a typical length  $l$  over which the local wavevector changes to the typical pattern wavelength  $\lambda$ . The dimension  $l$  is usually taken to be the size of the container but, depending on the dynamics of the pattern itself, may turn out to be smaller. In fact, the most appropriate choice for  $l$  is the distance between pattern singularities and, as the stress parameter

$R$  is increased well above its onset value  $R_c$ , the number and density of defects tend to increase. This immediately brings to light one of the difficulties with the theory. Its small parameter,  $\epsilon$ , depends on  $R$  and will generally increase with  $R$ . Furthermore, there is no a priori estimate yet available on the range of stress parameter (and other parameters that may be relevant) for which  $\epsilon$  is small. To date, all we know is what we observe. A typical pattern consists of a mosaic of patches, usually consisting of almost straight or circular rolls, which are separated by isolated point defects called disclinations and line defects joining disclinations called phase grain boundaries across which the phase is continuous but the wavevector is discontinuous. The pattern may or may not be stationary. Time dependence is usually connected with the presence of dislocations and amplitude grain boundaries. (These terms will be defined later). Nevertheless, it is clear that there are ranges of  $R$  for which  $\epsilon$  is small and where a suitably regularized phase diffusion equation should be relevant.

### 1.2.2. The CN equation; some heretofore overlooked yet important results, and its apparent gradient property

Given the basic premise that the pattern wavevector changes slowly almost everywhere, the basic idea of Cross–Newell theory is to seek a solution  $w_0(\theta = \int \mathbf{k} \cdot d\mathbf{x})$  of the underlying microscopic field equations that is a modulation of the locally periodic structure. In Section 2.1, we review the derivation of the phase diffusion equation from two viewpoints. Here we simply state that it is a constraint on the evolution of the change in phase induced by the translational symmetry of the original system, which also respects its rotational invariance, and write it down:

$$\tau(k)\theta_t - kD_{\perp}(k)\nabla \cdot \hat{\mathbf{k}} - D_{\parallel}(k)(\hat{\mathbf{k}} \cdot \nabla)k = 0. \quad (1.2)$$

By construction (they are inner products of products of  $w_0(\theta)$  and its derivatives), the

perpendicular ( $D_{\perp}(k)$ ) and parallel ( $D_{\parallel}(k)$ ) diffusion coefficients are analytic in  $k$ ,  $\mathbf{k} = \nabla\theta$ ,  $k = |\mathbf{k}|$ ,  $\hat{\mathbf{k}} = \mathbf{k}/k$ .

The first new result we introduce in this paper (section 2b) is that there is a special condition, namely

$$r = \operatorname{res}_{k=k_B} \frac{D_{\parallel}(k)}{kD_{\perp}(k)} = 1, \quad D_{\perp}(k_B) = 0, \quad (1.3)$$

under which (1.2) can be written in flux divergence form,

$$\tau(k)\theta_t + \nabla \cdot \mathbf{k}B(k) = 0, \quad (1.4)$$

with

$$\mathbf{k}B(k) = (kB)_0 \exp \int_{k_0}^k \frac{D_{\parallel}(k)}{kD_{\perp}(k)} dk, \quad (1.5)$$

analytic over wavenumbers within the neutral stability boundaries ( $k_l(R), k_r(R)$ ), the domain over which the underlying finite amplitude planform exists. We assume here, there are profound consequences if this is not true, that the transition at the neutral stability boundary is supercritical. The typical shape of the graph of  $kB(k)$  as function of  $k$  is shown in Fig. 1.

The condition (1.3) is important for at least two reasons. First, it allows us to write the spatial part of the phase diffusion equation in flux divergence form. This is important because it means that the jump or Rankine-Hugoniot conditions which relate the values of the wavevector across curves where it is discontinuous are independent (within a certain class) of the exact form of regularization. Second, the amount by which  $r$  differs from unity provides one measure of the nongradient character of the system. When  $r = 1$ , one can establish the formal existence of a free energy (derived in [9])

$$\bar{F} = \int \int \bar{G} dx dy, \quad \bar{G} = - \int_{k_B}^k kB(k) dk, \quad (1.6)$$

where

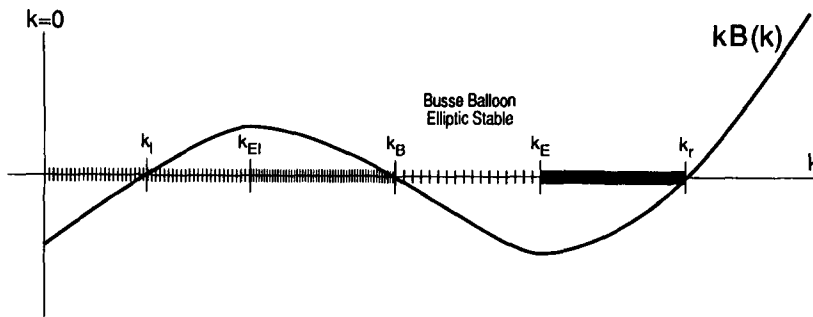


Fig. 1. Graph of  $kB(k)$ .

$$\frac{\delta \bar{F}}{\delta \theta} = \nabla \cdot kB(k). \tag{1.7}$$

If  $B(k)$  is not analytic,  $\bar{G}$  is not defined because, although one can choose the real branch for  $k \geq k_B$ , one cannot find a branch which is real throughout  $(k_l(R), k_r(R))$ . We will demonstrate explicitly in Section 4 that (1.4) is not formally gradient when  $r \neq 1$ . If the original system is gradient, then, as we will show in Section 2.1,  $\bar{F}$  is obtained from the original free energy  $F$  simply by averaging its integrand  $G$  over a period of the fast phase  $\theta$ , namely  $\bar{G} = \frac{1}{2\pi} \int_0^{2\pi} G d\theta$ . But there are systems, the Oberbeck-Boussinesq equations at very large Prandtl numbers being one example, where  $r$  is almost one and the phase diffusion equation behaves as if it were phase gradient even though the original microscopic equations are not. The notion of a phase gradient system is new. We will see in Section 4 how near stationary disclinations the far field wavenumber  $k$  approaches  $k_B$  exponentially fast, so that  $\bar{F}$  becomes vanishingly small.

However, it is not true that  $\bar{F}$  is a true gradient functional if there are dislocations in the pattern. The obstruction, identified in [9], that  $\bar{F}$  decreases with time if and only if the far field wavenumber  $k_d$  at which isolated dislocations are stationary is equal to  $k_B$ , still stands. However, the result (1.3) points out that there are two separate contributors to  $k_d$  and to the finite velocity of dislocations when the far field wavenumber is not equal to  $k_d$ . One arises from the non phase gradient character of the system

(if  $r \neq 1$ ). The other arises from the structure of the dislocation core peculiar to the particular system of interest. Our regularization will be consistent with keeping  $r = 1$ . It will not, however, be able to capture  $k_d$  nor dislocation velocities to within an order  $\epsilon$  accuracy.

1.2.3. *The regularization of (1.4) (the OPE) and the sense in which it represents a controlled approximation to the solution of the original microscopic equation. The use of wavelets*

As it stands, the CN phase diffusion equation is inadequate because it is ill-posed when the local wavenumber  $k$  lies outside of the Busse balloon  $(k_B(R), k_E(R))$  (See Fig. 1 for definition of  $k_l, k_{EI}, k_B, k_E, k_r$ ). Since there are many influences (e.g. curvature, induced by boundary conditions) which force the local wavenumber outside of this interval, we must add new terms to (1.4), which will be of order  $\epsilon^2$  almost everywhere, but which come into play and can balance  $\nabla \cdot kB$  in those regions (whose area tends to zero with  $\epsilon$ ) where the local wavenumber lies to the left of the zig-zag instability boundary  $k = k_B$  or to the right of the Eckhaus instability boundary  $k = k_E$ . This we do in Section 3. In principle, one can calculate the exact corrections by continuing the Cross–Newell method to higher orders thereby obtaining corrections involving higher order spatial derivatives to both the phase diffusion equation (the corrections involve fourth order derivatives in  $\theta$ ) and the algebraic equation giving the amplitude as a function of wavenum-

ber. The latter will involve second and higher derivatives in the amplitude. Indeed, one can often calculate the most important correction of the phase diffusion equation. However, except in a few special circumstances, it is impractical to compute all the corrections because the calculations are too formidable to be carried out analytically and numerical evaluations tend to obscure the important physics. Despite these difficulties, it may turn out to be essential to carry out this analysis if one is to accurately capture the influence of the cores of singularities such as dislocations on their speeds and interactive properties. A key theoretical challenge will be to separate those contributions that really matter from those which play only a perturbative role.

In this first attempt, our approach has been to build the regularized equation (the OPE) about the phase diffusion equation in a manner consistent with the following principles. The order parameter, which we will call  $W$ , is a real valued, monochromatic, periodic function of the phase  $\theta$ ,  $W = a \cos \theta$ . It is very important that the order parameter be real as otherwise the OPE would not support disclinations whose local wavevector field is double valued. It satisfies the equation

$$\chi(-\nabla^2)W_t + (A(-\nabla^2) + a^2\Gamma(-\nabla^2))W = 0, \quad (1.8)$$

which reduces via the Cross–Newell formalism to the *same* phase diffusion equation as the original microscopic system. We stress this crucially important feature. We build the OPE on that one foundation, the phase diffusion equation, which is the central means of encoding the pattern behavior of a particular system in a macroscopic format and which is readily calculable. The original field  $w$  can be reconstructed from  $W$  as  $w_0(\arccos \frac{1}{a}W)$ . It will in general contain higher harmonics of the fundamental local period. The amplitude  $a$  and phase  $\theta$  of  $W$  are recovered from the real signal  $W$  by wavelet analysis. This is another important addition to the study and

understanding of patterns. While we choose to use the wavelet algorithm directly in the OPE to define the quantity  $a^2$ , it is also a crucial aid in determining the wavevector field of the patterns.

Our assertion is that in the limit  $\epsilon \rightarrow 0$ , (1.8) and the original microscopic system describe the same pattern behavior, except for defect velocities. The fact that it shares the same phase diffusion equation certainly supports this. We provide additional support with the aid of several numerical experiments which simulate nontrivial pattern behaviors. In particular, the choices of coefficients in (1.8) allow us to capture the nucleation of dislocations with great accuracy. Moreover, we are also able to capture the instability of dislocations and their gliding properties. Indeed, we will see a dramatic affirmation of the necessity for using a real order parameter  $W$  when we study how well the OPE simulates the instability of moving dislocations. Perhaps somewhat fortuitously, the defect velocities are captured to within a reasonable accuracy. The reason for this is that the velocity of dislocations driven by an instability in the phase field, as is the case when the far field wavenumber lies to the right of the Eckhaus instability boundary, far exceeds that of dislocations which move so as to adjust to a change of wavenumber within the Busse balloon. We note that it is possible to add terms to (1.8) which would ensure that  $k_d$  is correctly identified but our prescription for doing so involves no general principle so we will leave this as an open challenge until we gain a more complete understanding of the role of defect cores.

Two other challenges, connected with the practical implementation of (1.8) in general circumstances, remain open, or at least partially open. The first has to do with an accurate two dimensional wavelet transform that can successfully resolve scales down to the size of a wavelength. This will be important if we are to attempt to compare the behaviors of solutions of (1.8) with solutions of the original microscopic system, particularly with respect to the morphology of defects and their dissociation into

their elementary components. The second is the question of the choice of appropriate conditions to apply at horizontal boundaries. Clearly in the fluid context, for  $R - R_c = O(1)$ , one of them should be that the normal gradient of  $\nabla W$  is zero to leading order. But what should the second one be, and how does the first depend on  $R - R_c$  as this quantity becomes small?

#### 1.2.4. The point and line singularities of patterns, and weak solutions of (1.4)

One of the most important contributions of this paper is the demonstration that the stationary phase diffusion equation

$$\nabla \times \mathbf{k} = 0, \quad \nabla \cdot \mathbf{k} B = 0, \quad (1.9)$$

admits weak solutions that we can identify with the point and line defects of patterns. We will show that the elementary point defects are convex and concave disclinations (Figs. 2a, b, d, e) and from them one can build composites such as saddles, targets, vortices, handles (each contains two disclinations) and dislocations and bridges (each contains four disclinations). It is important to emphasize that these solutions are significantly different from the harmonic solutions (valid if  $B \equiv 1$ ) which arise as the level curves of quadratic differentials and which are sometimes drawn in the literature to represent the phase field near disclinations. The solutions we find not only have the correct topological properties but also the correct energetic ones in that the local wavenumber almost everywhere in their far field lies within the Busse balloon. Indeed, it will turn out to be very close to  $k_B$ . In contrast, the harmonic solutions have wavenumbers which lie well outside the Busse balloon and therefore are not seen in real patterns.

The solutions are weak in the sense that they are the  $\epsilon \rightarrow 0$  limit of the smooth solutions of

$$\nabla \cdot \mathbf{k} B + \epsilon^2 \frac{|B'(k_B)|}{4k_B} \nabla^2 \nabla \cdot \mathbf{k} = 0, \quad (1.10)$$

which is the stationary part of (1.8) when amplitude corrections are ignored. For concave discli-

nations, the wavenumber  $k$  approaches  $k_B$  from below. In that case,  $\nabla \cdot \mathbf{k} B$  is a hyperbolic operator and the characteristics, Riemann invariants and Rankine-Hugoniot conditions for (1.9) are exactly calculated. It turns out (1.9) is isomorphic to one dimensional compressible gas flow and the shallow water equations when  $k$  is close to, but less than,  $k_B$ . The importance of condition (1.3), namely  $r = 1$ , emerges again and again. The shock solutions correspond to phase grain boundaries which emanate from the cores of concave disclinations. They are called phase grain boundaries because, while the wavevector is discontinuous across them, the phase is continuous. Amplitude grain boundaries (Fig. 2f) on the other hand, are very different. They are the boundaries between two patches of rolls, each of which is described by a different phase, and across which the respective amplitudes decay. They usually consist of a line of dislocations.

As we have already said, an important realization of this work is that the building blocks of all point defects are convex and concave disclinations. For example, it is very clear that the vortex is the coincidence of two convex disclinations. We will also demonstrate by examining an exact solution of the regularized phase equation (1.10) how dislocations are composed of four disclinations, two convex and two concave. These elementary defects are bound as composites as long as the dislocation is stable. We shall also see, however, that moving dislocations can destabilize, essentially by a process that involves the dissociation of the disclinations, and the formation of two new pairs of convex and concave disclinations. The dislocation is then reformed by a combination of the old convex disclinations and the new concave ones, and in its wake leaves a bridge structure. The latter has been frequently observed in experiment.

A more detailed discussion of the rich character and properties of the solution of (1.9) corresponding to singularities will be given in [16]. In particular, we will discuss their connection with the canonical singularities (folds, cusps, umbil-

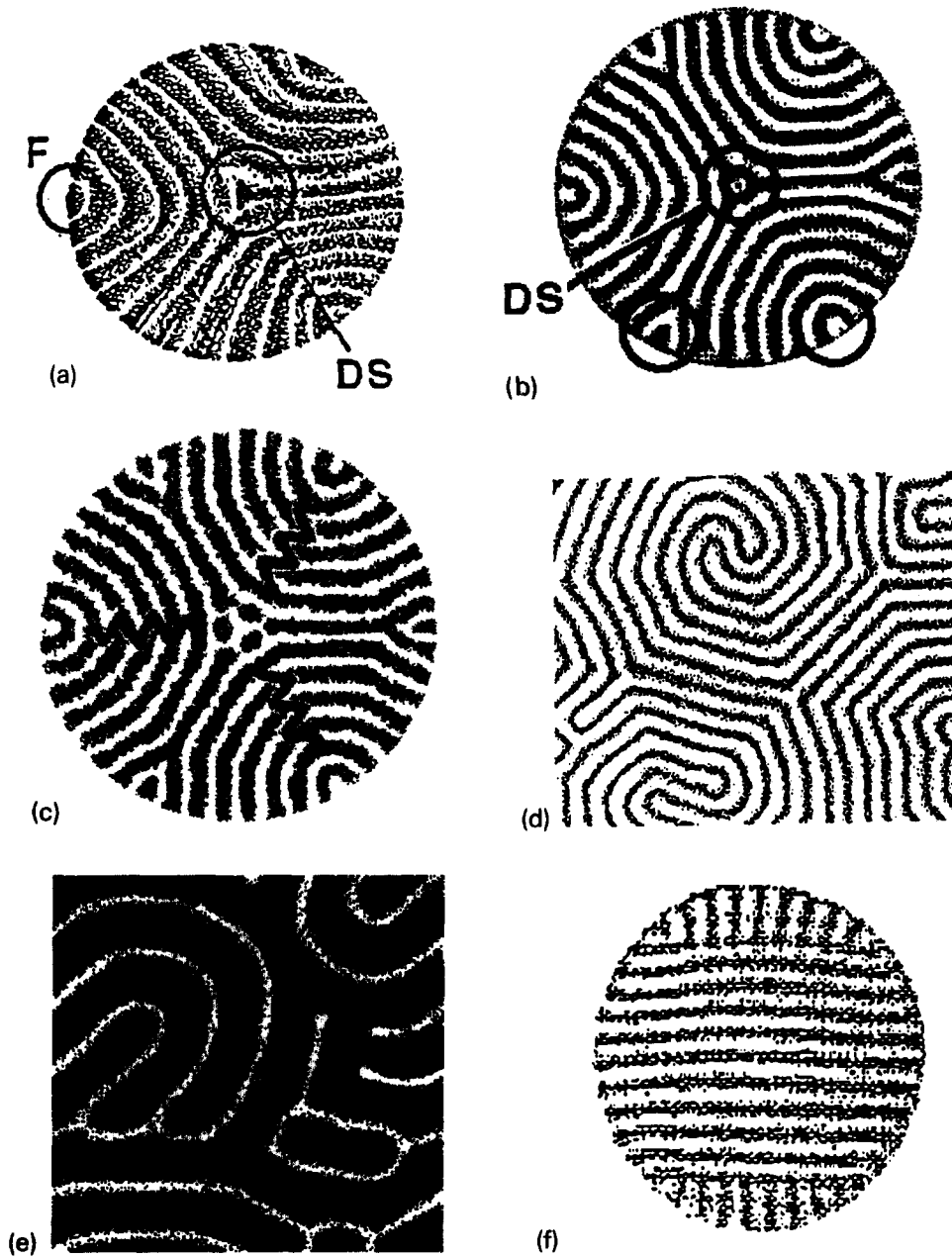


Fig. 2. (a), taken from [35], shows a concave disclination (DS) and three sidewall foci in a convecting fluid at a value of the Rayleigh number  $R = 2.61R_c$ ,  $R_c = 1708$  and  $Pr = 2.5$ . (b) is a numerical simulation of the SH equation for  $R = 0.1$  with boundary conditions  $w = \nabla w \cdot \hat{n} = 0$ . (c) is (b) with shock lines marked. (d) is a pattern showing many concave and convex disclinations and phase grain boundaries in a magnetically driven ferrofluid taken from [36]. (e) is a Roman Arch (regularized convex disclination) seen in a numerical simulation of a pattern created by an instability of copropagating optical beams [37]. (f) shows an example of an amplitude grain boundary.

ics) of two dimensional maps, with quasiconformal maps and quadratic differentials, and with measured foliations.

The outline of this paper is as follows. In Section 2, we revisit the phase diffusion equation, its derivation and introduce the  $r = 1$  condition. In Section 3, we show how the OPE is built from the phase diffusion equation and a knowledge of the relaxation rate, as function of  $k$ , of the amplitude to its slaved value. We also carry out three experiments to illustrate the effectiveness of the OPE. In Section 4, we introduce the new weak and singular solutions of the stationary phase diffusion equation. In Appendix A, we discuss the wavelet transform. In Appendix B, we show how to find, in very general terms, the CN equation for the OPE. In Appendix C, we provide further and a more detailed motivation for the choices made in constructing the OPE.

## 2. The phase diffusion equation

### 2.1. Its derivation

We shall show briefly how to obtain the phase diffusion equation and, using the Swift-Hohenberg model,

$$w_t + (\nabla^2 + 1)^2 w - R w + w^3 = 0, \quad (2.1)$$

describing the evolution of a scalar field  $w(\mathbf{x}, t)$  in two space dimensions  $\mathbf{x} = (x, y)$ , we review how to do this two ways.

First, we use general perturbation theory which uses no special property of (2.1) other than the fact that rolls are the stable planform for a certain range of values of the stress parameter  $R$ . We assume that there is a small parameter  $\epsilon$ , which in the case of Rayleigh-Bénard convection is the inverse aspect ratio of the container and which here gives the order of magnitude of the roll curvature. This assumption is valid in real convection (and also for (2.1) as confirmed by numerical simulations) away from defects. Large scale coordinates are defined according to

$X = \epsilon x, Y = \epsilon y, T = \epsilon^2 t$ , and it is important to stress that both space directions are scaled the same way since we want to preserve rotational invariance. Our aim is to derive equations for the macroscopic order parameters, the wavevector and amplitude, of the pattern. The method for achieving this description is analogous to the Whitham averaging theory [17] of slowly modulated nonlinear waves. The small scale coordinate upon which averaging is performed is the phase  $\theta$  of the basic nonlinear roll solution. The wavevector  $\mathbf{k}$  is assumed to be slowly varying and in turn this defines a large scale phase  $\Theta = \epsilon \theta$  such that  $\mathbf{k} = \nabla_x \theta = \nabla_X \Theta$ . The field  $w(\theta, X, Y, T)$  is expanded in powers of  $\epsilon$  as  $w = w_0 + \epsilon w_1 + \epsilon^2 w_2 + \dots$  and the differential operators take the following forms:

$$\partial_t = \epsilon \Theta_T \partial_\theta + \epsilon^2 \partial_T, \quad (2.2)$$

$$\nabla_x = \mathbf{k} \partial_\theta + \epsilon \nabla_X. \quad (2.3)$$

We also find,

$$(1 + \nabla^2)^2 = \mathcal{L}_0 + \epsilon \mathcal{L}_1 \partial_\theta + \epsilon^2 \mathcal{L}_2 + \epsilon^3 \mathcal{L}_3 \partial_\theta + \epsilon^4 \mathcal{L}_4, \quad (2.4)$$

where

$$\mathcal{L}_0 = (1 + k^2 \partial_\theta^2)^2, \quad (2.5)$$

$$\mathcal{L}_1 = (1 + k^2 \partial_\theta^2) D_1 + D_1 (1 + k^2 \partial_\theta^2), \quad (2.6)$$

$$\mathcal{L}_2 = (1 + k^2 \partial_\theta^2) D_2 + D_2 (1 + k^2 \partial_\theta^2) + D_1^2 \partial_\theta^2, \quad (2.7)$$

$$\mathcal{L}_3 = D_1 D_2 + D_2 D_1, \quad (2.8)$$

$$\mathcal{L}_4 = D_2^2, \quad (2.9)$$

and

$$D_1 = 2\mathbf{k} \cdot \nabla + \nabla \cdot \mathbf{k}, \quad (2.10)$$

$$D_2 = \nabla^2. \quad (2.11)$$

$\mathcal{L}_j^p$  means that we replace  $\frac{\partial^2}{\partial \theta^2}$  in  $\mathcal{L}_j$  by  $-p^2$  and  $k$  is the amplitude of the vector  $\mathbf{k}$ . Substituting into (2.1), we obtain the equation for the stationary straight roll solution  $w_0$  at leading order in  $\epsilon$ ,

$$(\mathcal{L}_0 - R)w_0 + w_0^3 = 0. \quad (2.12)$$

This equation has non-zero periodic solutions only when  $R$  and  $k$  are such that  $R - (1 - k^2)^2 > 0$ . The graph  $R = (k^2 - 1)^2$  is called the marginal or neutral stability curve. The minimum value of  $R$ ,  $R = 0$  is realized for  $k = 1$ . Let  $w_0(\theta)$  be a periodic solution of (2.12). We will assume here we are in a range of wavenumber where the solution is unique. The amplitude  $A$  (norm of  $w_0$ ) is determined as a function of the wavenumber  $k$  once we fix the periodicity of the solution to be  $2\pi$ . Since  $\mathbf{k}$  and  $A$  are not exact constants, then  $w_0$  is not an exact solution of (2.1) and its first correction  $w_1$  satisfies

$$Lw_1 = (\mathcal{L}_0 - R + 3w_0^2)w_1 = -(\partial_\theta w_0)\Theta_T - \mathcal{L}_1(\partial_\theta w_0). \tag{2.13}$$

The linear operator  $L$  acting on  $w_1$  is singular since, due to translational invariance,  $\partial_\theta w_0$  is an element of its null space. As a consequence, the phase must obey a solvability condition before  $w_1$  can be found. This condition, which is necessary and sufficient if we demand that  $w_1$  belongs to a space of  $2\pi$ -periodic functions in  $\theta$ , will simply read ( $L$  is self-adjoint)

$$\langle \partial_\theta w_0 | \partial_\theta w_0 \rangle \Theta_T + \langle \partial_\theta w_0 | \mathcal{L}_1 \partial_\theta w_0 \rangle = 0, \tag{2.14}$$

where  $\langle a | b \rangle$  denotes the scalar product  $\frac{1}{2\pi} \int_0^{2\pi} d\theta ab$ . Note that the large scale derivatives of  $w_0$  are found as

$$\frac{\partial w_0}{\partial X} = \frac{\partial w_0}{\partial k^2} \frac{\partial k^2}{\partial X}, \tag{2.15}$$

which reflects the fact that all the large scale dependencies are included in the wavenumber  $k$ . Expanding out the second term in (2.14) we get an equation of the form

$$\Theta_T - kD_\perp(k)\nabla \cdot \hat{k} - D_\parallel(k)(\hat{k} \cdot \nabla)k = 0, \tag{2.16}$$

where  $\hat{k}$  is the unit vector associated with the vector  $\mathbf{k}$ . The coefficients  $D_\perp(k)$  and  $D_\parallel(k)$  are called the perpendicular and parallel diffusion

coefficients respectively. By construction, they are analytic in  $k$ .

Multiplication by an integration factor gives formally

$$\tau(k)\Theta_T + \nabla \cdot (\mathbf{k}B(k)) = 0. \tag{2.17}$$

As we will discuss, an extra condition must be satisfied if  $\tau(k)$  and  $B(k)$  are to be analytic at  $k = k_B$ . In the particular case of the Swift–Hohenberg equation, it is possible to calculate the functions  $\tau(k)$  and  $B(k)$  explicitly in terms of  $w_0$ . After a little calculation, one finds,

$$\tau(k) = \overline{(\partial_\theta w_0)^2}, \tag{2.18}$$

$$B(k) = \frac{1}{2} \frac{d}{dk^2} \overline{w_0^4}. \tag{2.19}$$

where  $\overline{f}$  is  $\frac{1}{2\pi} \int_0^{2\pi} f d\theta$ .

Second, we use the gradient property of (2.1) to obtain the phase diffusion equation by directly averaging (2.1) over the pattern periodicity. We shall consider a more general microscopic equation of the form

$$w_t = -\frac{\delta F}{\delta w}, \tag{2.20}$$

which can be written as

$$\iint dx dy w_t \delta w = -\delta F \tag{2.21}$$

where  $F[w] = \iint G dx dy$ . In (2.20),  $\delta F/\delta w$  is the variational derivative of  $F$ , namely the expression in the integrand for the integral  $\delta F$  which multiplies  $\delta w$ . Assume that the variation of the field  $w$  is totally contained in the evolution of the phase  $\theta$ . Averaging over  $\theta$  on the approximate solution  $w_0(\theta)$  and taking the variation  $\delta w$  in the “direction”  $\theta$ , we get,

$$\epsilon \Theta_T \iint dx dy \overline{|\partial_\theta w_0|^2} \delta \theta = -\delta \overline{F}. \tag{2.22}$$

It is important to remark now that due to translational and rotational invariance,  $\overline{F}$  depends solely on the wavenumber  $k$ . As a consequence  $\delta \overline{F} = \iint (d\overline{G}/dk^2) \delta k^2 dx dy =$

$\epsilon \int \int (\overline{dG/dk^2}) 2\mathbf{k} \cdot \nabla \delta \theta \, dx \, dy$ . Integrating by parts we get finally,

$$\Theta_T \overline{|\partial_\theta w_0|^2} = \nabla_X \cdot 2\mathbf{k} \frac{d\overline{G}}{dk^2}, \quad (2.23)$$

so that  $\tau(k) = \overline{(\partial w_0/\partial \theta)^2}$  and  $B(k) = -2(\overline{d/dk^2})\overline{G(k)}$  are both analytic functions of  $k$ . Another reason for the existence of these explicit formulae is that when the basic equation is a gradient flow, the linearized operator is self-adjoint and the solvability condition is obtained after multiplying by  $\partial_\theta w_0$ . For the Swift–Hohenberg model,

$$F = \int \int dx \, dy \left\{ -\frac{1}{2} R w^2 + \frac{1}{4} w^4 + \frac{1}{2} [(\nabla^2 + 1)w]^2 \right\} \quad (2.24)$$

and using (2.12), we find  $\overline{G} = -\frac{1}{4} \overline{w_0^4}$ .

To determine the higher order corrections of the phase diffusion equation, it is possible, but in general difficult, to proceed to the next orders of the expansion. For example the function  $w_1$  is the sum of terms coming from the inversion of (2.13) after imposing the solvability condition, and of another term, an element of the kernel of  $L$ , to be determined by the  $O(\epsilon^2)$  compatibility condition. It is however possible to incorporate this latter term in the definition of a “phase-shift”  $\Psi$ . The redefinition of a new phase equal to  $\Theta + \epsilon \Psi$  (as part of a systematic expansion:  $\theta = \frac{\theta_0}{\epsilon} + \Theta_1 + \epsilon \Theta_2 + \dots$ ), allows us to recombine (2.14) and the next order solvability condition into a single equation for this new phase. In fact this procedure is equivalent to summing the different compatibility conditions of the successive orders. We state here, and prove in Appendix B, that, for the case of the regularized equation, and near  $k_B$  where  $B(k)$  is small, the higher order term that balances  $\frac{1}{\tau} \nabla \cdot \mathbf{k} B$  is  $\epsilon^2 \nu \nabla^2 \nabla \cdot \mathbf{k}$  where  $\nu = D_{\parallel}(k_B)/4k_B^2$ . The fact that it is a gradient is important.

## 2.2. Phase gradient systems

There are several reasons for which it is useful to write (2.16) in conservation (flux divergence) or Cross–Newell form (2.17). First, many of the properties such as wavenumber selection (not only by roll curvature but also by boundary geometry effects) are more easy to glean. Second, the conservation law form allows us to compute uniquely the wavevector jump (shock) conditions associated with weak solutions of (2.16) for  $k$  in the hyperbolic region  $k < k_B(R)$ . Third, the form (2.1) allows us to identify a candidate for a free-energy functional

$$\overline{F} = \int \int \left( -\frac{1}{2} \int_0^{k^2} B(s) \, ds \right) dX \, dY, \quad (2.25)$$

because then

$$\tau \Theta_T = -\frac{\delta \overline{F}}{\delta \Theta} = -\nabla \cdot \mathbf{k} B(k). \quad (2.26)$$

However, there is an obstruction, heretofore overlooked, to writing (2.16) as (2.17). Identifying coefficients of  $\nabla \cdot \mathbf{k}$  and  $(\mathbf{k} \cdot \nabla)k^2$  in (2.16) and (2.17), we get

$$D_{\perp}(k) = -\frac{1}{\tau(k)} B(k), \quad (2.27)$$

$$\frac{D_{\parallel}(k) - D_{\perp}(k)}{k} = -\frac{1}{\tau} \frac{dB(k)}{dk}, \quad (2.28)$$

from which we find, upon dividing and integrating, that

$$kB = (kB)_0 \exp \int_{k_0}^k \frac{D_{\parallel}(k)}{k D_{\perp}(k)} dk. \quad (2.29)$$

Since  $D_{\parallel}(k)$  and  $D_{\perp}(k)$  are analytic in  $k_l(R) < k < k_r(R)$ ,  $kB$  is analytic everywhere providing that the residue

$$r = \frac{D_{\parallel}(k_B)}{k_B D'_{\perp}(k_B)} \quad (2.30)$$

of the integrand in (2.29) at its pole  $k = k_B$  is unity. If  $r$  is not unity,  $B(k)$  is not single valued

p	R	$r - 1$
$\infty$	2000	$5 \times 10^{-4}$
$\infty$	4500	$5 \times 10^{-2}$
$\infty$	6000	0.118
1	2000	0.108
1	4500	0.18

Table 1  
The value of the residue  $r$  for several values of Prandtl and Rayleigh number.

and real within the marginal stability band. For example, we could define it to be real for  $k > k_B$  but then it is not real for  $k < k_B$ . Furthermore, the free energy functional (2.25) would not make sense for all  $k$  in  $(k_l(R), k_r(R))$ .

Therefore, we define a new category of pattern forming systems, named phase gradient systems, to be one for which the residue  $r$  is unity. This category includes microscopic systems which are gradient, but also contains a large class of microscopic flows which do not possess a free energy. For example, the Oberbeck-Boussinesq equations either at high Prandtl numbers  $p$  or near onset fall into this category. (The onset value  $R = R_c$  is 1708).

This result is consistent with the observations of Pocheau and Croquette [18] who find that the dislocation velocity in high Prandtl number ( $Pr = 70$ ) fluids obeys the 3/2 law, namely is proportional to  $(k - k_d)^{3/2}$ , and that the dynamics is close to being variational. We have also done several numerical simulations on a variation of the Swift–Hohenberg equation, suggested by Greenside and Cross [19]

$$w_t + (\nabla^2 + 1)^2 w - R w + w^3 + a w (\nabla w)^2 + b w^2 \nabla^2 w = 0. \quad (2.31)$$

Eq. (2.31) is a gradient flow for  $a = b$ . In this case  $r = 1$  and  $k_d = k_B$ . For  $R = 1, a = 0, b = -1, r = 1.03, k_d = 1.02k_B$ ; for  $R = 1, a = 0, b = -2, r = 1.06, k_d = 1.02k_B$ , and maximal velocities when  $(k - k_d)/k_d$  is between 0 and 0.2 are of the order of  $10^{-2}$ , slower than one roll wavelength per horizontal diffusion time. For

$R = 1, a = 0, b = -1$ , and  $w$  complex with  $w^3$  replaced by  $|w|^2 w, w^2 \nabla^2 w$  by  $|w|^2 \nabla^2 w, r = 1$ , but the flow is nongradient and  $(k_d - k_B)/k_B = .08$ .

The residue  $r$  also depends on the stress parameter. Because the phase equation (2.16) with the regularization term  $-\epsilon^2 (D_\perp(k_B)/4k_B^2) \nabla^2 \nabla \cdot k$  added must (and does) reduce to the phase component of the NWS equation (with the amplitude determined algebraically in terms of  $\nabla \theta$ ),  $r$  tends to unity as  $R \rightarrow R_c$ .

When  $r = 1, \bar{F}$  defined by (2.25) is a formal free energy functional. It is natural to ask if  $\bar{F}$  decreases with time. This question was addressed in [9] and the conclusion there was that moving dislocations may cause  $\bar{F}$  to increase unless the far field wavenumber  $k_d$  at which dislocations are stationary is  $k_B$  and that dislocations move so as to bring the wavenumber of the pattern towards  $k_B$ . That conclusion still stands even if  $r = 1$ . What is new here is the realization that the nongradient character of the original systems can manifest itself in two ways. It can cause the phase equation to be nongradient or, even if the phase equation is formally gradient, it can manifest itself in the dislocation core and thereby influence dislocation velocities. In the regularization of (2.17) that follows in Section 3, we will respect the condition  $r = 1$  and ignore the defect velocity difficulty. The fact that we cannot accurately reproduce defect velocities measured on the horizontal diffusion time scale  $T_s$  (one roll wavelength per  $T_s$  unit) is not too serious when we consider that it is even less reasonable to expect a general theory to capture dislocation velocities when the far field wavenumber  $k$  is greater than  $k_E$ . Whereas our inclusion in the OPE of the relaxation rate of the amplitude mode to its slaved value will ensure that the dislocation nucleation time is captured accurately, the dislocation velocities will be of the order of one roll wavelength per vertical diffusion time scale which is  $\epsilon^{-2} T_s$ , in other words infinite when measured on the horizontal diffusion time scale. Therefore, the best one can hope

for is a qualitative agreement.

### 3. The regularization of the phase diffusion equation

#### 3.1. The order parameter equation

In this Section, we propose a two-dimensional order parameter equation (OPE) that reproduces the dynamics of phase gradient patterns for all values of the stress parameter for which the phase diffusion equation obtains. Our goal is to write down a regularized form of the phase diffusion equation, uniformly valid for all  $k$ , inside and outside the marginal stability curve and, in the former domain, inside and outside the Busse balloon. For  $k < k_B(R)$ , a situation forced on the pattern (see the center of the cylinder in Figs. 2a, 2b) by curved roll patches induced by boundary constraints, the rolls undergo a supercritical instability called the zig-zag instability because the mode with wavevector  $(k, 0)$  gives up its energy to the modes with wavevectors  $(k, \pm\sqrt{k_B^2 - k^2})$  which produce a zig-zag pattern of wavenumber  $k_B$ . The bifurcation is supercritical and the instability is saturated. The behavior for  $k < k_B(R)$  can be regularized by introducing a biharmonic term  $\varepsilon^2 \nu \nabla^2 \nabla \cdot \mathbf{k}$  into the phase diffusion equation, a term which arises naturally as the most important contribution at the next order of approximation. Furthermore, we can view the saturated state, which often contains concave disclinations (see Figs. 2a, 2b), from another point of view. For  $k < k_B(R)$ , the stationary phase diffusion equation is hyperbolic and it is not hard to show that, in general, characteristics from the same family will intersect and shocks will form. The resulting shock (weak) solutions give a good approximation to the pattern structure near concave disclinations. The biharmonic term will act to smooth the discontinuities in the wavevector (strictly director) field along

the shock lines, lines which join concave disclinations to sidewall foci (Figs. 2b, 2c). Thus, on the left of the Busse balloon, the phase equation can be itself regularized.

To the right of the Busse balloon, however, another kind of regularization is required. In distinct contrast to the zig-zag instability, the Eckhaus instability triggered when  $k > k_E(R)$  is a subcritical one [20] and does not saturate in a new state close to the unstable one. Rather the instability very quickly takes the local wavenumber  $k$  far outside the Busse balloon  $k_E$  and also outside the right hand border  $k_r$  of the marginal stability curve. At this value of  $k$ , the amplitude  $A^2$  becomes zero and the basic premise of the theory, namely the existence of a finite amplitude periodic state, is violated. To regularize in this case, we need to add back in the amplitude  $A$ , which to date has been slaved to, that is, determined algebraically by, the wavenumber  $k$  through  $A^2 = \mu^2(k^2, R)$ , as an active parameter. One might argue that when the amplitude of the total field is zero, modes with wavevectors in all directions can become active. But they will be rapidly suppressed by the bias introduced by the direction of the wavevector in the far field because the roll planform is locally stable. Therefore, only the amplitude associated with that mode is considered. The importance of this amplitude when  $\mu^2$  is close to zero is evidenced by the existence of a second solution  $v_2$  for the homogeneous equation  $Lw_1 = 0$  given by

$$v_2 = \frac{dw_0}{dA} = \frac{\partial w_0}{\partial A} + \frac{\partial w_0}{\partial \theta} \cdot \frac{\theta}{2k^2} \left( \frac{\partial A}{\partial k^2} \right)^{-1}, \quad (3.1)$$

which becomes  $2\pi$ -periodic at the marginal stability boundary  $A^2 = \mu^2(k, R) = 0$ . Therefore we need a prescription in which both the amplitude and the phase are order parameters at the core of dislocations (points where  $A = 0$ ) and at the center of certain target patterns where the local wavenumber becomes infinite, but only the phase is an order parameter elsewhere.

The order parameter equation must have the following properties:

(a) It must be an equation for a real order parameter that is a periodic function of the phase (e.g.  $a \cos \theta$ ) in order to remove the multivaluedness of the phase introduced by local periodicity. Complex order parameters, that define a wavevector field without directional ambiguity, cannot describe disclinations because these defects are defined by the behavior of a local director (vector without an arrow) rather than a vector field.

(b) The OPE must reduce to the Cross–Newell equation for  $\epsilon \rightarrow 0$  and inside the marginal stability curve with analytic function  $B(k)$ .

(c) The OPE must lead to the same Newell–Whitehead–Segel equation as the original equation near onset. The amplitude of the order parameter must go to zero both at  $k_l$  and  $k_r$ .

(d) The transition from the null solution to the roll solution at the marginal curve must be a forward pitchfork bifurcation.

(e) We must recover the correct decay rate  $\lambda_{1S}$  (see Appendix C) of perturbations to all finite amplitude patterns with wavenumbers in the marginal stability band. This property is important if we wish to follow the dynamics of all events (such as the nucleation of dislocation pairs) that are connected with the horizontal diffusion time scale. We do not require that we recover the higher order terms of the phase diffusion equation from the OPE.

We propose the following equation:

$$\chi(-\nabla^2)W_t + A(-\nabla^2)W + a^2\Gamma(-\nabla^2)W = 0, \quad (3.2)$$

for the order parameter  $W = a \cos \theta$ . The term  $a^2$ , the squared amplitude, is a functional of the real field  $W$  extracted for example by wavelet analysis (see Appendix A). The functions  $\chi$ ,  $A$ ,  $\Gamma$  are given by combinations of  $\lambda_{1S}$ ,  $B$  and  $\tau$ . A term like  $A(-\nabla^2)W$  is by definition  $\int_{-\infty}^{\infty} A(k^2)e^{ik \cdot x} \widehat{W}(\mathbf{k}) d\mathbf{k}$  where  $\widehat{W}(\mathbf{k})$  is the Fourier transform of  $W(x)$ .

Let us now show that (3.2) satisfies points (a)–(e) mentioned above:

(a) It is clear from the form of the equation itself that it satisfies point (a) and (d) provided  $A(k^2)$  and  $\Gamma(k^2)$  have a correct sign on the marginal curve. It is important to make explicit the link between its solution and the original pattern. The OPE is not meant to give the correct short scale structure. For example, the solutions of the OPE are monochromatic and periodic whereas the original equation may have many harmonics in its periodic structure. However, given a solution  $W$  of (3.2) it is possible to reconstruct the phase  $\theta$  of the true solution and with that phase and the amplitude  $a$  determine  $w_0(\theta)$  which is a close approximation to the exact solution. Namely, away from singularities,

$$w(x, y, t) \sim w_0\left(\arccos\left(\frac{1}{a}W\right)\right) \quad (3.3)$$

for  $a$  of order one and this reduces to  $W$  in the limit of small amplitude  $a$ . The amplitude  $a$  of the order parameter  $W$  is not an approximation to the amplitude  $A$  of the real pattern, except near onset where the single Fourier mode approximation of the true solution is valid. The solution  $W$  will produce, however, the same overall pattern with the same topology (smooth patches, defect singularities, etc.) as the original field  $w(x, y, t)$ .

(b) The Cross–Newell limit of this equation is derived in Appendix B and we obtain the following phase diffusion equation

$$\chi A \theta_t - \nabla \cdot (\mathbf{k} A \Gamma (\frac{A}{F})') = 0. \quad (3.4)$$

This calculation is straightforward because (3.2) admits monochromatic solutions. This latter property allows us also to find  $\lambda_{1S} = -2A/\chi$ . In order to satisfy (b) and (e), we find

$$\chi = \sqrt{\frac{2\tau}{\lambda_{1S}}}, \quad (3.5)$$

$$A = -\sqrt{\frac{\tau \lambda_{1S}}{2}}, \quad (3.6)$$

$$\frac{\Gamma'}{\Gamma} = \frac{A'}{A} + \frac{\chi}{A} \frac{B}{\tau}. \tag{3.7}$$

The choice of integration constant for (3.7) ensures that the pseudo-amplitude is the real amplitude at the right border of the neutral stability curve  $k = k_r$ . Close to  $k_r$  we choose  $\Gamma(k^2) = \lambda_{1S}/2\mu^2$  so that  $\chi(k^2) = 1$  at  $k_r$ . Outside the band of wavenumbers  $k$  between  $k_l$  and  $k_r$  we define  $\chi(k^2)$  and  $\Gamma(k^2)$  by the constant values they assume on the marginal stability curve.

(c) The functions  $\chi, A, \Gamma$  are also functions of the stress parameter  $R$  through  $\tau, B$  and  $\lambda_{1S}$ . When this stress parameter is close to its critical value  $R_c$ , and if we denote by  $k_0$  the critical wavenumber, we derive from (3.2) the following NWS equation:

$$\begin{aligned} &\chi(k_0)A_t + (R - R_c)\left(\frac{\partial A}{\partial R}\right)_0 A \\ &- \frac{1}{2}\left(\frac{\partial^2 A}{\partial k^2}\right)_0 (\partial_x - (i/2k_0)\partial_y^2)^2 A \\ &+ \Gamma(k_0)|A|^2 A = 0. \end{aligned} \tag{3.8}$$

Equation (3.2) can be immediately transformed into Eq. (3.8) when  $\chi, A$  and  $\Gamma$  are expanded about  $\mathbf{k} = (k_0, 0)$ ,  $A$  is taken to be small and the stress parameter  $R$  close to  $R_c$ . Under these assumptions, the real and complex order parameters are also equivalent and we can take  $W$  in (3.2) to be  $Ae^{i\theta}$  and  $a^2$  to be  $|A|^2$ . The coefficient of  $\partial_{YYY}W$  identifies with the coefficient of the most important next correction to the phase diffusion equation (3.4) derived from (3.2) near  $k_B$ .

### 3.2. Numerical simulations

The goal of the first experiment is to show that the OPE correctly reproduces the dynamics of the original microscopic equation. Here, we choose the model (2.31) with  $a = b$ ,

$$\begin{aligned} \partial_t w - (R - (1 + \nabla^2)^2)w + w^3 + b(w(\nabla w)^2 \\ + w^2 \nabla^2 w) = 0 \end{aligned} \tag{3.9}$$

The reason for this choice is that its OPE is significantly different from the original equation. For the SH model ( $b = 0$ ), the form of the OPE is very close to the SH equation itself and its coefficients  $\chi, A, \Gamma$  do not show a significant difference from 1,  $R - (1 - k^2)^2$  and  $-\frac{3}{4}$ , respectively. This is mainly due to the fact that the ratios of the coefficient of the higher harmonics to the leading order coefficient of the solution  $\omega_0(\theta)$  are very small. However, by choosing  $b \neq 0$  we also change completely the form of the nonlinear terms and the solution  $\omega_0(\theta)$  has a Fourier spectrum with a significant amount of energy in the higher harmonics. Therefore, the comparison between the microscopic model and the OPE is less trivial. This equation derives from a potential and thus its phase diffusion equation falls in the category of models on which it is possible to apply the construction of Section 2. The functions  $\chi(k^2), A(k^2)$  and  $\Gamma(k^2)$  corresponding to this equation are plotted in Fig. 3 for  $b = -5$  and  $R = 1$ . This model and the OPE derived from it are integrated in parallel, in order to test the validity of the regularization. The integration of the OPE as it stands is easy when using a pseudo-spectral method with Fourier Series in a periodic domain. The temporal scheme mixes an Adams-Bashforth for the nonlinear terms, the  $a^2 \Gamma W$  term in (3.2), and an exact integration of the linear terms with a time step of 0.05 for a spatial resolution of  $64 \times 64$  grid points. We usually take initially eight rolls oriented along the  $y$  direction. A large number of rolls would necessitate a higher resolution. For Eq. (3.9) above, the cutoff wavenumber of the spectral range, must be at least three times the dominant wavenumber of the pattern. This constraint is strict because the nonlinear term contains derivatives and a small truncation error would completely modify the longwavelength instability boundaries. This constraint does not apply as strictly for the OPE since the roll solutions are monochromatic. This remark shows that the comparison between (3.9) and its OPE is far from being trivial. Since we are working with a field of almost straight

parallel rolls, the computation of the amplitude  $a^2$  is done by using the Hilbert transform to construct  $w^*$  and then  $a^2 = w^2 + w^{*2}$ . This procedure gives a very satisfactory answer as long as the rolls do not make a large angle with the  $y$  axis.

First of all, we made some tests to verify that the borders of the Busse balloon indeed coincide for both the microscopic model and the OPE. They do. Next we tested some very nontrivial behavior connected with dislocations, their motion and their instabilities. We started with straight parallel rolls at  $b = -5$  and wavenumber  $k_0 = 1.3$  with some perturbation  $w(t = 0) = A \cos(k_0(x + \alpha \sin x \cos y))$  tending to squeeze the rolls in the middle of the container. We observe the formation of a pair of dislocations which then move apart in a climbing motion along the  $y$  axis. The solutions of both model (3.9) and the OPE are in very good agreement for as long as we calculated. Let us stress here that in principle we cannot expect a perfect agreement when defects are close to each other or are moving, but in fact there is in this case. In order to test what happens for different wavenumbers of the far field, we did the following experiment. After the pair of dislocations have moved a certain distance from each other, we stop the runs and change the spatial scaling so as to change the effective wavenumber of the background pattern. We then restart the run. The defects then move in one direction or the other, according to the new wavenumber of the pattern  $k_0$ . We show in Figs. 4a, b, c, d the state of the pattern after some time for both model (3.9) and the OPE, and for  $k_0 = 0.85$  and  $k_0 = 1.2$ . The global topology is in agreement, but also the positions of the defects agree. The agreement is even better if the inverse aspect ratio is larger (not shown).

The OPE reproduces the behavior of solutions of the original equation reasonably well because the pattern is not “turbulent” and the distance between defects is large. However, we do not claim that this would hold if many defects were

nucleated. Indeed, we tried also to test more disordered situations. At higher values of the stress parameter ( $R = 3$ ) and with a larger number of rolls ( $n = 15$ ) we begin to observe serious discrepancies between the OPE and the original equation. This in fact is not very surprising since the pattern, when initially prepared in an Eckhaus unstable regime, is rapidly driven into a state of “defect mediated turbulence”. In such regimes, small differences in the initial conditions are exponentially amplified, and at best, we could only expect to recover an agreement in the statistics of the solutions. Indeed it would be of interest to investigate whether the same OPE obtains in a statistical sense for turbulent patterns.

The goal of the second experiment is to demonstrate a very nontrivial behavior of the pattern, the development of the bridge instability [21] (a finite amplitude instability of a moving dislocation), and to show the inability of an OPE for a complex order parameter to capture it. Our OPE correctly reproduces all stages of this instability. For this experiment we take the SH equation ( $b = 0$ ) at  $R = 3$  with  $k_0 = 1.5$ . The borders of the nonlinear stability region in this case is  $k_B = 0.98$  and  $k_E = 1.45$ . Taking the same initial conditions as in the second experiment, we also obtain a pair of dislocations which move upwards and downwards. When we consider the local wavenumber in the region where the pair of dislocations is forming, we see that there is a patch of wavenumber of approximately  $k_0/3$  just behind each dislocation, which rapidly disappears by contraction of the rolls as the defects separate. Here, however, the mode  $k_0/3$  is more linearly unstable and the amplitude of the Fourier components at that wavenumber, generated by the modulation of the mode  $k$  and the existence of the defect, have time to grow and reach significant values. Locally, it corresponds to a fully developed (nonlinear) patch of rolls whose wavenumber has now increased but stays well below the value  $k$  of the surrounding rolls. Its amplitude is well above the amplitude of these rolls and thus there is a tendency to bridge

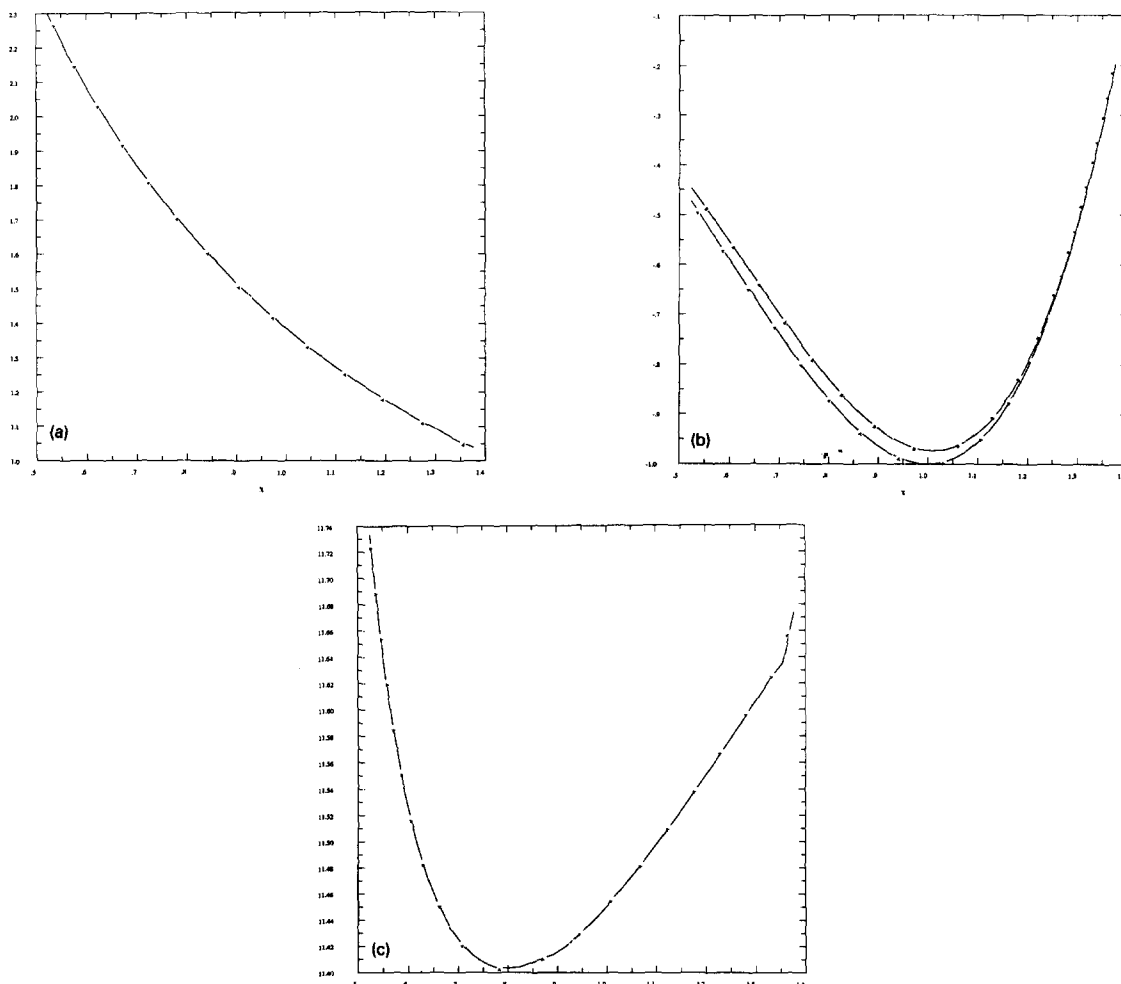


Fig. 3. A plot of the coefficients  $\chi(k)$  (a),  $\frac{A(k)}{\chi(k)}$  (b, bottom curve) and  $\Gamma(k)$  (c) for equation (2.31) at  $R = 1, a = b = -5$ . The upper curve in (b) corresponds to the quantity  $R - (k^2 - 1)^2$ .

the gaps at the edges of the dislocation. The competition between these two solutions eventually leads to the formation of a downflow just behind the core of the defect and this completes the process. This process is illustrated in more detail in [21]. We show in Figs. 5a, b, c, a picture of the resulting pattern after some time for (a) the real SH equation, (b) the real OPE and (c) the complex OPE. The agreement between the solutions of the SH equation and those of the real OPE is very satisfactory, even though, as we can expect, the defects are not at exactly the same location. But the topology is the same

and this is the main point. We see, however, in Fig. 5c that the correct topology is not at all recovered using the complex OPE. This might be interpreted by looking at the dotted lines in Fig. 5b compared to Fig. 5c. In Fig. 5b, the dotted lines are the lines of the zero of  $HW$ , the Hilbert transform of the real order parameter  $W$  which solves (3.2). In Fig. 5c, they are the lines of the zeros of  $\text{Im}W$ . We see that the field  $\text{Im}W$  is a regular dislocation for all times and thus the fields  $\text{Re}W$  and  $\text{Im}W$  cease to be intimately coupled in such a way that  $|W|^2$  is a slowly varying quantity. The coupling is forced in the

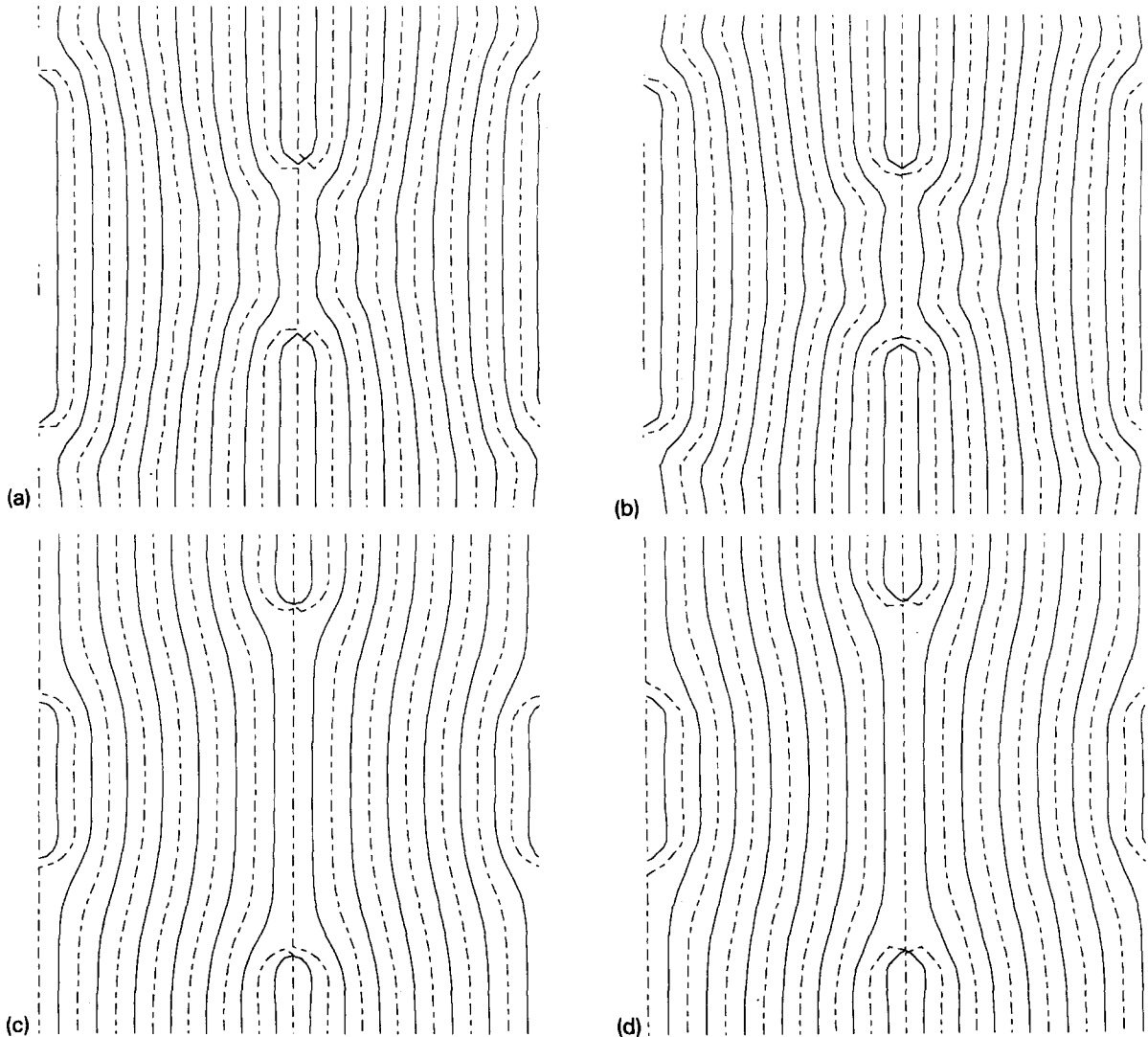


Fig. 4. (a) and (c) show snapshots of level curves of  $w = 0$  and  $w^* = 0$  for solutions of equation (2.31) with  $R = 1$ ,  $a = b = -5$  with  $k_0 = 0.85$  and  $1.2$  respectively. The quantity  $w^*$  is computed by the one dimensional Hilbert transform. (b) and (d) are the same level curves calculated for the OPE. In (a),(b) the defects are moving towards each other.

case of the real equation. Let us emphasize this crucial point: the dynamics causes the two fields  $\text{Re } W$ ,  $\text{Im } W$  of the equation for the complex order parameter  $W = \text{Re } W + i \text{Im } W$  to evolve in such a way that  $\sqrt{(\text{Re } W)^2 + (\text{Im } W)^2}$  varies on short time scales. On the other hand, Eq. (3.2) forces the fields  $W$  and  $HW$  to remain intimately coupled.

The wavevector fields at three stages of the

dissociation and reformation process of the instability are shown in Fig. 6. Bridges have been observed in real experiments [22, 23].

Finally, we want to present in experiment 4 the results of using a two dimensional wavelet algorithm for the calculation of the amplitude. The experiment is exactly the same as experiment 2 for  $k_0 = 1.3$ , except that the resolution is only  $32 \times 32$  grid points. We observe the formation of



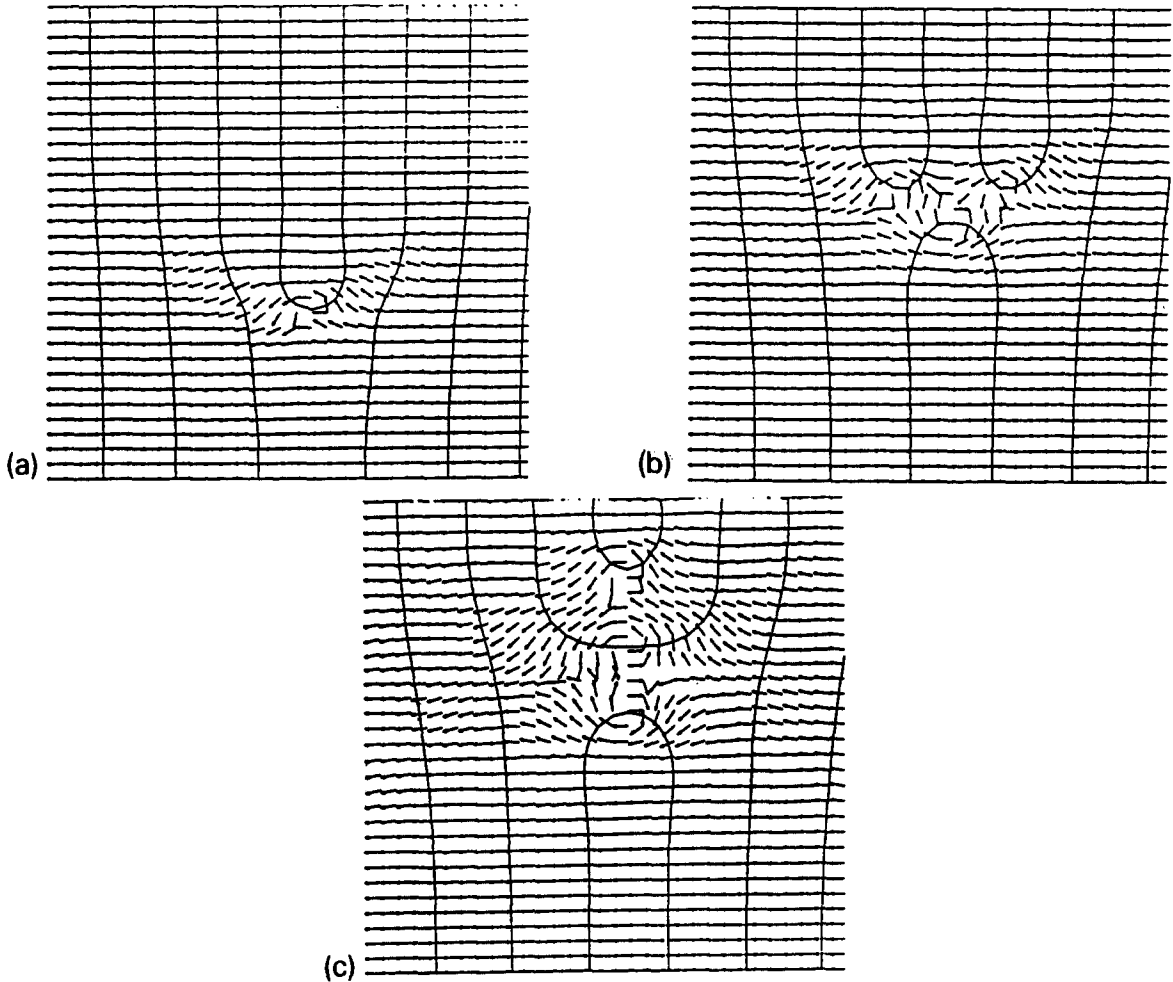


Fig. 6. Three stages of the instability, dissociation and re-formation of the dislocation leaving a bridge in its wake.

mation of defects. The wavevector field is accurately captured in the far field but does not have the resolution of that determined by the exact solution. The calculations are performed with the values of  $\alpha_1 = 1, \alpha_2 = 3, \omega = 3$  (see Appendix A).

#### 4. Towards a general theory of stationary pattern singularities

##### 4.1. Preamble

To this point, our regularization procedure has adopted the following viewpoint. A pattern consists of a mosaic of relatively smooth patches of locally periodic rolls separated by point and curve singularities at which the wavevector changes suddenly. In the smooth regions, the Cross–Newell equation holds but in order to make sense of the global behavior, one must solve the regularized order parameter equation

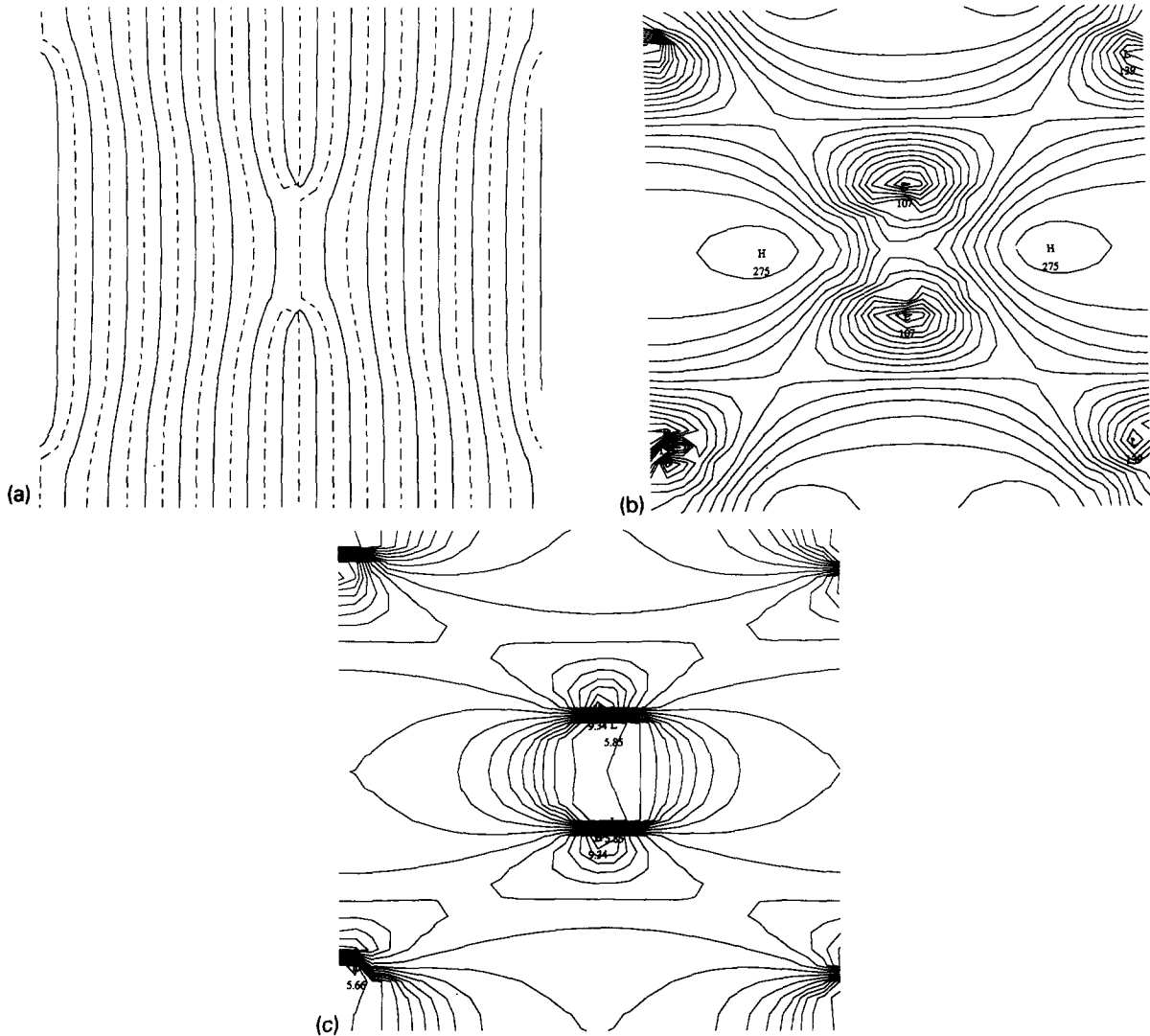


Fig. 7. (a) is the same pattern as is obtained in Fig. 4a except here  $k_0 = 1.3$  at a time just after the dislocation pair has formed using the OPE and the two dimensional wavelet algorithm. (b),(c) show, respectively, the constant amplitude (multiplied by 103) levels and the constant wavenumber (multiplied by  $8/1.3$ ) level curves.

constructed in Section 3. In other words, the CN equation is fine as long as one does not expect it to hold globally. It provides extremely useful qualitative information and it is the skeleton on which we build the OPE, but for general time dependent patterns, in order to make use of its content, we must return from an equation written in large scale coordinates to one which is written in small scale coordinates. In spite of

the fact that the OPE is usually simpler than the original system, we have lost the advantage of averaging.

The purpose of this Section is to show how we can recover some of that advantage when we deal with stationary patterns. In particular, we assert and now demonstrate that the far fields of point and line singularities are captured by weak and singular solutions of the stationary phase diffu-

sion equation which describes that far field. Concretely, we will seek solutions of the stationary CN equation

$$\nabla \times \mathbf{k} = 0, \quad (4.1)$$

$$\nabla \cdot \mathbf{k} B(k) = 0, \quad (4.2)$$

which are realized as asymptotic (time  $T \rightarrow \infty$ ) and therefore stable solutions of

$$\tau(k)\Theta_T + \nabla \cdot \mathbf{k} B(k) + \epsilon^2 R_g = 0 \quad (4.3)$$

in the limit  $\epsilon \rightarrow 0$ . Because these solutions may not be smooth, we call them weak solutions. In (4.3),  $R_g$  represents the regularization. It is  $e \frac{|B'(k_B)|}{4k_B} |\nabla^2 \nabla \cdot \mathbf{k}|$  for  $k_{E_l} < k < k_B$  with  $e = 1$  when  $k$  is close to  $k_B$ . For  $k > k_E$  or  $k < k_{E_l}$ , it represents the amplitude regularization obtained by embedding the phase diffusion equation in (3.2). In what follows, we will indeed find new solutions which capture the nature (the topology and the energetics) of point and line defects. Moreover, it turns out that the building blocks of all point defects are convex and concave disclinations, to which objects we have given the name *monofects*, whose topologies have already been discussed in the literature [24, 25, 26]. What is new in the present work is that we find weak solutions of (4.1), (4.2) which not only have the correct topologies but which also satisfy the energetic (stability) constraints imposed by insisting that they are stable ( $T \rightarrow \infty$ ) solutions of (4.3) in the limit  $\epsilon \rightarrow 0$ .

Solutions of (4.1), (4.2) give rise to a map

$$\begin{aligned} X(X = r \cos \alpha, Y = r \sin \alpha) \\ \rightarrow \mathbf{k}(f = k \cos \varphi, g = k \sin \varphi), \end{aligned} \quad (4.4)$$

from physical space to wavevector space with Jacobian matrix (subscripts refer to partial derivatives)

$$J = \begin{pmatrix} f_x & f_y \\ g_x & g_y \end{pmatrix}, \quad (4.5)$$

with determinant

$$|J| = f_x g_y - f_y g_x = \frac{k}{r} (k_r \varphi_\alpha - k_\alpha \varphi_r). \quad (4.6)$$

This map is singular when  $|J| = \infty$ . If the rank of the Jacobian matrix  $J$  is one, the singularity is a fold. If  $J$  has rank zero, the singularity is an umbilic. Note that the fact that  $f(X, Y), g(X, Y)$  satisfy (4.1), (4.2) applies a constraint so that not all generic singularities of two dimensional maps are necessarily realized here. The Jacobian matrix of the inverse map is

$$J^{-1} = \begin{pmatrix} X_f & X_g \\ Y_f & Y_g \end{pmatrix}.$$

Rotational invariance means that  $B$  is a function of wavenumber  $k$  only and it is therefore more convenient to analyze the map from  $X$  to the wavevector angle  $\varphi$  and wavenumber  $k$ . This map is not trivial for two reasons. First, in addition to the singular vectorfield solutions of (4.1), (4.2) for which the map  $X \rightarrow \varphi$  is singlevalued in the neighborhood of the singularity, there are director field (a vectorfield without arrows) solutions, corresponding to convex and concave disclinations, for which the map  $X \rightarrow \varphi$  is doublevalued. In those cases,  $\varphi$  is only determined modulo  $\pi$  or up to sign. In the neighborhood of point singularities where  $\mathbf{k}$  is a vectorfield, one can define the invariant,  $\Gamma$ , called the circulation and defined as

$$\Gamma = \frac{1}{\epsilon} \int_C \mathbf{k} \cdot d\mathbf{X}, \quad (4.7)$$

where  $C$  is a curve which circumscribes the singularity in a counterclockwise direction. In the neighborhood of point singularities, such as disclinations, where  $\mathbf{k}$  is only a director field,  $\Gamma$  is not defined. There is, however, another invariant, the twist  $T$ , which is the winding index of the map  $X$  to  $\mathbf{k}$  or, more simply stated, the amount by which a director rotates about its midpoint as the latter circumscribes the singularity on the curve  $C$ . For disclinations,  $T$  is either  $+\pi$  (convex) or  $-\pi$  (concave). The twist of each of the composite defects is simply the sum of the twists of the disclinations from which it is built.

Second, while the map  $X \rightarrow \varphi$  tells us much about the defect topology, the map  $X \rightarrow k$  tells us about energetics. This map is also multivalued because of the nontrivial shape of  $k_B(k)$ . The energetically correct solution branch is chosen uniquely by the constraint that the wavenumber  $k$  must lie between  $k_B$  and  $k_E$  almost everywhere. Only in an order  $\sqrt{\epsilon}$  neighborhood of certain curves (phase grain boundaries along which the regularization  $R_g = e^{\frac{|B'(k_B)|}{4k_B}} \nabla^2 \nabla \cdot \mathbf{k}$  obtains) or in an order  $\epsilon$  neighborhood of point defects (where amplitude regularization is usually required) can  $k$  lie outside of  $(k_B, k_E)$ . Moreover, the requirement that the wavenumber lies in the band  $(k_B, k_E)$  almost everywhere means that the orders of magnitudes of various constants that arise in the singular solutions are determined. The result is that, in the neighborhoods of point defects and phase grain boundaries,  $k$  is  $k_B$  to within an exponentially small correction in those regions where the rolls are straight, and to within order  $\epsilon$  in regions where the rolls are circular, in the far field of stationary dislocations. Therefore, concave and convex disclinations, as do target patterns, select a preferred wavenumber in their far fields.

In Section 4.2, we introduce the solutions corresponding to point defects, convex and concave disclinations, saddles, targets, vortices and spirals. Handles, dislocations and bridges are also discussed. The first two are called *monofects*. The next five are each composed of two disclinations and are therefore called *difects*. The last two require four disclinations and are called *quadrafects*. We identify these solutions by applying the hodograph transformation which converts (4.1), (4.2) into a linear, separable equation. In Section 4.3, we examine the quasilinear system (4.1), (4.2) directly, and identify its characteristics and the Rankine-Hugoniot conditions associated with its discontinuous solutions. It turns out that, when  $k$  is close to  $k_B$ , as is almost always the case of interest, the system (4.1), (4.2) is isomorphic to compressible gas flow and the

shallow water wave equations. Because of the flux divergence form of the stationary equation

$$\nabla \cdot \mathbf{k} B(k) + \epsilon^2 \frac{|B'(k_B)|}{4k_B} \nabla^2 \nabla \cdot \mathbf{k} = 0, \quad (4.8)$$

the jump conditions at discontinuities are unique and independent of the exact form of the regularization. In Section 4.4, we introduce exact solutions of (4.8) corresponding to dislocations and to phase grain boundaries with weak discontinuities. Again we will see the importance of the  $r = 1$  condition.

#### 4.2. Elementary and composite defects of roll patterns

Since (4.1), (4.2) are quasilinear, we can use the hodograph transformation

$$\begin{aligned} f_X &= |J| Y_g, f_Y = -|J| X_g, g_X \\ &= -|J| Y_f, g_Y = |J| X_f \end{aligned} \quad (4.9)$$

to express  $X$  and  $Y$  as functions of  $f$  and  $g$ . Equation (4.1) then allows us to introduce the potential  $\hat{\theta}(f, g)$ ,

$$X = \frac{\partial \hat{\theta}}{\partial f} = \cos \varphi \frac{\partial \hat{\theta}}{\partial k} - \frac{\sin \varphi}{k} \frac{\partial \hat{\theta}}{\partial \varphi}, \quad (4.10)$$

$$Y = \frac{\partial \hat{\theta}}{\partial g} = \sin \varphi \frac{\partial \hat{\theta}}{\partial k} + \frac{\cos \varphi}{k} \frac{\partial \hat{\theta}}{\partial \varphi}, \quad (4.11)$$

and, after a little analysis, (4.2) becomes

$$k \frac{\partial}{\partial k} k_B \frac{\partial \hat{\theta}}{\partial k} + \frac{\partial}{\partial k} (k_B) \frac{\partial^2 \hat{\theta}}{\partial \varphi^2} = 0, \quad (4.12)$$

a linear and separable equation in  $k, \varphi$ . Observe that  $\Theta(X, Y)$  and  $\hat{\theta}(f, g)$  are related via the Legendre transform

$$\Theta(X, Y) + \hat{\theta}(f, g) = \mathbf{k} \cdot \mathbf{X} = k \frac{\partial \hat{\theta}}{\partial k} = r \frac{\partial \Theta}{\partial r}. \quad (4.13)$$

Thus a solution  $\hat{\theta}(k, \varphi)$  gives us a map between  $(k, \varphi)$  and  $(X, Y)$  (Eqs. (4.10) and (4.11)) and the constant phase contours are given by

$$k \frac{\partial \hat{\theta}}{\partial k} - \hat{\theta} = \Theta, \quad (4.14)$$

and can be drawn either in the  $k(f, g)$  or  $X(X, Y)$  planes.

We now analyze several of these solutions in detail. It is useful for illustrative purposes to begin with a class of solutions, called harmonic, corresponding to the choice  $B(k) = 1$ , even though they are irrelevant for patterns because of energetic considerations. In this case (4.1) and (4.2) are the Cauchy Riemann conditions from which we can deduce that  $w = f - ig$  is an analytic function of  $z = X + iY$ . The singularities of analytic functions corresponding to vectorfields  $(f, -g)$  are well known. They are associated with the level curves corresponding to the integration of the one-forms

$$d\Omega = d\Theta + id\Psi = w dz \quad (4.15)$$

for  $w = z^l = r^l e^{il\alpha}$ ,  $l$  an integer. The constant phase contours are given by

$$\Theta = r^{l+1} \cos(l+1)\alpha. \quad (4.16)$$

The canonical singularities are zeros ( $l = 1$ ) and poles ( $l = -1$ ). Director field solutions on the other hand derive from square root singularities,  $w = z^{\pm 1/2}$ , and are associated with the level curves corresponding to the integration of the quadratic differentials

$$\sqrt{w^2} dz^2. \quad (4.17)$$

For  $w = z^m$ , the constant phase contours are

$$\Theta = r^{(m+2)/2} \cos\left(\frac{m+2}{2}\alpha\right). \quad (4.18)$$

For  $m = 2l$ , (4.18) is (4.16). The solutions (4.18) correspond to taking the exact solutions of (4.12),

$$\hat{\theta} = \frac{1}{n} k^n \cos n\varphi, \quad n = 1 + 2/m, \quad (4.19)$$

which gives

$$r = k^{n-1}, \quad (4.20)$$

$$\alpha = (n-1)\varphi, \quad (4.21)$$

and

$$\Theta = \frac{n-1}{n} r^{n/(n-1)} \cos\left(\frac{n}{n-1}\alpha\right). \quad (4.22)$$

The constant phase contours for  $m = 1, -1, 2$ , or  $n = 3, -1, 2$  corresponding to the concave and convex disclinations, and a saddle respectively, are drawn in Figs. 8c, 8a, 8k. Note that the twists are  $-\pi, \pi$  and  $-2\pi$  respectively. Note that the wavenumbers of the harmonic solutions fall well outside the Busse balloon over large areas near the singularity. For this reason, the harmonic representations only give the correct topologies of the solutions of (4.1), (4.2) we shall shortly discuss. Nevertheless, they help us understand the morphology of the composite defects because the  $w(z)$  representations of the latter can be found by multiplying together the harmonic representations of each of the elementary disclinations from which that particular composite is built. We list the composites, their representations, their twists and their circulations in the following Table. Note in particular that, in the limit  $\mu \rightarrow 0$ , the wavevector field for the dislocation is given by

$$\begin{aligned} f &= k_0 + \epsilon \frac{Y}{X^2 + Y^2}, & g &= -\epsilon \frac{X}{X^2 + Y^2}, \\ \Theta &= k_0 X - \epsilon \alpha, \end{aligned} \quad (4.23)$$

and is clearly the superposition of a vortex at  $X = Y = 0$  and a saddle at  $X = 0, Y = -\epsilon/k_0$  (Fig. 8q).

We now turn to the construction of the energetically correct weak solutions of (4.1), (4.2) with nontrivial topologies. It is instructive to begin with the target pattern because in this context it is easy to see how the energetic considerations come into play.

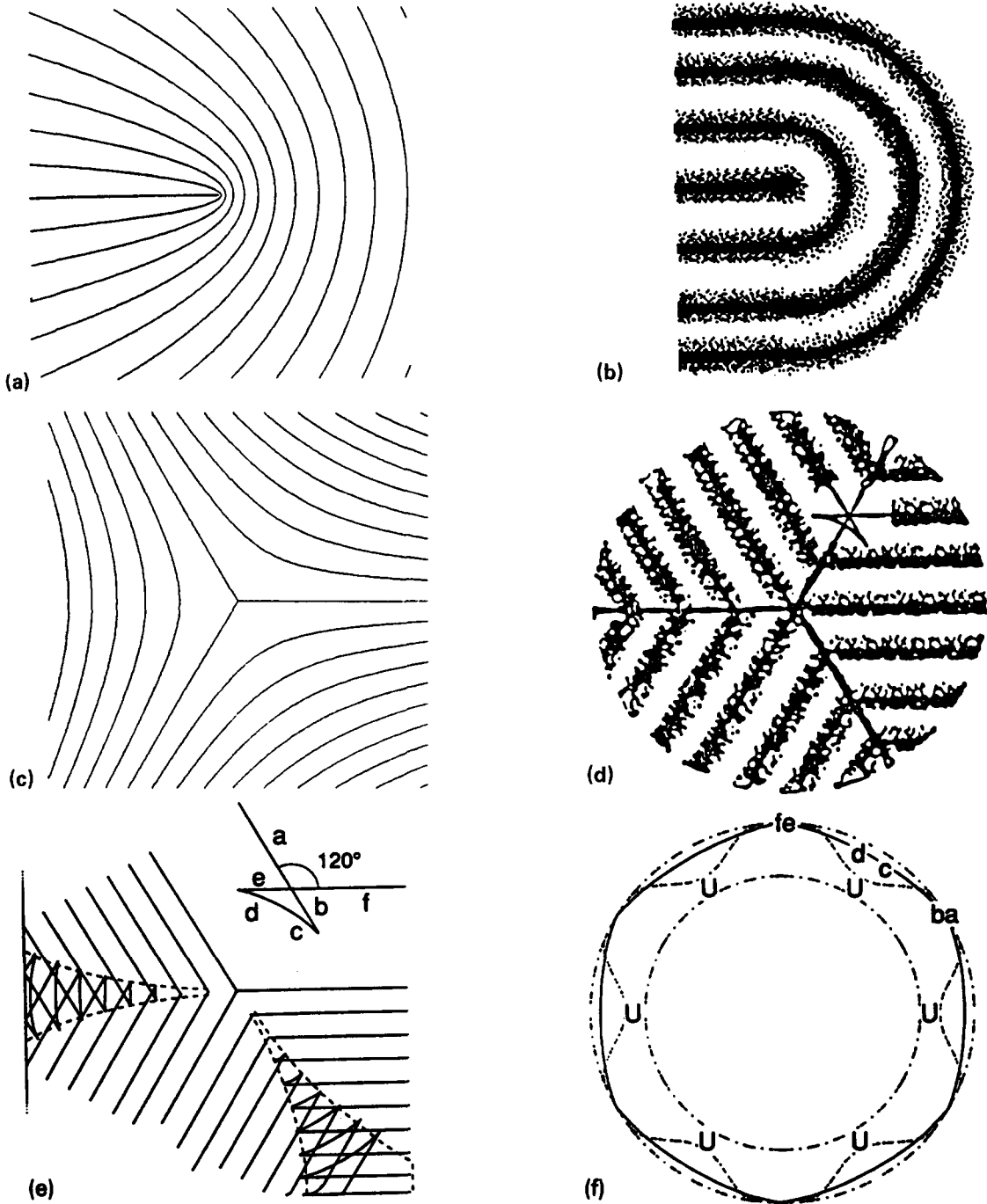


Fig. 8. (a) Isophase contours for the harmonic convex disclination. Note  $k \rightarrow \infty$  as  $x^2 + y^2 \rightarrow 0$ . (b) Isophase contours for regularized convex disclination or Roman Arch. (c) Isophase contours for harmonic concave disclination. Note  $k \rightarrow 0$  as  $x^2 + y^2 \rightarrow 0$ . (d) Isophase contours of regularized concave disclination with phase grain boundaries along  $\alpha = \pi/3, \pi, 5\pi/3$ . (e) Isophase contours for exact solution of unregularized solution of (4.1), (4.2) with concave disclination topology. The sector  $0 < \alpha < 2\pi/3$  shows a blown up version of a single phase line in which the multivaluedness of the unregularized solution is apparent. (f) The corresponding path in  $k$  space (bold line)  $fedcba$  to the one marked in (e). The dotted line is the locus of folds. The outer and inner circles are  $k = k_B$  and  $k = k_{E1}$  respectively. (g) Isophase contours of harmonic target pattern. Note  $k \rightarrow \infty$  as  $r \rightarrow 0, k \rightarrow 0$  as  $r \rightarrow \infty$ . (h) Isophase contours of regularized target pattern. (i) Separated target pattern. (j) Vortex.  $\theta = -\alpha$ . (k) Isophase contours of harmonic saddle. (l) Isophase contours of regularized saddle with phase grain boundaries along  $\alpha = \pi/4, 3\pi/4, 5\pi/4, 7\pi/4$ . (n) Isophase contours of a separated harmonic saddle. (m) Wavevector field for the separated harmonic saddle. (o) Isophase contour for Type I handle. (p) Isophase contours for Type II handle. (q) Isophase contours of harmonic dislocation. (r) Wavevector field for harmonic bridge.

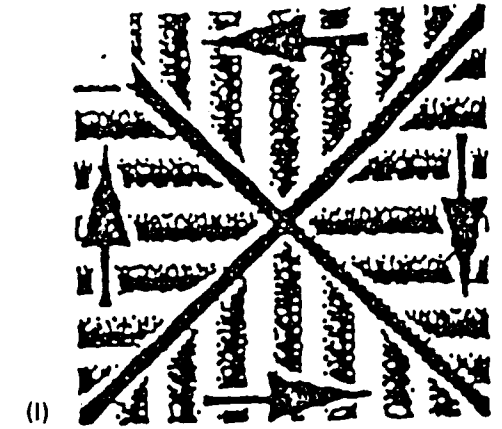
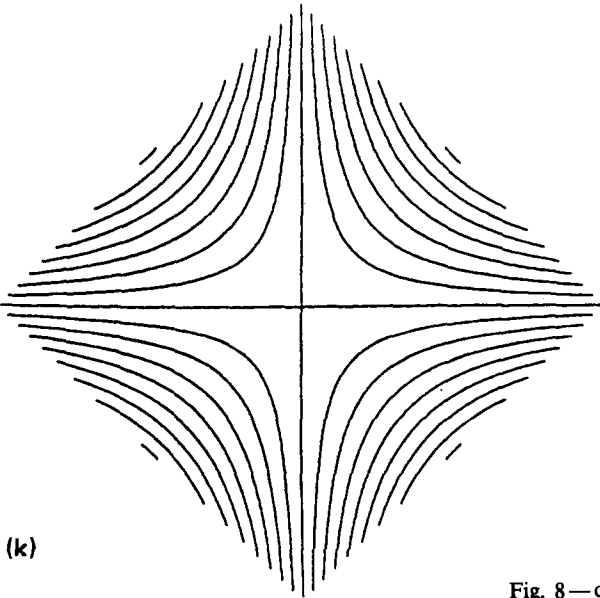
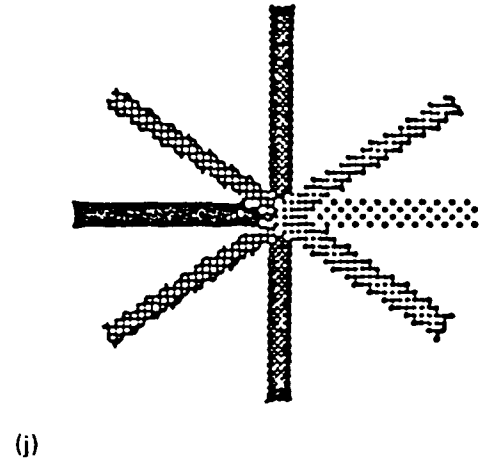
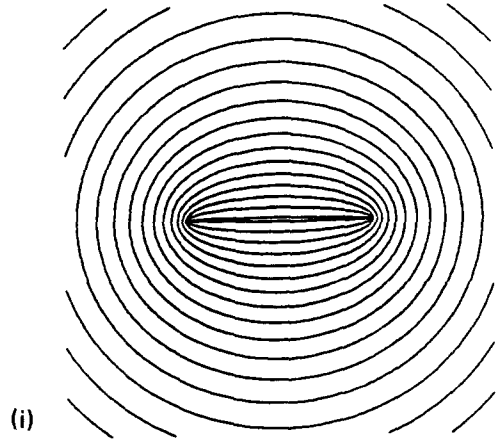
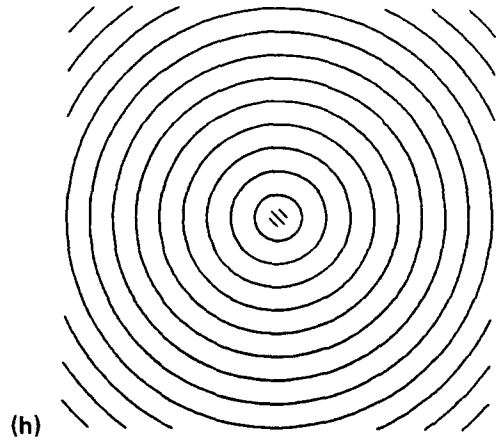
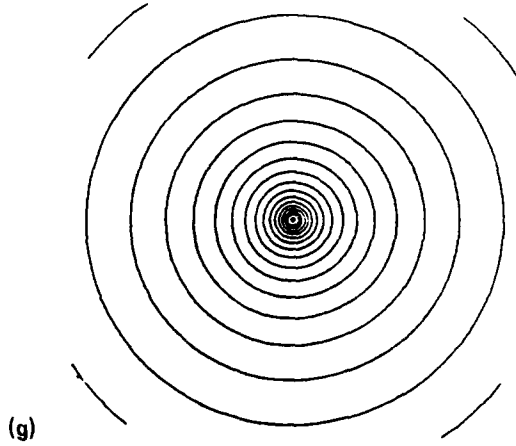


Fig. 8 — continued.

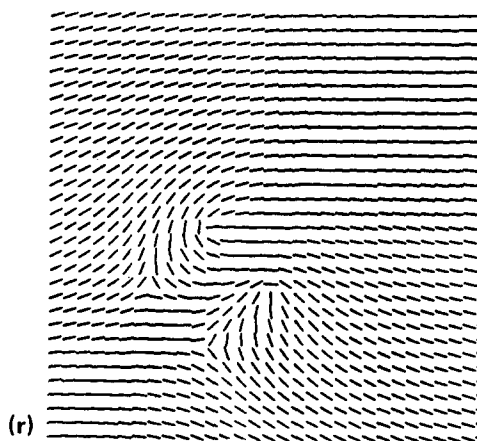
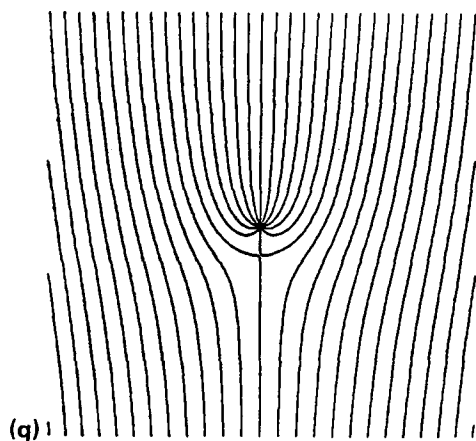
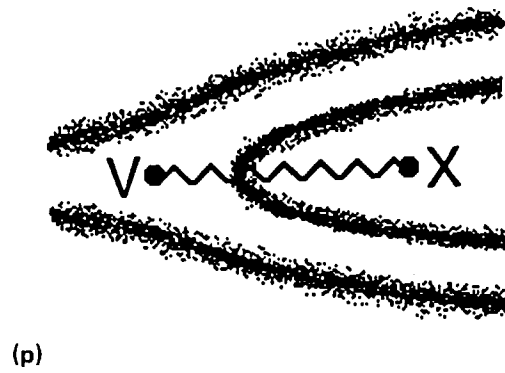
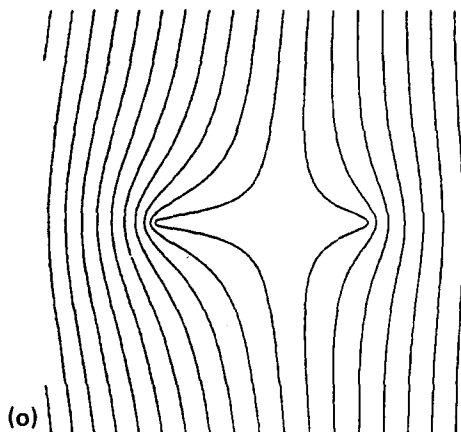
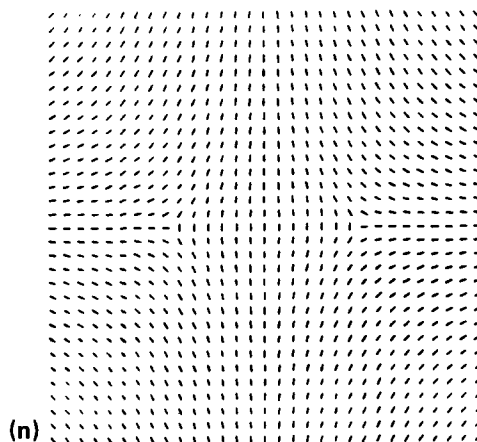
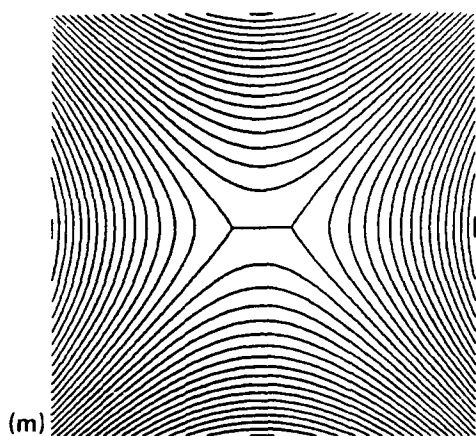


Fig. 8—continued.

Symbol	Name	Representation	Twist ( $T$ ) and Circulation ( $\Gamma$ )
$X$ (Fig. 8a)	Convex disclination	$w = (z - a)^{-1/2}$	$T = \pi$
$V$ (Fig. 8c)	Concave disclination	$w = (z - a)^{1/2}$	$T = -\pi$
$XX$ (Fig. 8i)	target	$w = (z^2 - a^2)^{-1/2}$	$T = 2\pi, \Gamma = 0$
(Fig. 8j)	vortex	$w = i(z^2 - a^2)^{-1/2}$	$T = 2\pi, \Gamma = -2\pi$
	spiral	$w = (\alpha + i)(z^2 - a^2)^{-1/2}$	$T = 2\pi, \Gamma = -2\pi$
$VV$ (Fig. 8m)		$w = i(z^2 - a^2)^{1/2}$	$T = -2\pi, \Gamma = -\pi Rl a^2$
$XV$ (Fig. 8o)	Handle	$w = \left(\frac{z-a}{z+a}\right)^{1/2}$	$T = 0, \Gamma = -2\pi \text{Im } a$
$\begin{pmatrix} XX \\ VV \end{pmatrix}$ (Fig. 8q)	Dislocation	$w = k_0 \sqrt{\frac{(z+a^*)(z-a)}{(z+b^*)(z-b)}}$ $a = \frac{-ie}{k_0} + \mu, b = \mu$	$T = 0, \Gamma = -2\pi$
$\begin{pmatrix} X \\ V \ V \\ X \end{pmatrix}$ (Fig. 8r)	Bridge	$w = (z^2 - a^2)^{1/2} (z^2 + b^2)^{-1/2}$ $a, b$ real	$T = 0, \Gamma = 0$

Table 2  
A list of the harmonic representations.

(1) Target:

$$\hat{\theta} = c \int^k \frac{dk}{kB}, \tag{4.24}$$

$$r = \sqrt{X^2 + Y^2} = c/kB, \tag{4.25}$$

$$\alpha = \tan^{-1} Y/X = \varphi, \tag{4.26}$$

$$\theta = \frac{c}{B} - c \int^k \frac{dk}{kB}. \tag{4.27}$$

From (4.26), we see that  $\varphi$  is determined uniquely as function of  $\alpha$ . In particular,  $T = 2\pi$ . The more interesting map is between  $r$  and  $k$  which, for  $c$  negative, is drawn in Fig. 9. Observe that in order to obtain a solution which covers all the regions in the  $(X, Y)$  plane down to the target core  $r = 0(\epsilon)$  and for which the wavenumber  $k$  is the stable band  $(k_B, k_E)$ , we must choose  $c = -\epsilon c_0$ . That choice pushes the relevant branch  $AD$  close to  $k_B$  almost everywhere. In the core region  $r = 0(\epsilon)$ ,  $k$  increases to  $k_E$  but the amplitude regularization will already have come into play at that stage. This argument is very similar to the one used by Pomeau and Manneville [27] to show how circular roll patterns select the wavenumber  $k_B$ . Write (4.25) as

$$kB = \frac{c}{r} \tag{4.28}$$

and it is clear that in order to keep  $kB$  finite for  $r$  of order  $\epsilon$ , the constant  $c$  must be of order  $\epsilon$ . Then, in the far field, where  $r$  is order one,  $B(k)$  is of order  $\epsilon$ , meaning that  $k = k_B + 0(\epsilon)$ . In our discussion here, we draw one extra conclusion, namely that  $c$  must be negative so that  $k$  approaches  $k_B$  from above. For target patterns, the circulation  $\Gamma$  is zero. We also note from (4.6) that

$$|J| = -\frac{k}{r^2} \frac{kB}{(kB)'} \tag{4.29}$$

from which we see why, unless  $c_0$  is identically zero, which can be arranged but is not typical for circular patches in natural patterns, it is very important to have regularization in the core region. The amplitude regularizations for target patterns is discussed by Pomeau and Manneville [28] and by Newell, Passot and Souli [12].

(2) Convex Disclination.

The convex disclination is captured by another exact solution of (4.12),

$$\hat{\theta} = \left( ck \int^k \frac{dk}{k^3 B} \right) \cos \varphi, \tag{4.30}$$

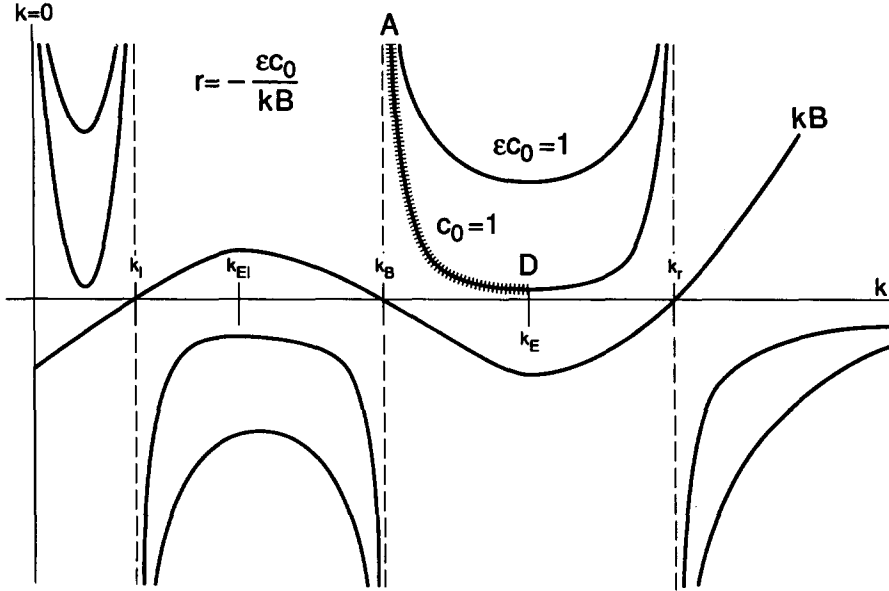


Fig. 9. The graph of  $r$  versus  $kB$  for the target pattern. Note that the only acceptable solution is the branch  $AD$ . The value of  $r$  at  $D$  is less than  $\epsilon$ , the core size.

from which we find

$$X = r \cos \alpha = c \int \frac{dk}{k^3 B} + \frac{c}{k^2 B} \cos^2 \varphi, \quad (4.31)$$

$$Y = r \sin \alpha = \frac{c}{k^2 B} \sin \varphi \cos \varphi, \quad (4.32)$$

and

$$\theta = \frac{c}{kB} \cos \varphi. \quad (4.33)$$

Note that if  $B = 1$ ,  $\hat{\theta}$  is exactly given by (4.19) with  $n = -1$ . In order that this solution covers all but a core region of diameter  $\epsilon$ ,  $c$  must be of order  $\epsilon$ . We write  $c = -\epsilon c_0$ . Therefore  $k = k_B + O(\epsilon)$  almost everywhere. The isophase contours are drawn in Fig. 8b (see also Figs. 2e and 10) and take the form of a Roman Arch. In Fig. 2d we show Roman Arches in a ferrofluid pattern and in Fig. 2e reproduce a Roman Arch observed in a numerical experiment involving two copropagating optical beams. This shape can be solved for explicitly by inverting (4.31), (4.32) (choosing the  $k$  branch that lies in  $(k_B, k_E)$ ) and drawing  $\theta = \theta_0$  for several values of  $\theta_0$ . The shape can also be heuristically argued as follows.

For  $\cos \varphi$  of order one, namely for  $|\varphi|$  strictly less than  $\frac{\pi}{2}$ , the dominant term in (4.31) is the second and, from (4.31), (4.32),

$$r = -\frac{\epsilon c_0}{kB} \cos \varphi, \quad \alpha = \varphi, \quad (4.34)$$

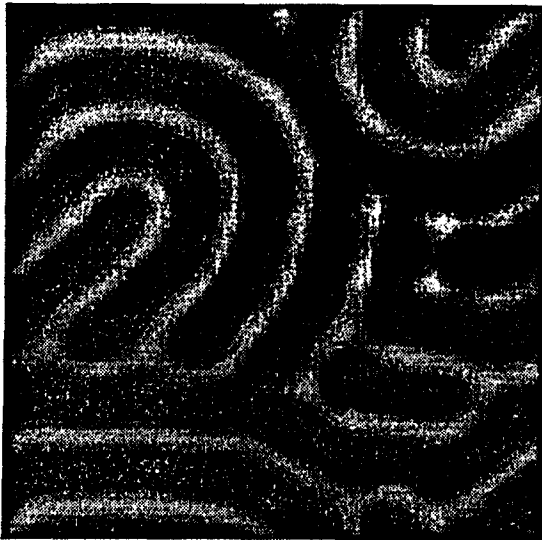
and the constant  $\theta$  contours are semicircles. For  $\varphi \simeq \frac{\pi}{2}$ , however, or  $\cos \varphi = O(k - k_B)$ , it is the logarithm terms in (4.31) which dominates and

$$k - k_B = \exp \frac{k_B^3 |B'(k_B)|}{\epsilon c_0} X, \quad (4.35)$$

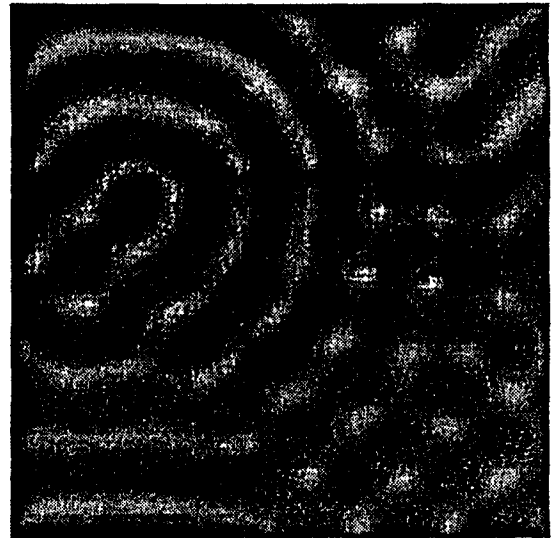
namely  $k$  approaches  $k_B$  exponentially fast as  $X$  tends to negative infinity. For  $X < 0$ , the constant phase contours are straight lines. There is no discontinuity in any derivative between the semi circular and straight regions. The twist  $T$  of a convex disclination is  $\pi$ . Circulation is not defined.

The choice of the sign of  $c$  (or  $c_0$ ) gives the direction of the Roman arch. For  $c > 0$  or  $c_0 < 0$ , the semicircular component occurs for  $X < 0$ ,  $\frac{\pi}{2} < \varphi < \frac{3\pi}{2}$  and the straight component occurs for  $X > 0$ .

(3) *Vortices and spirals.*



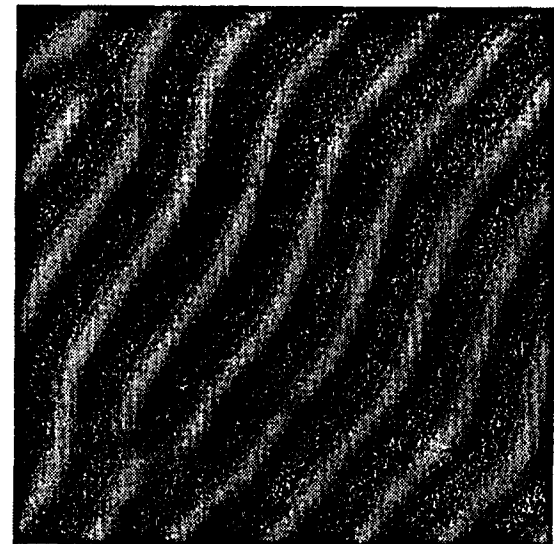
(a)



(b)



(c)



(d)

Fig. 10. A sequence of snapshots showing the instability of the convex disclination (Roman Arch) as the stress parameter is taken close to its onset value. These patterns occurred in a pattern formed by copropagating optical beams [37].

The exact solution

$$\hat{\theta} = -\epsilon c_0 \int \frac{dk}{kB} + \epsilon c_1 \varphi \tag{4.36}$$

leads to targets ( $c_1 = 0$ ), vortices ( $c_0 = 0, c_1 = 1$ ) and spirals ( $c_0, c_1$  non zero). From (4.10), (4.11),

$$r = \epsilon \sqrt{\frac{c_0^2}{(kB)^2} + \frac{c_1^2}{k^2}}, \tag{4.37}$$

$$\alpha = \varphi + \beta(r), \tag{4.38}$$

where  $\cos \beta(r) = -\epsilon c_0/kBr, \sin \beta(r) = \epsilon c_1/kr$ . They have twist  $2\pi$ . The pure vortex ( $c_0 = 0$ ) has a circulation of  $-2\pi$  whereas the spiral, like the target pattern, has zero circulation. The pure vortex can be regularized by the correction terms at its core but not in its far field. In certain cases, for example, the complex Ginzburg-Landau equation,  $k_B$  is zero and then the regularized vortex is a stable object. When  $k_B > 0$ , however, the far field can only be “regularized” by introducing another nearby singularity, a saddle. As we have remarked after (4.23), the juxtaposition of a vortex and a saddle gives a dislocation (see also Fig. 13).

(4) *Concave Disclination.*

The solution

$$\hat{\theta} = F(k) \cos 3\varphi \tag{4.39}$$

leads to the concave disclination. In this case,  $F(k)$  cannot be expressed in terms of elementary functions but it is readily calculated. As before, however, on the branch which is energetically relevant,  $k \simeq k_B$  and then we can approximate  $F(k)$  by  $\epsilon c_0 \ell n|k - k_B|$ . We obtain

$$X = r \cos \alpha = \frac{\epsilon c_0}{k - k_B} \cos 3\varphi \cos \varphi + \frac{3\epsilon c_0 \ell n|k - k_B|}{k_B} \sin 3\varphi \sin \varphi, \tag{4.40}$$

$$Y = r \sin \alpha = \frac{\epsilon c_0}{k - k_B} \cos 3\varphi \cos \varphi - \frac{3\epsilon c_0 \ell n|k - k_B|}{k_B} \sin 3\varphi \cos \varphi. \tag{4.41}$$

Almost everywhere on the constant  $\Theta$  contours,

$$\cos 3\varphi = 0(k - k_B), \tag{4.42}$$

so that the logarithm terms dominates in (4.40), (4.41) in the sectors  $-\frac{\pi}{3} < \alpha - \frac{2n\pi}{3} < \frac{\pi}{3}, n = 0, 1, 2$ . In each of these sectors respectively,  $\varphi = \frac{\pi}{2}, \frac{\pi}{6}$  and  $-\frac{\pi}{6}$ , and  $k$  approaches  $k_B$  exponentially fast from below as  $X^2 + Y^2 \rightarrow \infty$ ,

$$k_B - k = \exp \frac{k_B}{3\epsilon c_0} (\sin 3\varphi)^{-1} \times (X \sin \varphi - Y \cos \varphi). \tag{4.43}$$

For example, in the first section,  $\varphi \simeq \pm \frac{\pi}{2}$  and  $k_B - k = \exp[-(k_B/3\epsilon c_0)X]$ . The transition between roll directions is made in a region close to the rays  $\alpha = \frac{\pi}{3}, \pi$  and  $\frac{5\pi}{3}$ . Along these rays, the  $\sin 3\varphi$  term vanishes,  $\cos 3\varphi$  becomes of order one and the first terms in (4.40), (4.41) dominate. In Figs. 8f and 8e we draw the constant phase contours both in  $k$  space and in  $X$  space. Several key features should be noted.

- (1) The dashed lines in Fig. 8f correspond to folds, namely a locus of singularities of the matrix  $J$  ( $|J| = \infty$ ) of rank one.
- (2) In wavevector space, the constant phase contour  $\Theta = \text{constant}$ ,  $fedcba$  stays close to  $k = k_B, \varphi = \frac{\pi}{2}$ , ( $f$ ) until it crosses the fold close to  $e$ . At this point (a cusp in  $X$ -space; see Fig. 8e), the solution transfers onto the branch on which  $\varphi$  makes a transition from  $\frac{\pi}{2}$  to  $\frac{\pi}{6}$ . When this locus crosses the fold close to  $b$ , it transfers again onto a branch  $ba$  where  $\varphi$  is almost constant ( $\frac{\pi}{6}$ ). Again, the transition in  $X$ -space occurs at a cusp.
- (3) Note that as  $\alpha$  goes from zero to  $2\pi$  around the singularity at  $r = 0, \varphi$  winds clockwise through the angle  $-\pi$ . The twist  $T$  of a concave disclination is  $-\pi$ .
- (4) The singularity at  $r = 0$  and the points marked  $U$  on Fig. 8f are umbilics.
- (5) Generically, umbilics, being the interaction of folds, are isolated singularities.
- (6) The number of solutions at any point  $(X, Y)$  is eight.

- (7) The presence of a concave disclination acts to select the far field wavenumber to be exponentially (not just  $k_B + 0(\epsilon)$  but  $k_B + 0(\exp(-1/\epsilon))$ ) close to  $k_B$ !

The new feature in the concave disclination is the regularization of the transition regions along the rays  $\alpha = \pi/3, \pi$  and  $5\pi/3$ . As one goes from the sector  $-\pi/3 < \alpha < \pi/3$  to the sector  $\pi/3 < \alpha < \pi$ , the phase remains continuous but the roll direction changes by  $\pi/3$ . The multivalued solution is regularized in an order  $\sqrt{\epsilon}$  boundary layer obtained by a balance between  $\nabla \cdot \mathbf{k}B(k)$ , which is small because  $k \simeq k_B$ , and the phase regularization  $\epsilon^2 (|B'(k_B)|/4k_B) \nabla^2 \nabla \cdot \mathbf{k}$ , namely is a solution of (4.8). Since  $k$  is below  $k_B$ ,  $\nabla \cdot \mathbf{k}B$  is hyperbolic and can support shocks. The shock relations, derived in the next Section 4.3, are that the constant phase contours on opposite sides of the shockline meet the shock line, here  $dX/dY = \tan \pi/6$ , at the same angle, exactly what we see in the concave disclination. Because the equation (4.2) and the regularization is in flux divergence (conservation) form, the shock conditions (the Rankine-Hugoniot conditions) are independent of the exact form of regularization. Therefore the concave disclination is a singularity which is associated with wavenumbers  $k$  below  $k_B$ , and the potential instability (the zig-zag) is regularized (saturated) by the presence of the next correction in the phase diffusion equation. In Section 4.4, we work out the exact solution of (4.8) in the case where the change in roll direction is small.

In principle, one should also be able to have convex disclinations analogous to concave disclinations in which the semicircular cap in Fig. 8b is replaced by a rectangular cap with shocks along the direction  $\alpha = \pm\pi/4$  joining phase contours with wavevector angles  $\varphi = \pi/2$  to phase contours with wavevector angle  $\varphi = 0$ . For these solutions  $k$  will approach  $k_B$  from above. They will, however, have a higher free energy than the Roman arch but may be important near lateral boundaries.

We have frequently said that concave and convex disclinations cannot be present in pat-

terns which can be described by a complex order parameter. Therefore as  $R$  decreases to  $R_c$ , there comes a point  $R_d(\epsilon)$ , depending on  $\epsilon$ , at which disclinations must destabilize because near onset, where both amplitude and phase are active order parameters, the wavevector field is uniquely defined. In Figs. 10 and 11, we show numerical simulations of the instabilities of both the Roman Arch (as occurred in a problem of counterpropagating optical beams) and the concave disclination (as it arises in a simulation of the SH equation in a cylinder). The former ends up in a state of almost parallel straight rolls. The latter ends up as a pattern with two distinct phases separated by an amplitude grain boundary.

#### (5) Saddle.

The saddle is the merger of two concave disclinations and is given by

$$\hat{\theta}(f, g) = F(k) \sin 2\varphi, \quad (4.44)$$

where again, on the energetically relevant branch,  $F(k)$  can be approximated by  $\epsilon c_0 \ell n(k - k_B)$ . The constant phase contours are shown in Figs. 8l. The twist  $T = -2\pi$ . The circulation is zero. The shocks (phase grain boundaries) occur along the rays  $\alpha = \frac{\pi}{4}, \frac{3\pi}{4}, \frac{5\pi}{4}, \frac{7\pi}{4}$ . Saddles, being the direct superposition of two concave disclinations or umbilics, are non generic. They are exact solutions but, unless there are external influences to make the coincidence of concave disclinations energetically favored, a perturbation to the system will cause them to separate. Fig. 12a shows a saddle computed as an exact solution of the Swift-Hohenberg equation in a circle. Fig. 12b shows how the saddle separates when noise is added to the exact solution and the perturbed pattern is allowed to evolve further in time. The saddle separates along one of its shocks to create two concave disclinations. The direction of separation keeps the total circulation zero. This is consistent with the separated harmonic saddle of Fig. 8m. Note the circula-

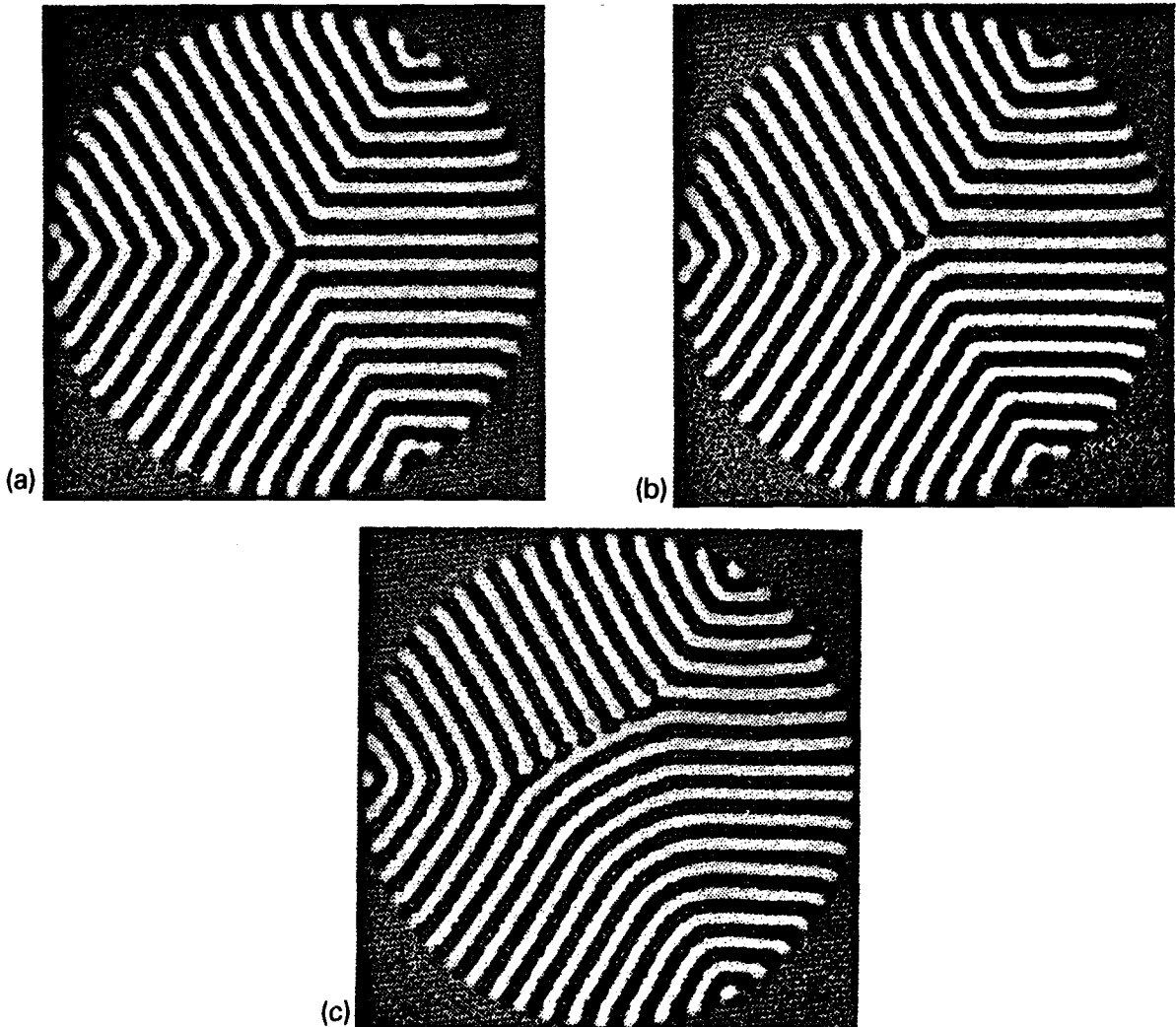


Fig. 11. Three snapshots of a concave disclination. (a) Stable concave disclination at a finite value of  $R$ . (b) Its destabilization as  $R$  is taken below some critical value  $R_d$ . The dependence of  $R_d$  on  $\epsilon$  has yet to be determined. (c) The eventual formation of an amplitude grain boundary.

tion of the separated pairs is zero if  $Rl a^2 = 0$  or  $a = |a|e^{\pm i\pi/4}$ .

Energetically acceptable solutions corresponding to collections of isolated disclinations in close proximity will be discussed in another paper. They involve a complicated superposition of angle harmonics  $\Sigma(F_n(k) \cos n\varphi + G_n(k) \sin n\varphi)$  but as yet we have no simple superposition rule. The advantage of the harmonic representation for composites is that these solutions are constructed simply by multiplication

of the individual solutions. It is therefore easier to understand the morphology of defects. Three interesting composites, one familiar, two new, are the dislocation, the handle and the bridge. Dislocations correspond to a vortex bound with a saddle, the singularities being separated by distances of the order of a wavelength or  $k_B^{-1}$ . In Section 4.4, we give an exact solution for the stationary dislocation of the stationary regularized phase diffusion equation (4.8). Although this solution does not contain all the informa-

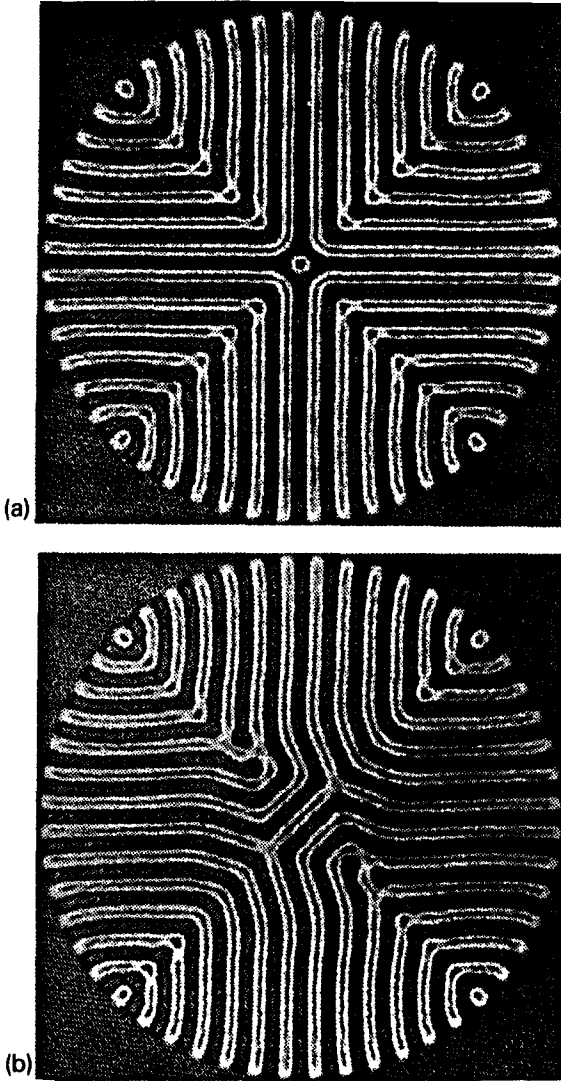


Fig. 12. (a) saddle, an exact and apparently stable solution to the SH equation in a cylinder. (b) with a finite amount of noise added, the saddle naturally splits into two concave disclinations revealing the nongeneric character of that structure.

tion about the core, it does clearly illustrate that there are four singular regions, two where  $k$  becomes larger than  $k_E$  and two where  $k$  becomes smaller than  $k_{E_1}$ . Around each of the former  $T = \pi$ . Around each of the latter  $T = -\pi$ . Handles are pairs of nearby concave and convex disclinations. They have a total twist of zero and therefore can appear out of the vacuum

state when it is energetically favorable for them to do so. There are two types. Type I consists of a loop in the constant phase contours shown in Fig. 8a, around which pair the circulation is zero. They often arise at larger values of the stress parameter when the zig-zag instability is not saturated by the zig-zag Chevron pattern. Type II (Fig. 8b) handles which look like dislocations, but do not have a far field consisting of straight parallel rolls, have finite circulation. They arise in the formation of bridges after the instability of dislocations. As the saddle under the dislocation separates horizontally ( $a$  in Table 1 is real), there is a finite circulation  $-\pi a^2$  created. This can be offset by the creation of a handle with zero twist and opposite circulation. This process has been discussed in Section 3.

Bridges are essentially two pairs of handles arranged so that both the total twist and the total circulation is zero. We have already met them in Section 3 (Fig. 5).

### 4.3. Characteristics, Riemann invariants and shocks

We write (4.1), (4.2) in matrix form as

$$A_1 F_X + A_2 F_Y = 0, \tag{4.45}$$

with

$$F = (f, g)^T, \quad A_1 = \begin{pmatrix} 0 & -1 \\ B + 2f^2 B' & 2fgB' \end{pmatrix},$$

$$A_2 = \begin{pmatrix} 1 & 0 \\ 2fgB' & B + 2g^2 B' \end{pmatrix}, \tag{4.46}$$

where  $B' = dB/dk^2$ . Next, write  $A_1^{-1}A_2$  in Jordan form

$$A_1^{-1}A_2 = PAP^{-1}, \tag{4.47}$$

with

$$A = \begin{pmatrix} \lambda_+ & a \\ 0 & \lambda_- \end{pmatrix},$$

$$P = \begin{pmatrix} \lambda_+ & a + \lambda_- \\ -1 & -1 \end{pmatrix}, \tag{4.48}$$

so that (4.45) becomes

$$P^{-1}F_X + AP^{-1}F_Y = 0. \tag{4.49}$$

If  $\lambda_+ = \lambda_-$ ,  $a = 1$ . If  $\lambda_+ \neq \lambda_-$ ,  $a = 0$ . The diagonal components of  $A$  are

$$\lambda_{\pm} = \frac{2fgB' \pm \sqrt{-B \left( \frac{d}{dk} kB \right)}}{B + 2f^2B'}, \tag{4.50}$$

which, after replacing  $f$  and  $g$  by  $k \cos \varphi$  and  $k \sin \varphi$ , becomes

$$\lambda_{\pm} = \frac{\pm \sqrt{-s(kB)_k} \sin \varphi - \sqrt{sB} \cos \varphi}{\sqrt{sB} \sin \varphi \pm \sqrt{-s(kB)_k} \cos \varphi}, \tag{4.51}$$

where we take  $s = 1$  in the hyperbolic region  $k_{E_l} < k < k_B$  where  $B > 0$ ,  $(kB)_k < 0$  and  $s = -1$  in the hyperbolic region  $k_E < k < k_r$  where  $B < 0$ ,  $(kB)_k > 0$ . It is the former region in which we are most interested. Unless  $B(kB)_k = 0$ , i.e. at  $k = k_{E_l}, k_B, k_E$ ,  $\lambda_+ \neq \lambda_-$  and  $a = 0$ . We now take  $k_{E_l} < k < k_B$ . Then introducing the characteristic coordinates  $u(X, Y), v(X, Y)$  by

$$\begin{aligned} \frac{dY}{dX} &= -\frac{u_X}{u_Y} = \lambda_+, \\ \frac{dY}{dX} &= -\frac{v_X}{v_Y} = \lambda_-, \end{aligned} \tag{4.52}$$

we obtain

$$\begin{aligned} \frac{\partial f}{\partial u} + \lambda_+ \frac{\partial g}{\partial u} &= 0, \\ \frac{\partial f}{\partial v} + \lambda_- \frac{\partial g}{\partial v} &= 0, \end{aligned} \tag{4.53}$$

which, in polar coordinates and after a little analysis, become

$$\frac{\partial}{\partial u} \left( -\int_k^{k_B} \frac{\cot \rho(k)}{k} dk - \varphi \right) = 0, \tag{4.54}$$

$$\frac{\partial}{\partial v} \left( -\int_k^{k_B} \frac{\cot \rho(k)}{k} dk + \varphi \right) = 0, \tag{4.55}$$

where

$$\tan \rho(k) = \frac{\sqrt{B}}{\sqrt{-(kB)_k}}. \tag{4.56}$$

The Riemann invariants of the Cross–Newell equation are:

$$R_{\pm} = \varphi \mp \int_k^{k_B} \frac{\cot \rho(k)}{k} dk. \tag{4.57}$$

$R_{\pm}$  are constant along the characteristic curves

$$\frac{dY}{dX} = \lambda_{\pm} = \tan(\varphi \mp \rho(k)), \tag{4.58}$$

respectively. Defining  $\lambda_{\pm} = \tan \chi_{\pm}$ ,  $R_{\pm}$  are constant along the directions  $\varphi \mp \rho(k)$  respectively. We also point out that if the Cross–Newell equation is not in flux divergence form, these results still hold with

$$\tan \rho(k) = \frac{\sqrt{-D_{\perp}}}{\sqrt{D_{\parallel}}}. \tag{4.59}$$

Observe that near the left Eckhaus boundary  $k_{E_l}$ ,  $\rho(k) \rightarrow \pi/2$  and the characteristic directions are almost parallel to the isophase contours. Near  $k_B$ ,  $\rho(k) \rightarrow 0$  and the characteristics become parallel to the wavevector direction. In all cases, the wavevector bisects the characteristics. In the vicinity of  $k_B$ , we can approximate  $D_{\perp}$  by  $-D'_{\perp}(k_B^2 - k^2)$  where  $D'_{\perp}$  is  $dD_{\perp}/dk^2$  estimated at  $k_B$ . Then from (4.56),

$$\tan \rho(k) \simeq \frac{1}{\sqrt{2r}} \frac{(k_B^2 - k^2)^{1/2}}{k_B}, \tag{4.60}$$

where  $r$ , the residue of  $\frac{D_{\perp}}{kD'_{\perp}}$  at  $k = k_B$ , is equal to unity if  $B(k)$  is analytic at  $k_B$ . In the same approximation

$$\int_k^{k_B} \frac{\cot \rho(k)}{k} dk \simeq \sqrt{\frac{r}{2}} \frac{(k_B^2 - k^2)^{1/2}}{k_B}. \tag{4.61}$$

Therefore we have that

$$\varphi \mp r \frac{1}{\sqrt{2r}} \frac{(k_B^2 - k^2)^{1/2}}{k_B} \tag{4.62}$$

are constant along the directions

$$\frac{dY}{dX} = \varphi \mp \frac{1}{\sqrt{2r}} \frac{(k_B^2 - k^2)^{1/2}}{k_B}, \tag{4.63}$$

respectively. If we identify  $\varphi$  with the horizontal fluid velocity  $U$ ,  $(1/\sqrt{2r})(k_B^2 - k^2)^{1/2}/k_B$  with  $C$  the sound speed and call  $r = 2/\gamma - 1$ , (4.62), (4.63) are exactly the equations of one dimensional compressible gas dynamics. In the case where  $B(k)$  is analytic at  $k_B$  and  $r = 1, \gamma = 2$  and they are also isomorphic to the shallow water equations.

In general, such systems will form multivalued solutions and indeed we have already demonstrated the multibranch behavior of the map  $X \rightarrow k$ . When the Cross–Newell equation is regularized, however, as in (4.8), we expect that the multivalued solutions can be replaced by single valued solutions with discontinuities along certain lines called shocks

$$\frac{dX}{dY} = s = \cot \psi, \tag{4.64}$$

in the  $X, Y$  plane. Because (4.8) is in flux divergence form, in the small  $\epsilon$  limit the Rankine–Hugoniot (jump) conditions are independent of the exact form of the regularization term, provided that it too is in conservation form, as indeed it is. The reason is straightforward. Write (4.3) as

$$\partial_X(fB + \epsilon^2 F) + \partial_Y(gB + \epsilon^2 G) = 0, \tag{4.65}$$

with  $(F, G) = (|B'(k_B)|/4k_B)\nabla\nabla \cdot \mathbf{k}$ . Then seeking “travelling wave” solutions which depend only on  $Z = X - sY$ , we find on integrating across the value  $Z = 0$  at which a large transition in the values of  $f, g$  occurs,

$$[fB + \epsilon^2 F] - s[gB + \epsilon^2 G] = 0, \tag{4.66}$$

where  $[h]$  represents the difference between the asymptotic values of  $h$  on one side of  $Z = 0$  and the other. Then, as long  $F, G$  asymptote to zero on either side of  $Z = 0$ , the “shock” conditions can be determined by taking the  $\epsilon = 0$  limit. If (4.8) is not in flux divergence form, as is the

case when  $r \neq 1$ , one does not have the freedom to integrate once and prove that the jump condition produced by the smooth solution of (4.8) with  $\epsilon$  finite will give rise to a jump condition independent of the exact form of regularization in the  $\epsilon \rightarrow 0$  limit. For (4.1), (4.2), the jump conditions are

$$s[f] + [g] = 0, \tag{4.67}$$

$$[fB] - s[gB] = 0. \tag{4.68}$$

We examine several cases.

- (1) *The wavenumber  $k$  is continuous across the shock.* Since  $k$ , and therefore  $B$  is continuous, (4.67) and (4.68) together imply that  $[f] = [g] = 0$  or that  $B(k) = 0$ . Therefore,  $k = k_B$  on each side. As a direct corollary, we can argue that if  $k < k_B$  on one side of the shock, then it cannot be continuous across the shock. We consider Figs. 8d,e. Take the pattern wavenumber on the negative side to be  $k_B(0, 1)$ , and the angle that the shock makes with the  $X$  axis to be  $\psi$ . Then  $s = \cot \psi$ . If  $k$  is continuous, then that condition and (4.67) gives

$$\begin{aligned} f_+^2 + g_+^2 &= k_B^2, \\ sf_+ + g_+ &= k_B, \end{aligned} \tag{4.69}$$

so that

$$f_+ \left( (1 + s^2)f_+ - 2sk_B \right) = 0. \tag{4.70}$$

If  $f_+ = 0$ , then  $g_+ = k_B$  and there is no discontinuity. Therefore, at a shock we must have that

$$\begin{aligned} f_+ &= \frac{2s}{1 + s^2} k_B = k_B \sin 2\psi, \\ g_+ &= \frac{1 - s^2}{1 + s^2} k_B = -k_B \cos 2\psi. \end{aligned} \tag{4.71}$$

Therefore the constant phase contours make equal angles with the shock line as shown in Fig. 6b. In particular we note as special case the limit  $\psi = 0$  for which the wavevector  $\mathbf{k}$  reverses direction across the shock. We also

note that the shock angle is simply the average of the angles of the level phase curves on either side of the shock. Since this angle  $\varphi$  is analogous to  $U$ , the condition is equivalent to the shock speed being the average of flow speeds front and back as is. These shock conditions are precisely what is seen along the phase grain boundaries emanating from concave disclinations and saddles.

- (2)  $k_- = k_B, k_+ < k_B$ . In that case, from (4.68), we have that  $f_+ - sg_+ = 0$  because  $B_+ \neq 0$ . Then,  $sf_+ + g_+ - k_B = 0$  and therefore

$$\begin{aligned} f_+ &= \frac{sk_B}{1+s^2} = k_+ \cos \psi, \\ g_+ &= \frac{k_B}{1+s^2} = k_+ \cos \psi, \end{aligned} \tag{4.72}$$

where  $k_+ = k_B \sin \psi$ . In this case, the rule is that the phase contours as the side where  $k < k_B$  are perpendicular to the shock line. Note that as  $\psi \rightarrow 0$ , the wavelength on the plus side increases to infinity so that  $k_+ \rightarrow 0$ . In that case, the plus side of the shock is open to a new instability of the zero state and will generally give rise to a roll planform with another phase. Observe in neither of these cases is there any restrictions on  $\psi$  the shock angle.

- (3) *General case*  $k_- = (0, k_-)$ . In this case, the two equations (4.67), (4.68),

$$sf_+ + g_+ - k_- = 0, \tag{4.73}$$

$$B_+(f_+ - sg_+) = B_-(f_- - sg_-), \tag{4.74}$$

give two relations between,  $f_+, g_+, s$  and  $f_- = 0, g_- = k_-$ . We will choose to write  $f_+, g_+$  in terms of  $s, k_-$ .

$$f_+ = \frac{sk_-}{1+s^2} \left(1 - \frac{B_-}{B_+}\right), \tag{4.75}$$

$$g_+ = \frac{k_-}{1+s^2} \left(1 + \frac{s^2 B_-}{B_+}\right), \tag{4.76}$$

where  $k_+$  and  $B_+$  is a solution of the nonlinear equation

$$k_+^2 = \frac{k_-^2}{1+s^2} \left(1 + s^2 \frac{B_-^2}{B_+^2}\right). \tag{4.77}$$

Note if  $B_-/B_+ \ll 1, k_- \rightarrow k_B$  and we recover case 2.

#### 4.4. Weak shocks and stationary dislocations

We now examine a special class of solutions of the regularized phase diffusion equation

$$\begin{aligned} \tau(k)\Theta_T - kD_\perp(k)\nabla \cdot \hat{k} - D_\parallel(k)(\hat{k} \cdot \nabla)k \\ + \epsilon^2 \nu \nabla^4 \Theta = 0, \end{aligned} \tag{4.78}$$

in the case when  $k \simeq k_B, \nu = \frac{D_\parallel(k_B)}{4k_B^2}$  and the far field is almost a field of straight parallel rolls. Let

$$\begin{aligned} \Theta(X, Y, T) = k_B X \\ + \epsilon \Psi \left( \xi = \frac{1}{k_B} X, \eta = \frac{1}{\sqrt{\epsilon}} Y, s = \frac{D_\parallel(k_B)}{4k_B^2} T \right) \end{aligned} \tag{4.79}$$

and find

$$\begin{aligned} \Psi_s - 4\Psi_{\xi\xi} - 4\Psi_\xi\Psi_{\eta\eta} - 8\Psi_\eta\Psi_{\xi\eta} - 6\Psi_\eta^2\Psi_{\eta\eta} + \Psi_{\eta\eta\eta\eta} \\ - 4\frac{1-r}{r} \left( \Psi_\xi + \frac{1}{2}\Psi_\eta^2 \right) \Psi_{\eta\eta} = 0, \end{aligned} \tag{4.80}$$

$$= -\frac{\delta\bar{F}}{\delta\Psi} - 4\frac{1-r}{r} \left( \Psi_\xi + \frac{1}{2}\Psi_\eta^2 \right) \Psi_{\eta\eta}, \tag{4.81}$$

where

$$\bar{F} = \int \left( 2 \left( \Psi_\xi + \frac{1}{2}\Psi_\eta^2 \right)^2 + \frac{1}{2}\Psi_\eta^2 \right) d\xi d\eta. \tag{4.82}$$

We now have in a very explicit form what we have said before. The two cases  $r = 1$  and  $r \neq 1$  are different in a substantial way. For  $r = 1$ , (4.80) is relaxational; for  $r \neq 1$ , it is not! We also point out that when  $r = 1$  it is simply the Newell–Whitehead–Segel equation from which the amplitude has been eliminated by assuming it slaved to the phase gradient. In this context, and in the small amplitude limit, Pomeau [29] has also obtained the first of the two solutions which follow.

There are two solutions of particular interest. The first corresponds to a weak shock, a phase grain boundary which occurs when the wavevector discontinuity is small. Let

$$\Psi = -\kappa\xi + G(\eta) \tag{4.83}$$

and find

$$\alpha G_{\eta\eta} - 6\beta G_{\eta}^2 G_{\eta\eta} + G_{\eta\eta\eta\eta} = 0, \tag{4.84}$$

with

$$\alpha = 4\kappa \left(1 + \frac{1-r}{r}\right), \quad \beta = 1 + \frac{1-r}{3r}. \tag{4.85}$$

Now  $f = \frac{\partial\theta}{\partial X} = k_B - \epsilon\kappa/k_B$  and  $g = \sqrt{\epsilon}G_{\eta}$  so that  $g(\eta)$  satisfies

$$\alpha g - \beta/\epsilon g^3 + g_{\eta\eta} = \gamma, \tag{4.86}$$

where  $\gamma$  is the integration constant. We seek solutions where  $g(\eta)$  approaches constant values as  $\eta \rightarrow \pm\infty$ . Note  $\kappa$  must be positive. Thus in the far field of the grain boundary,  $k$  approaches  $k_B$  from below. If we demand reflection symmetry of the phase pattern about the  $y = 0$  axis, a natural assumption since there should be no preferred side, then  $\gamma = 0$  and

$$\begin{aligned} g(\eta) &= \sqrt{\frac{\epsilon}{2\beta}} \tanh \sqrt{\frac{\alpha}{2}} \eta \\ &= \sqrt{\frac{\alpha\epsilon}{2\beta}} \tanh \sqrt{\frac{\alpha}{2\epsilon}} Y, \end{aligned} \tag{4.87}$$

so that  $k_{\infty}^2 = f^2 + g_{\infty}^2 = k_B^2 + \frac{4}{3}\kappa\epsilon(r-1)/r + 0(\epsilon^2)$ . The far field wavenumber is an order  $\epsilon$  distance away from  $k_B$  unless  $r = 1$ . Furthermore for  $r < 1$ , it would lie in the zig-zag unstable region which is unacceptable because the regularizing contribution in zero in the far field and cannot come into play to balance the nonzero value of  $\nabla \cdot \mathbf{k}B(k)$ . On the other hand, if we choose  $\gamma$  so that  $g(-\infty) = -\sqrt{2\kappa\epsilon}$  whence  $f^2(-\infty) + g^2(-\infty) = k_B^2 + 0(\epsilon^2)$ , then  $g(+\infty) = \sqrt{2\kappa\epsilon}(1 + 0(r-1))$  and wavenumbers on opposite sides of the shock are unequal. Indeed there is no shock solution to link patterns with wavenumbers  $k_B$  on either side of the shock

unless  $r = 1$ . When  $r = 1$ , the constant phase contours do indeed meet the shock at equal angles. In this case,  $\frac{1}{2\epsilon}g_{\eta}^2 = 2(g^2/2\epsilon - \kappa)^2$ , the solution (4.87) is linearly stable and

$$\bar{F} = \frac{1}{\epsilon} \int g_{\eta}^2 d\xi d\eta = 4/3(2\kappa)^{3/2}L, \tag{4.88}$$

where  $L = \int d\xi$ . Note that the contributions from  $\nabla \cdot \mathbf{k}B$  and  $(D_{||}(k_B)/4k_B^2)\nabla^4\theta$  to the free energy are the same. So, as we have noted, the free energy grows linearly with the length of the phase grain boundary. Solutions periodic in  $\eta$  can also be found. They correspond to orbits in the  $(g, g_{\eta})$  phase plane inside the separatrix joining  $(-\sqrt{2\kappa\epsilon}, 0)$  to  $(\sqrt{2\kappa\epsilon}, 0)$ . They have a higher free energy. They appear as wavy rolls undulating between the zig and zag directions.

The second solution of interest corresponds to a stationary dislocation and has self similar structure. Let

$$\Psi(\xi, \eta, s) = \text{sgn } \xi F \left( \zeta = \frac{\eta}{\sqrt{2|\xi|}} \right) \tag{4.89}$$

and find

$$\begin{aligned} F'''' &= 4\zeta^2 F'' + 12\zeta F' - 12\zeta F' F'' \\ &\quad - 8F'^2 + 6F'^2 F'' \\ &\quad + 4\frac{1-r}{r} \left( \frac{1}{2}F'^2 - \zeta F' \right) F''. \end{aligned} \tag{4.90}$$

Eq. (4.90) has a remarkable property. It satisfies the Painlevé test when  $r = 1$  and not otherwise. This means that its only moveable singular points, points that depend on initial data such as the value of  $F$  and its first three derivatives at a given  $\zeta$ , are poles. This strongly suggests that (4.90) for  $r = 1$  is integrable. Maaron Zou, who verified the Painlevé property of (4.90) with  $r = 1$  also was able to construct the integral

$$\begin{aligned} I &= 2(F' - 2\zeta)F'''' - F''^2 + 4F'' + 16\zeta^3 F' \\ &\quad - 28\zeta^2 F'^2 + 16\zeta F'^3 - 3F'^4. \end{aligned} \tag{4.91}$$

Indeed, it turns out that not only is (4.90) integrable but so is (4.80) when  $r = 1$  and  $\Psi_s =$

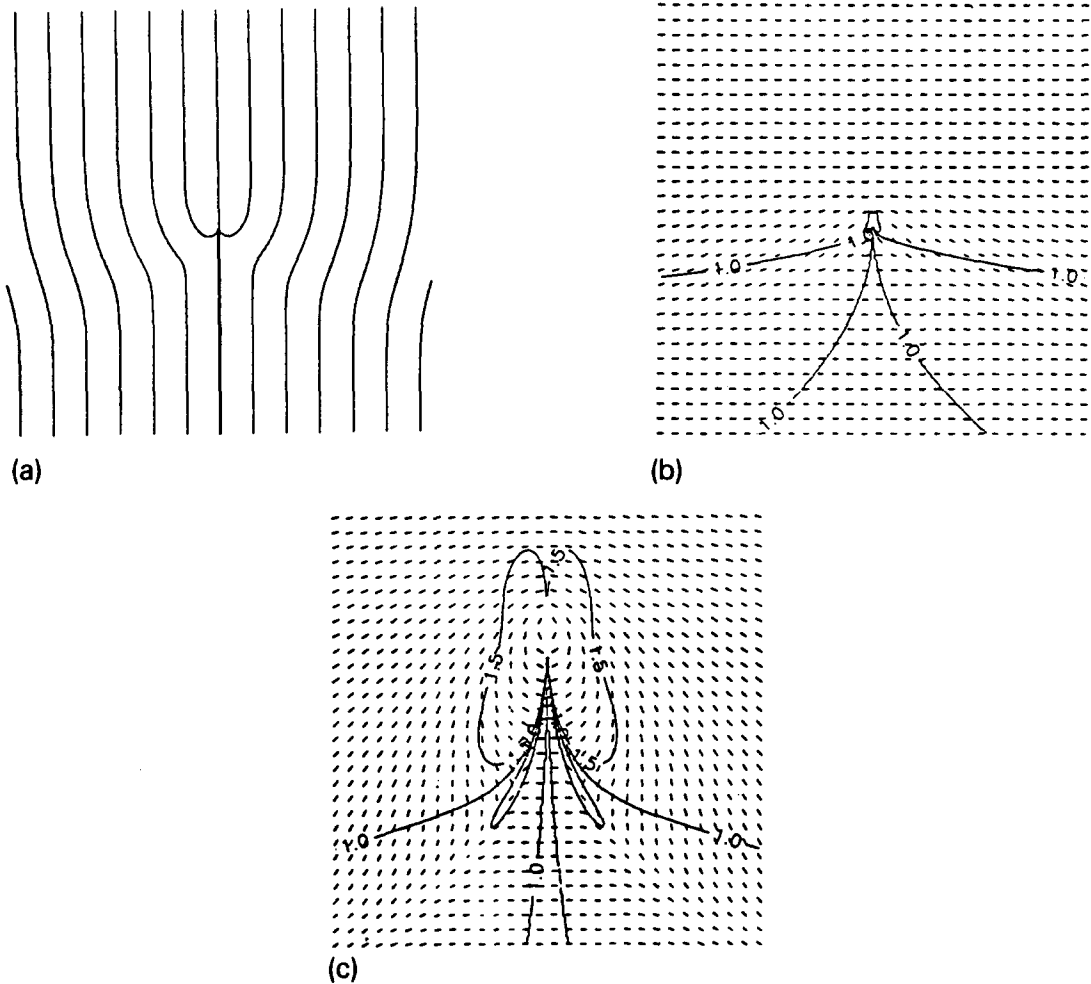


Fig. 13. The morphology of a stationary dislocation as represented by the solution (4.94). (a) shows the isophase contours and (b) the wavevector field.  $k > k_B$  north and south of the lines marked 1.0 where  $k = k_B$  and approaches  $k_B$  from above in the far field.  $k < k_B$  and approaches  $k_B$  from below in the far field of the west-east-sectors. (c) is a magnification of the wavevector field within a roll wavelength of the origin. The region of the two convex disclinations, the vortex, is circumscribed by the contour  $k = 1.5k_B$ . The two narrow regions ( $k < 0.5k_B$ ) below the origin contain the concave disclinations. One can clearly see the vortex-saddle nature of the two components.

O. Nepomanyashchy and Pismen [30] observed that all solutions of

$$\Psi_{\eta\eta} = \text{sgn} \xi (2\Psi_\xi + \Psi_\eta^2),$$

namely Burger's equation, satisfy (4.80). One sees this directly by noting that (4.80) with  $\Psi_s = 0$  and  $r = 1$  can be written,

$$-4 \frac{\partial}{\partial \xi} \left( \Psi_\xi + \frac{1}{2} \Psi_\eta^2 \right)$$

$$-4 \frac{\partial}{\partial \eta} \left[ \Psi_\eta \left( \Psi_\xi + \frac{1}{2} \Psi_\eta^2 \right) \right] + \frac{\partial^4 \Psi}{\partial \eta^4} = 0, \tag{4.92}$$

and replacing  $\Psi_\xi + \frac{1}{2} \Psi_\eta^2$  by  $\Psi_{\eta\eta}$  twice gives the stated result. The solution corresponding to the stationary dislocation is

$$\Psi(\xi, \eta) = \text{sgn} \xi [(\ln 2 - \ln(1 + e^{-\pi})) + (1 - e^{-\pi}) \text{Erf} \zeta] \tag{4.93}$$

and then

$$\begin{aligned} \Theta(X, Y) = & k_B X + \epsilon \operatorname{sgn} X \left\{ \ell n 2 \right. \\ & - \ell n \left[ 1 + e^{-\pi} + (1 - e^{-\pi}) \right. \\ & \left. \left. \times \operatorname{Erf} \left( \sqrt{\frac{k_B}{2|X|\epsilon}} Y \right) \right] \right\}. \end{aligned} \quad (4.94)$$

Note that for  $Y < 0$ ,  $\Theta(X = 0, Y) = \pi \operatorname{sgn} X$ . The constant phase contours, the wavevector field and the wavenumber field is plotted in Fig. 13. In particular we note that in this approximation the dislocation consists of a vortex (two neighboring convex disclinations, each with twist  $T = \pi$ ) and a saddle (two neighboring areas of twist  $T = -\pi$ ) although the actual structure of the region of the net “concave” disclination is complicated.

These solutions had been first suggested by Newell [31], and later Meiron and Newell [32] verified that their shape corresponded very accurately with the numerically calculated shape of a stationary dislocation of the Swift–Hohenberg equation.

Again, on this solution, the two contributions, from  $\nabla \cdot \mathbf{k} B$  and the regularizing term  $\epsilon^2 \nu \nabla^4 \Theta$ , to the free energy are equal (because of (4.89)) and

$$\begin{aligned} \bar{F} = & \int \Psi_{\eta\eta}^2 d\xi d\eta \\ = & \int \Psi_{\zeta\zeta}^2 d\zeta \int \frac{d\xi}{(2\xi)^{3/2}}. \end{aligned} \quad (4.95)$$

## Appendix A

In this Appendix we describe the algorithm that calculates the slowly varying amplitude  $A$  from the real field  $u(x, y)$ . The reader might want to refer to the papers by Tchamitchian and Torresani [33] and Delprat et al. [34] for further details on the one dimensional version of the algorithm we use here.

The extraction of amplitude and frequency from time signals, such as might be recorded from a sound wave, has been important for a long time. It requires the use of tools such as the Wigner distribution or the Gabor transform (sliding window Fourier transform). This last representation is now advantageously replaced by the wavelet transform, which basically has the same structure, the frequency translations being replaced by dilatations. Before describing the general algorithm,

This integral converges in the far field but requires the amplitude regularizations near the core in order to remove the divergence there.

## Acknowledgements

We want to thank N. Ercolani, R. Indik, J. Lega and P.L. Sulem for valuable discussions and in particular want to thank Ph. Tchamitchian and B. Torrèsani who taught us about the wavelet transform and how to implement it. We are also indebted to Kjartan Emilsson for carrying out the numerical work which produced Figs. 11 and 12 and to John Giddes for allowing us to use his figure (Fig. 10) showing the destabilization of a convex disclination as the stress parameter is decreased towards its onset value. This work was supported by the Mathematics Division of the Air Force Office for Scientific Research under contract number AFOSR900021 and NATO grant 9.25, 921149. Part of the numerical simulations were carried out on the CRAY/YMP of the Inst. Méditerranéen de Technologie (Marseille, France).

let us introduce the ideas and notations used in a simple case where the signal is one-dimensional, “asymptotic” (i.e. in the high frequency limit) and contains only one spectral line.

In this latter case, the modulations laws can be satisfactorily extracted using the Hilbert transform. A real signal can be non-uniquely represented in the form

$$f(x) = A(x) \cos \phi(x). \tag{A.1}$$

Among pairs of  $(A, \phi)$ , there exists a canonical one. Consider the Hilbert transform:  $\mathcal{H} = -i\mathcal{F}^{-1}\epsilon\mathcal{F}$ , where  $\mathcal{F}$  is the Fourier transform and  $\epsilon f(\omega) = \text{Sgn}(\omega)f(\omega)$ . (For example  $\mathcal{H} \cos(\alpha x) = \sin(\alpha x)$ .) The analytic signal of  $f(x)$ , called  $Z_f(x)$ , is obtained by linear filtering after cancelling negative frequencies:

$$Z_f(x) = (I + i\mathcal{H})f(x) = A_f(x) \exp(i\phi_f(x)). \tag{A.2}$$

From this representation it is now easy to define an instantaneous frequency (or wavenumber) as  $k_f(x) = d\phi_f/dx$ . It can be shown that this definition corresponds to what one looks for physically if the amplitude  $A_f$  varies slowly compared to  $\phi_f$ :  $|d\phi/dx| \gg |1/A dA/dx|$  and if the signal is locally monochromatic. The principal obstacles to the use of such an algorithm in our problem are (i) there is no analog of the Hilbert transform in two dimensions, although we are going to describe a possible way of handling the quasi one dimensional cases, (ii) the algorithm cannot be extended to the multiphase case.

Let us now describe briefly the Gabor transform. For any  $f$  in  $L^2(R)$ , it is defined as

$$G_b^\alpha f(\omega) = \int_{-\infty}^{+\infty} e^{-i\omega x} f(x) g_\alpha(x - b) dx \tag{A.3}$$

where  $g_\alpha(x)$  is a “window-function”. The optimal window with respect to the uncertainty principle, is given by the Gaussian  $g_\alpha(x) = (1/2\sqrt{\pi\alpha}) e^{-x^2/4\alpha}$ . This definition localizes the Fourier transform of  $f$  around  $x = b$ . The problem with that definition is that the width of the window (given by  $2\|xg_\alpha\|_2/\|g_\alpha\|_2 = 2\sqrt{(\alpha)}$ ) is constant. We would like however to have a small “space window” to analyze with precision “high frequency” bursts and vice-versa. We will see now that the wavelet transform has this zoom in and zoom out property.

Wavelets constitute new basis for representing functions. We know that every function of  $L^2(0, 2\pi)$  can be decomposed into a sum of many mutually orthogonal components ( $c_n e^{inx}$ ). The Fourier basis in this case is generated by dilatation of a single function:  $e^{ix}$ . If we now want to construct such a basis in  $L^2(R)$ , we must look for small waves or wavelets that have fast decay at infinity. Thus we have to introduce not only dilatations of a generating function but also translations. The function  $\psi$  will be called an orthogonal wavelet in  $L^2(R)$  if  $\psi_{j,k} = 2^{j/2}\psi(2^jx - k)$ ,  $j, k \in \mathbf{Z}$ , is an orthonormal basis of  $L^2(R)$ . The Haar function ( $\psi_H(x) = 1$  for  $0 \leq x < \frac{1}{2}$ ,  $\psi_H(x) = -1$  for  $\frac{1}{2} \leq x < 1$  and  $\psi_H(x) = 0$  otherwise), is a simple example of an orthogonal wavelet. A wavelet is called an R-wavelet if the dual basis can be generated by translations and dilatations from a unique wavelet. We will not discuss here further the cases of a discrete wavelet basis but instead introduce directly the continuous wavelet transform which we will use in the following. It is defined for every  $f \in L^2(\mathbf{R})$  as

$$T_\psi f(b, a) = |a|^{-\frac{1}{2}} \int_{-\infty}^{+\infty} f(x) \overline{\psi}\left(\frac{x-b}{a}\right) dx. \tag{A.4}$$

In contrast to the case of Fourier series, there is a relation between the discrete and the continuous wavelet transform, namely  $\langle f | \psi_{j,k} \rangle = T_\psi f(\frac{k}{2^j}, \frac{1}{2^j})$ . The condition on  $\psi$  that allows it to be used as a basic wavelet for the integral wavelet transform is much weaker than the condition for it to be an orthogonal wavelet. It comes from the inversion formula,

$$f(x) = \frac{1}{C_\psi} \int \int_{\mathbf{R}^2} T_\psi f(b, a) \frac{1}{\sqrt{|a|}} \psi\left(\frac{x-b}{a}\right) \frac{da db}{a^2}, \quad (\text{A.5})$$

which is valid if  $C_\psi$  is finite and nonzero which implies:  $\int_{-\infty}^{+\infty} |\widehat{\psi}(\omega)|^2/|\omega| d\omega < \infty$ . Moreover, if we want to have a good localization of the basic wavelet both in physical and Fourier space we may want to have  $\psi \in L^1(\mathbf{R})$  so that the last condition reduces to  $\widehat{\psi}(0) = 0$ . Conditions are more restrictive if one considers only positive frequencies. It is easy to see using the above definition that the wavelet transform performs signal analysis using constant relative bandwidth and as a consequence it has the nice property to adapt its window with the frequency content of the given part of the signal. The analysing probe is also different. In the case of Gabor analysis, one has a given Gaussian profile, filled in by more or less periods of the oscillating exponential. In the case of the wavelet analysis, the number of oscillations in the wave profile is always the same, but the shape is more or less dilated.

Let us now introduce the one dimensional algorithm due to Tchamitchian and Torr sani [33]. This technique for the extraction of amplitude and frequency modulation laws works if the signal is asymptotic. Let us remark first that if the wavelet is also asymptotic, then the wavelet transform can be estimated using the stationary phase method. Restricting the transform on a certain curve in the  $(b, a)$  plane, called the ridge, this estimate will allow us to define the frequency modulation law. It is however not very natural to impose the asymptotic constraint on the wavelet itself since it will enforce its frequency localization and destroy its space localization, in contradiction to what one wants for a space-frequency analysis. This problem can be avoided if one uses a wavelet with Gaussian profile (e.g. the Morlet wavelet). In that case indeed the integral involved in the wavelet transform can again be approximated. We will show now how to proceed.

Let us write the basic wavelet  $\psi = A_\psi e^{i\phi_\psi}$  where now the amplitude  $A_\psi$  is the Gaussian function  $A_\psi(x) = e^{-\frac{1}{2}x^2}$  and let us denote by  $A_f$  and  $\phi_f$  the amplitude and phase of the analytic signal of  $f$ , that constitutes our unknown. Simplifying the notation and for convenience normalizing differently, we can simply write the wavelet transform of a signal  $f(x)$  as

$$Tf(b, a) = \frac{1}{2a} \int_{-\infty}^{+\infty} A_f(x) A_\psi\left(\frac{x-b}{a}\right) e^{i(\phi_f(x) - \phi_\psi(\frac{x-b}{a}))} dx. \quad (\text{A.6})$$

The factor  $\frac{1}{2}$  comes from the fact that we replaced the signal  $f$  by its analytic signal  $Z_f$ . If the amplitude of the signal varies slowly compared to the amplitude of the wavelet one can approximate this integral as follows,

$$Tf(b, a) \approx \frac{1}{2a} A_f(x_s) e^{i\Phi(x_s)} \int_{-\infty}^{+\infty} e^{-\frac{1}{2}(\frac{x-b}{a})^2} e^{i\frac{1}{2}(x-x_s)^2 \Phi''(x_s)} dx, \quad (\text{A.7})$$

where  $\Phi(x) = \phi_f(x) - \phi_\psi(\frac{x-b}{a})$  and  $x_s = x_s(b, a)$  is such that  $\Phi'(x_s) = 0$ . There might be several such points. This is not an obstruction as we shall see. It is not necessary to evaluate this integral for every  $b$  and  $a$ , but rather on the so-called ridge which is the set of  $(b, a)$  such that  $x_s(b, a) = b$ .

Choosing one solution of this equation for  $a$ , namely  $a_r(b)$ , we can evaluate the wavelet transform at this point as

$$Tf(b, a_r(b)) \approx \sqrt{\left(\frac{\pi}{2}\right)} \frac{e^{\frac{i}{2}\text{atan}(a_r(b)^2\Phi''(b))}}{(1 + a^4\Phi''(b)^2)^{\frac{1}{4}}} e^{-i\phi_\psi(0)} Z_f(b). \tag{A.8}$$

This is the first term in an asymptotic expansion whose next correction vanishes identically.

If we know the ridge, then the modulation laws for the wavenumber and amplitude follow. Indeed  $\Phi'(x_s) = 0$  leads to

$$k(b) = \phi'_f(b) = \frac{1}{a_r(b)}\phi'_\psi(0) \tag{A.9}$$

and the last evaluation of  $Tf$  leads to

$$A_f(b) = \sqrt{\left(\frac{2}{\pi}\right)} (1 + a^4\Phi''(b)^2)^{\frac{1}{4}} |Tf(b, a_r(b))|, \tag{A.10}$$

where  $\Phi''(b) = -\frac{1}{a_r(b)^2} (a_r(b)'\phi'_\psi(0) + \phi''_\psi(0))$  on the ridge.

We now need a procedure to determine the ridge. Let  $\Psi$  denote the phase of the wavelet transform. Taking the path in the  $(b, a)$  plane defined by  $x_s(b, a) = b_0$  to perform the derivative in the left hand side of the following equation, we have, at the intersection with the ridge,

$$\left[\frac{d\Psi}{db}\right]_{x_s(a,b)=b_0} = \frac{1}{a} \left[ \phi'_\psi(0) + \frac{1}{2} \left( \frac{\phi''_\psi(0)}{1 + (\phi_\psi(0)a'_r(b) + \phi''_\psi(0))^2} \right) \right]. \tag{A.11}$$

The path  $x_s(b, a) = b_0$  is also called a wavelet curve because it is determined uniquely by the analyzing wavelet. For example in the case of a fixed frequency wavelet (such as the one we use), the wavelet curve is simply given by  $a = a_r(b_0)$  and the last formula reduces to

$$\left[\frac{\partial\Psi}{\partial b}\right] (a_r(b), b) = \frac{1}{a_r(b)}\phi'_\psi(0). \tag{A.12}$$

A simple procedure to calculate the ridge is to solve this equation by iteration,

$$a^{n+1}(b) = \frac{\phi'_\psi(0)}{\frac{\partial\Psi}{\partial b}(a^n(b), b)}. \tag{A.13}$$

Several remarks have to be made at this point. First, it is possible to handle the case of several spectral components since the equation for the ridge is a nonlinear equation which might have several solutions. After finding one solution it is then possible to subtract the spectral line just found from the signal and to continue on the remaining signal. Second, we do not need to calculate the whole wavelet transform of the signal but just the coefficients corresponding to the values of  $a$  close to  $a_r$ . Since the iteration algorithm converges quickly, the procedure is quite fast. Third, the algorithm is meant to work on asymptotic signals and it is not obvious that it will give a good precision for convection patterns including defects. It has been successfully implemented in the one dimensional case using the Morlet wavelet:  $\psi(x) = e^{-\frac{1}{2}x^2} e^{i\omega x}$ . This wavelet is strictly speaking, not admissible (it could be made admissible by adding a correction term), but since we never use the reconstruction formula in the algorithm, it is not important. The value of the frequency  $\omega$  is chosen to be between 2 and 6.

We are now going to discuss the two dimensional version of this algorithm. The generalization is easy by considering rotations in addition to translations and dilatations of the basic wavelet. The wavelet transform of the signal  $f(x, y)$  will now be given by,

$$Tf(\mathbf{b}, a, \theta) = \frac{1}{a^2} \int_{\mathbf{R}^2} e^{-\frac{1}{2}|R_\theta(\frac{\mathbf{x}-\mathbf{b}}{a})|^2} e^{-i\boldsymbol{\omega} \cdot R_\theta(\frac{\mathbf{x}-\mathbf{b}}{a})} f(x, y) dx dy, \quad (\text{A.14})$$

where  $R_\theta$  is the rotation of angle  $\theta$ . Since we use a spectral method to solve the OPE, it is convenient to give the wavelet transform in terms of the Fourier components of  $f$ ,

$$Tf = \sum_{\mathbf{k}} \widehat{f}(\mathbf{k}) e^{i\mathbf{k} \cdot \mathbf{b}} e^{-(aR_\theta \mathbf{k} - \boldsymbol{\omega})^2/2}. \quad (\text{A.15})$$

In fact, since near dislocations, the scalings of across and along the axis are different, it is useful to choose a slightly different wavelet. We scale differently the direction parallel and perpendicular to the vector  $\boldsymbol{\omega}$  by choosing the wavelet to be  $\psi(\mathbf{x}) = e^{-\frac{1}{2}X^T R_\xi [\alpha] R_{-\xi} X + i\boldsymbol{\omega} \cdot X}$  where  $\xi$  is the angle of the constant vector  $\boldsymbol{\omega}$  with the  $x$  axis and  $[\alpha]$  the diagonal matrix of coefficients  $\alpha_1$  and  $\alpha_2$  which scale the two directions. The analysis follows just as in the preceding case and we obtain that the wavelet transform is given by

$$Tf = \frac{1}{\sqrt{\alpha_1 \alpha_2}} \sum_{\mathbf{k}} \widehat{f}(\mathbf{k}) e^{i\mathbf{k} \cdot \mathbf{b}} e^{-\frac{1}{2}((aR_\theta \mathbf{k} - \boldsymbol{\omega})^T R_\phi [\alpha^{-1}] R_{-\phi} (aR_\theta \mathbf{k} - \boldsymbol{\omega}))}, \quad (\text{A.16})$$

where  $[\alpha^{-1}]$  the diagonal matrix of coefficients  $1/\alpha_1$  and  $1/\alpha_2$ . The ridge is obtained by solving the two fixed point equations,

$$\tan(\theta) = \frac{\frac{\partial \Psi}{\partial b_1} - \frac{\partial \Psi}{\partial b_2}}{\frac{\partial \Psi}{\partial b_1} + \frac{\partial \Psi}{\partial b_2}}, \quad (\text{A.17})$$

$$a = \frac{\omega \sqrt{2}}{\sqrt{[(\frac{\partial \Psi}{\partial b_1})^2 + (\frac{\partial \Psi}{\partial b_2})^2]}}, \quad (\text{A.18})$$

where the indices 1 and 2 denote the  $x$  and  $y$  directions and  $\Psi$  is the phase of the wavelet transform. And finally the amplitude is obtained by,

$$A_f(b) = \frac{|Tf(\mathbf{b}, a_r, \theta_r)|}{\pi} \left( [a_r^4 (\Psi_{12}^2 - \Psi_{11} \Psi_{22}) + (\alpha_1 c^2 + \alpha_2 s^2)(\alpha_1 s^2 + \alpha_2 c^2) - c^2 s^2 (\alpha_2 - \alpha_1)^2]^2 + \{a_r^2 c s (\alpha_2 - \alpha_1) \Psi_{12} - a_r^2 [\Psi_{11} (\alpha_1 s^2 + \alpha_2 c^2) + \Psi_{22} (\alpha_1 c^2 + \alpha_2 s^2)]\}^2 \right)^{\frac{1}{4}}, \quad (\text{A.19})$$

where  $c = \cos(\theta_r - \xi)$ ,  $s = \sin(\theta_r - \xi)$  and  $\Psi_{ij}$  is the derivative of the phase of  $Tf$  with respect to  $b_i$  and  $b_j$ .

## Appendix B

We want here to show how to obtain the Cross–Newell equations for the OPE (3.2). Consider the term  $\mathcal{A}(-\nabla^2)W$  which by definition is equal to  $\int_{-\infty}^{\infty} \mathcal{A}(k^2) e^{i\mathbf{k} \cdot \mathbf{x}} \widehat{W}(\mathbf{k}) d\mathbf{k}$ . We are looking at the phase diffusion properties of this linear term in the case of slowly modulated rolls. This latter assumption means that  $\widehat{W}(k)$  has a narrow (of order  $\epsilon$ ) support centered about a wavenumber that we will call

$k_0$ . Since the width of the wavepacket is small compared with the absolute value of  $k_0$  we can take another representation of  $\widehat{W}(k)$  that is widely used in the context of envelope equations, namely, we set  $\widehat{W}(k) = A(k_0, X)\delta(k - k_0)$  where  $X = \epsilon x$  is a large scale on which modulation of the wavepacket takes place. The operator  $A$ , which in Fourier representation is simply a multiplicative term, will now become a very complicated operator acting on the function  $A$ , namely,  $A_0(k_0^2 - i\epsilon D_1 - \epsilon^2 \nabla^2)A(X)$  where  $D_1$  is the operator defined in Section 2. We will be looking at the first two terms in the asymptotic expansion of this term using powers of  $\epsilon$ . We will also calculate the contribution at order  $\epsilon^3$  in the special case when  $k_0$  is close to  $k_B$ . In order to be able to compute these terms it will be necessary to make further assumptions. Since the support of  $\widehat{W}$  is assumed to be small, it is possible to take for  $A(k^2)$  a Taylor expansion around  $k_0$ . We then only need to look at cases where  $A(k^2) = (k^2)^n$ . The result we will obtain will still be valid if the function  $A$  can be expanded in an infinite series of powers of  $k^2$  around  $k_0$ . The main difficulty in the computation is that we also take  $k_0$  to be a slowly varying function of  $X$  and thus the operator  $D_1$  and  $k_0^2$  do not commute.

The calculations of Section 2 suggest a possible formula of the form

$$A(k_0^2 - i\epsilon D_1)^n A = (k_0^2)^n A^2 - i\epsilon \nabla \cdot (kn(k_0^2)^{(n-1)} A^2) + O(\epsilon^2) \tag{B.1}$$

that we will prove by induction. This formula is certainly true for  $n = 1$ . Let us assume it holds for  $n$  and let us examine the case  $n + 1$ . We have, after a little algebra,

$$A(k_0^2 - i\epsilon D_1)^{n+1} A = A(k_0^2 - i\epsilon D_1)(k_0^2 - i\epsilon D_1)^n A \tag{B.2}$$

$$= A(k_0^2 - i\epsilon D_1) \frac{1}{A} ((k_0^2)^n A^2 - i\epsilon \nabla \cdot (kn(k_0^2)^{(n-1)} A^2) + O(\epsilon^2)) \tag{B.3}$$

$$= (k_0^2)^{n+1} A^2 - i\epsilon (AD_1(k_0^2)^n A + k_0^2 \nabla \cdot (kn(k_0^2)^{(n-1)} A^2)) + O(\epsilon^2) \tag{B.4}$$

$$= (k_0^2)^{n+1} A^2 - i\epsilon \nabla \cdot (k(n+1)(k_0^2)^n A^2) + O(\epsilon^2). \tag{B.5}$$

We see easily that for a general function  $A(k^2)$  the term  $W^* A(-\nabla^2)W$  in the slowly varying wave approximation will be up to order  $\epsilon$ ,

$$W^* A(-\nabla^2)W = A(k^2)|W|^2 - i\epsilon \nabla \cdot (k \frac{d}{dk^2} A(k^2)|W|^2) + O(\epsilon^2). \tag{B.6}$$

It is now straightforward to derive (3.4).

Our next task is to calculate the principal contribution at order  $\epsilon^3$  to the phase diffusion equation when  $k$  is close to  $k_B$ . A little analysis will show that the most important term is that proportional to  $\epsilon^3 \nabla^2 \nabla \cdot k$  which arises from the action of  $D_2$  on  $D_1$ .

It is then straightforward to show by induction that this contribution from  $(k_0^2 - i\epsilon D_1 - \epsilon^2 D_2)^n A$  is

$$i\epsilon^3 \frac{n(n-1)}{2} k_0^{2n-4} D_2 \cdot D_1 A. \tag{B.7}$$

Adding up these contributions gives us that the coefficient  $\eta$  of  $\epsilon^2 \nabla^2 \nabla \cdot k$  in the phase diffusion equation is

$$\eta = \left( \frac{A''}{2} + A^2 \frac{\Gamma''}{2} \right) \frac{1}{\chi}. \tag{B.8}$$

Differentiating (3.7) and using  $k = k_B$ , we find that

$$\eta = -\frac{1}{2\tau} \frac{dB}{dk^2} = \frac{1}{4k_B^2} D_{||}(k_B). \tag{B.9}$$

## Appendix C

In this appendix we discuss the coupling of the phase diffusion equation with the amplitude mode. We also try to motivate the choice of the OPE and discuss possible alternatives.

### C.1. The phase and amplitude equations near the border of the marginal stability curve

In the case where the amplitude is not of order one but of order  $\sqrt{\epsilon}$ , the corrections to the phase equation can be evaluated more easily. This will be illustrated using the SH equation. This intermediate scaling allows to calculate the nonlinear roll solution perturbatively and explicitly. Moreover, at small amplitudes,  $\lambda_{1S}(k^2, R)$ , the decay rate of an amplitude fluctuation about its slaved value, is small and the amplitude mode will also be marginal, allowing the coupling of phase and amplitude. The essential differences with the analysis of Section 2.1 are that now  $w = \sqrt{\epsilon}(w_0 + \epsilon w_1 + \dots)$ . At order  $O(\sqrt{\epsilon})$ , we get that  $w_0 = A_0 \cos \theta$ ,  $A_0$  is order one,  $R = R_0 = (1 - k^2)^2$ . The essential difference is that the linearized operator has now two null eigenmodes,  $\cos \theta$  and  $\sin \theta$ . A simple calculation leads to the following two equations,

$$(A_0^2 + O(\epsilon^2 A_0^6)) \Theta_T + A_0(\mathcal{L}_1^1 + \epsilon^2 \mathcal{L}_3) A_0 + O(\epsilon^2 A_0^6) = 0, \quad (\text{C.1})$$

$$\frac{(R - (1 - k^2)^2)}{\epsilon^2} A_0 - \frac{3 A_0^3}{4 \epsilon} = A_{0T} + (\mathcal{L}_2^1 + \epsilon^2 \mathcal{L}_4) A_0 + O(\epsilon^2 A_0^5), \quad (\text{C.2})$$

where  $R - (1 - k^2)^2$  is of order  $\epsilon$ . For the complex Swift–Hohenberg equation ( $w$  being now complex and  $w^3$  replaced by  $w^2 w^*$ ) the algebra is much simpler. The equations obtained are exact and given in [9]. In the case where the wavenumber of the pattern is close to the borders of the marginal stability curve (either  $k_l$  or  $k_r$ , both of which we denote as  $k_0$ ), Eqs. (C.1) and (C.2) simplify because we can identify the linear term to all orders and the first nonlinear correction proportional to the cube of  $A_0$ . We then obtain an equation for the complex order parameter  $W = \sqrt{\epsilon} A_0 e^{i\theta/\epsilon}$ ,

$$\partial_t W + A_0(-\nabla^2)W + |W|^2 \Gamma_0 W = 0. \quad (\text{C.3})$$

The term  $A_0(-\nabla^2)W$  is the inverse Fourier transform of  $\lambda(k^2)\widehat{W}$ . The term  $\lambda(k^2)$  is the eigenvalue of the operator  $L_0 = \frac{\delta H}{\delta w}|_{w=0}$  associated to the eigenmode  $\cos(k_0 x)$  for a microscopic equation of the form:

$$\partial_t w + H\left(\frac{\partial}{\partial x}, R, w\right) = 0. \quad (\text{C.4})$$

We denote  $\widehat{W}$  the Fourier transform of  $W$  and  $\Gamma_0 = g_0$ , the first Landau constant. For the Swift–Hohenberg model,  $g_0 = 3/4$ . Note that in this equation, time and space differentiation are performed with respect to small scales. While Eqs. (C.1) and (C.2) make no sense for  $k < k_l$  or  $k > k_r$ , (C.3) does make sense, and provides a natural extension for (C.1), (C.2) in these domains. It is also interesting to note that in the weakly nonlinear limit the three functions  $\tau(k)$ ,  $B(k)$  and  $\mu^2(k)$  can be derived from  $\lambda(k^2)$  and  $g_0$ . We find,

$$\tau \propto \mu^2 = -\lambda/g_0, \quad (\text{C.5})$$

$$B/\tau = -\lambda', \quad (\text{C.6})$$

where the prime denotes derivation with respect to  $k^2$ .

## C.2. A general approach

We can formally derive the phase and amplitude equation for an equation of the form (C.4) in the fully nonlinear regime by simply projecting this equation onto an appropriate set of basis modes. We begin by using (2.3) to expand  $H$  as  $\Sigma \epsilon^i H_i$ . Consider  $w_0$  of parity  $S$  (symmetric) to be the solution of  $H_0(w_0) = 0$ . A translation of the pattern by one quarter of a period exchanges the parity  $S$  with that of the antisymmetric or  $A$  mode. Denote by  $L$  the linear operator obtained by linearizing  $H_0(w)$  about  $w_0$ ,  $L = \frac{\delta H_0}{\delta w}|_{w_0}$ . The stability of  $w_0(\theta)$  is determined by the spectrum of the operator  $L$  acting on a suitably defined function space. The complete stability analysis in an infinite or nonperiodic domain leads to the full basis of Bloch functions and their associated Floquet exponents. However, since we are only going to consider large scale perturbations of the basic mode, we restrict ourselves to the study of a discrete set of periodic eigenmodes. The sidebands of each of these will be taken care of once we include dependence on the macroscopic coordinates  $X, Y$ . What then are the correct boundary conditions on  $Lw = \lambda w$ ? We surely have to consider all the higher harmonics of the basic period of  $w_0(\theta)$  but we also have to consider some of the subharmonics. The dangerous modes are those that can be sufficiently excited so as to replace patches of pattern with wavenumber  $k$  with finite amplitude patches of patterns with wavenumbers  $k' = nk$  or  $k' = k/n$  for integer  $n$  where both  $k'$  and  $k$  lie in the marginal stability band  $(k_l, k_r)$ . Modes lying outside the marginal stability band will be strongly damped and cannot attain finite amplitude states. The space of functions we should consider therefore is the space of periodic functions of basic period  $k/n$  such that  $k/n + 1 < k_l < k/n$ . Because we assume that  $w_0(\theta)$  is linearly stable, all the eigenvalues of  $L$ , except for the zero eigenvalue corresponding to an infinitesimal translation of the phase of  $w_0$ , namely  $\frac{\partial w_0}{\partial \theta}$ , will be positive. However, we must assume more. We assume that the least positive mode  $\lambda_{1S}(k^2, R)$  for all  $k$  in the marginal stability band has the same parity and period as  $w_0(\theta)$  and corresponds to an infinitesimal perturbation in the amplitude of the basic solution  $w_0(\theta)$ . If the parity of the least-damped eigenmode of  $L$  is opposite to that of  $w_0$ , then the manifestation of this mode through a finite amplitude instability leads to a global translation of the pattern. Indeed, in a previous paper [21], we have illustrated the triggering of a parity breaking instability in a numerical simulation of a climbing dislocation of the Swift–Hohenberg equation. The instability leads to a gliding motion. In that same paper, we also illustrated the finite amplitude instability and awakening of a mode with a different periodicity from  $w_0(\theta)$ . This was the case of “bridge formation” in which a dislocation core can be locally destabilized by a subharmonic instability of the  $k/3$  mode when the latter lies sufficiently to the right of the left boundary  $k_l$  of the marginal stability curve. Therefore in our analysis we assume that the only modes which locally play any role are the phase (i.e.  $\frac{\partial w_0}{\partial \theta}$  corresponding to a zero eigenvalue of  $L$ ) and “amplitude” modes. The latter has the same parity (and periodicity) as  $w_0(\theta)$  and, at least near the marginal stability boundary where the amplitude  $A$  is not slaved, is  $\frac{\partial w_0}{\partial A} = \frac{1}{A} w_0$ , directly proportional to  $w_0$ . Its damping rate  $\lambda_{1S}(k^2, R)$  approaches zero at  $k_l$  and  $k_r$ . This is what we mean when we say  $w_0(\theta)$  is stable and unique. Strictly, of course,  $w_0(\theta)$  is not unique. Depending on the wavenumber  $k$  and stress parameter  $R$ , there may be other finite amplitude solutions with different periodicities. But they are all more damped than either the phase or “amplitude” modes. If they can be present, then we must enrich the analysis by including new phases.

We are thus led to consider a discrete set of eigenmodes  $\xi_i$  (and  $\xi_i^\dagger$  for the adjoint operator  $L^\dagger$ ) corresponding to the eigenvalues  $\lambda_i$ , where  $\lambda_{i+1} \geq \lambda_i$ . We have  $\lambda_0 = 0$  and  $\xi_0 \propto \partial_\theta w_0$ . We normalize the eigenmodes by imposing  $\langle \xi_i^\dagger | \xi_j \rangle = \delta_{ij}$  and  $\langle \xi_i | \xi_i \rangle = 1$ . Due to the assumption about the parity of the basic solution, the eigenmodes are either symmetric ( $\xi_{iS}$ ) or antisymmetric ( $\xi_{iA}$ ). The marginal

mode  $\xi_0$  is of parity  $A$ , the least damped mode is of parity  $S$ , at least in a neighborhood of  $k_r$  where it corresponds to the amplitude mode. We will consider an even parity perturbation  $w_S$  and write  $w = w_0 + w_S$ ,  $w_S = \alpha_S \xi_{1S}$ . Substituting this expression into (C.4), we then project the equation onto the adjoint modes  $\xi_0^\dagger$  and  $\xi_{1S}^\dagger$  and obtain, respectively, the usual phase equation, containing the dominant correction terms, and an equation for the evolution of the amplitude  $\alpha_S$ . To order  $\epsilon^2$ , they are

$$\langle \xi_0^\dagger | \partial_\theta (w_0 + w_S) \rangle \Theta_T + \langle \xi_0^\dagger | H_1 (w_0 + w_S) \rangle + \epsilon^2 \langle \xi_0^\dagger | H_3 (w_0 + w_S) \rangle = 0, \quad (\text{C.7})$$

$$\epsilon^2 \langle \xi_{1S}^\dagger | \partial_T (w_0 + w_S) \rangle + \langle \xi_{1S}^\dagger | H_0 (w_0 + w_S) \rangle + \epsilon^2 \langle \xi_{1S}^\dagger | H_2 (w_0 + w_S) \rangle = 0. \quad (\text{C.8})$$

Away from the borders of the neutral stability curve,  $\lambda_{1S}$  is not small and (C.8) can be used to solve algebraically for  $\alpha_S$ , thus expressing the slaving of the amplitude to the wavenumber. If we linearize the term  $\langle \xi_{1S}^\dagger | H_0 (w_0 + w_S) \rangle$  as  $\langle \xi_{1S}^\dagger | H_0 (w_0) \rangle + \langle \xi_{1S}^\dagger | \frac{\partial H_0}{\partial w} \cdot w_S \rangle = 0 + \lambda_{1S} \alpha_S$ , the coupling between phase and amplitude is too weak and adiabatic elimination of the amplitude is not valid. By the same token, equation (C.8) becomes interesting and nontrivial when  $\lambda_{1S}$  is close to zero, e.g. in the low amplitude limit. In this limit, the amplitude mode is  $\xi_{1S} = \frac{\partial w_0}{\partial A} = \frac{w_0}{A}$ , so that  $w_0$  can be approximated by  $\mu \xi_{1S}$  and  $w_0 + w_S$  is  $(\mu + \alpha_S) \xi_{1S} = A \xi_{1S}$ . The term  $\langle \xi_{1S}^\dagger | H_0 (w_0 + w_S) \rangle$  is in first approximation equal to  $g(k) A (A^2 - \mu^2)$  where  $g(k)$  is given by  $\frac{\lambda_{1S}}{2\mu^2}$ . This estimate reflects the fact that there is a supercritical pitchfork bifurcation when we cross the marginal curve and the formula will still be valid as long as the nonlinear solution  $w_0$  stays unique and the eigenvector associated with  $\lambda_{1S}$  is close to  $w_0$ . In the low amplitude limit, one can neglect the contribution of the nonlinear terms in  $H_1$  and after multiplying (C.7) by  $A$ , we shall obtain the following equations,

$$\Theta_T + \frac{1}{\tilde{\tau}(k) A^2} \nabla \cdot (\mathbf{k} A^2 \tilde{B}(k)) + O(\epsilon^2) = 0, \quad (\text{C.9})$$

$$\epsilon^2 A_T + g(k) A (A^2 - \mu^2(k)) + O(\epsilon^2) = 0, \quad (\text{C.10})$$

which are the usual phase and algebraic amplitude equations when  $O(\epsilon^2)$  terms are neglected. We have deliberately written (C.9) in a form which identifies those places in the phase diffusion equation where the square of the “free” amplitude  $A^2$  has been replaced by its slaved valued  $\mu^2(k, R)$ . We recover the phase diffusion equation (2.17) by setting  $\tilde{\tau} \mu^2 = \tau$  and  $\tilde{B} \mu^2 = B$ . Note that it is possible to write the phase equation in conservative form because we kept only the linear terms in  $H_1$ . For the real Swift–Hohenberg equation at small amplitudes, where we can approximate  $w$  by a one Galerkin mode expansion for the basic roll solution (i.e.  $w = A \cos \theta$ ), we have  $\tilde{\tau}(k) = 1$ ,  $\tilde{B}(k) = (1 - k^2)$  and  $g(k) = \frac{3}{4}$ .

We can obtain these equations directly when the microscopic model derives from a Lyapunov functional. We begin from equation (2.21), allowing for variations in both the phase and amplitude “directions”. Defining the amplitude  $A$  by  $w = A f(\theta)$  where  $\bar{f} = 1$ , we get,

$$\int \int dx dy \Theta_T \overline{\left( \frac{\partial w_0}{\partial \theta} \right)^2} \delta \theta + A_t \overline{\left( \frac{\partial w_0}{\partial A} \right)^2} \delta A = \int \int dx dy \nabla \cdot \left( 2\mathbf{k} \frac{\partial \mathcal{G}}{\partial k^2} \right) \delta \theta - \int \int dx dy \frac{\partial \mathcal{G}}{\partial A} \delta A. \quad (\text{C.11})$$

Note that the integrand  $\mathcal{G}(A, k^2)$  is obtained by averaging  $G$  over  $\theta$ .  $\mathcal{G}$  is  $\bar{G}$  only when  $A^2$  is replaced by  $\mu^2(k^2, R)$ . From (C.11),

$$A^2 \Theta_T + \nabla \cdot \left( -2\mathbf{k} \frac{\partial \mathcal{G}}{\partial k^2} (A, k^2) \right) = 0, \quad (\text{C.12})$$

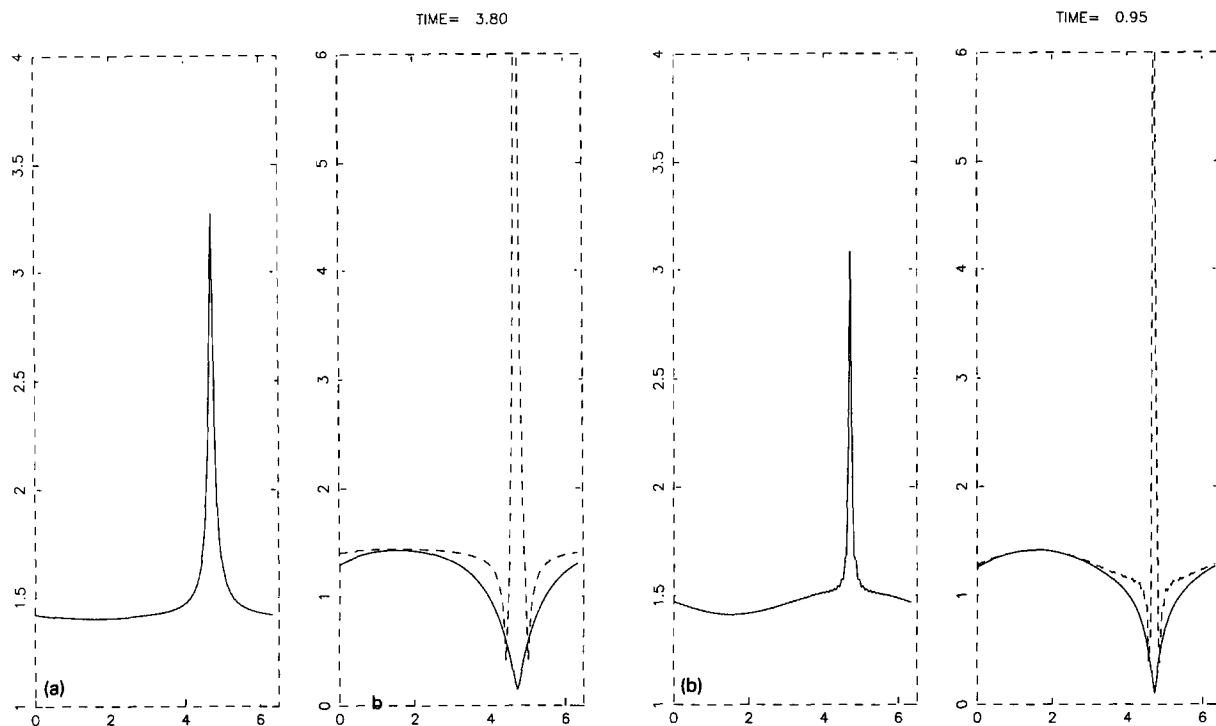


Fig. C.1. The left and right panels of (a), (b), (c), show respectively the graphs of the wavenumber  $k$  and amplitude  $A$  (solid) and slaved amplitude (dashed) as function of  $x$  at the time just before the singularity is reached for  $g = 0.1, 1.0$  and  $10$ . They were obtained by solving (C.9), (C.10) for an initial condition corresponding to a wavenumber in the right Eckhaus unstable band. Note that the slaving of the amplitude is much more pronounced for larger values of  $g$  and the time of formation of the singularity is shorter.

$$A_t = -\frac{\partial \mathcal{G}}{\partial A}(A, k^2). \tag{C.13}$$

In particular, for the case of SH,  $\mathcal{G} = \frac{1}{4}f^4 A^4 - \frac{1}{2}f^4 A^2 \mu^2$  which of course is equal to  $\bar{\mathcal{G}} = -\frac{1}{4}f^4 \mu^4$  when  $A^2 = \mu^2$ . We recover the phase-amplitude equations written above in (C.9), (C.10) without assuming a single Fourier mode basic solution. Note that we have  $\lambda_{1S} = \frac{\partial^2 \mathcal{G}}{\partial A^2}(\mu, k^2)$  only in the one mode approximation.

We now want to give numerical evidence that, at least in the large aspect ratio limit, the amplitude is indeed slaved to the wavenumber even when the latter takes values between  $k_E$  and  $k_r$ . This point is important because it shows that the regularized phase diffusion equation will suffice in this domain. We need this because the coupling to the amplitude in the OPE is justified only close to  $k_r$ . A second point addressed by this experiment concerns the time scale of amplitude relaxation and the size of the defect core. We show it is crucial to have the correct value of  $\lambda_{1S}$  if one wants to describe correctly the defect core and the time of formation of dislocation pairs.

We integrate numerically the phase and amplitude equations (C.9), (C.10) derived for the complex Swift–Hohenberg equation. The equations are solved for the wavenumber and amplitude in one space dimension, starting with  $k = k_0 + a \sin x$  and  $A = \mu(k)$ , with  $k_0$  in the right Eckhaus band ( $k_E, k_r$ ). As a typical example, we chose the stress parameter  $R = 3$  and took  $k_0 = 1.5, a = 0.6$ . (Note that in the one dimensional case investigated here, the  $k/3$  mode cannot be excited through a finite amplitude

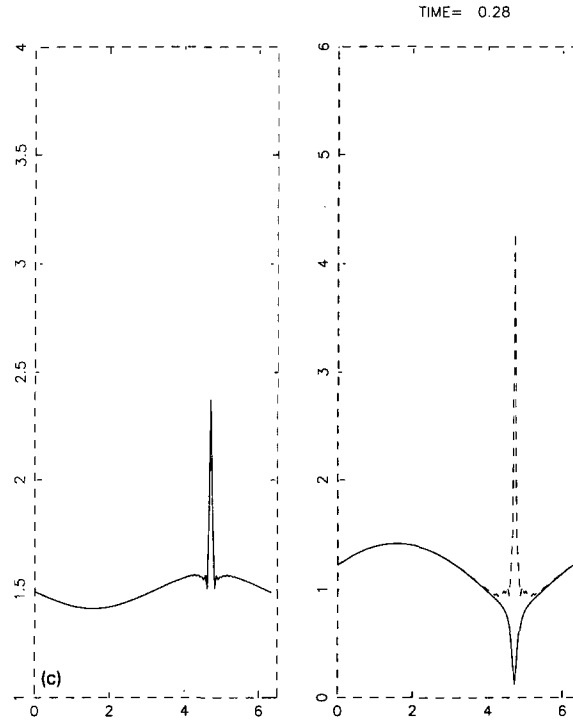


Fig. C.1—continued.

instability as it is in the two dimensional case after the formation of a dislocation [21], because in the finite amplitude stage of the one dimensional Eckhaus instability, the local wavenumber never reaches such low values.) The spatial scale is chosen so that  $\epsilon = 0.1$ . Since the equations are not well posed as they stand, we must find an appropriate numerical algorithm. Our procedure, which turns out to work well, consists in adding and subtracting in (C.9), the same quantity equal to a constant coefficient  $\eta$  multiplying the biLaplacian of  $\Theta$ . One term (the one leading to an instability) is integrated explicitly together with the nonlinear terms using an Adam's Bashforth scheme, the other one is evaluated implicitly using a Crank-Nicholson scheme. This algorithm stabilizes the small scales and the solution is not very sensitive to the value of  $\eta$ . Larger values of this parameter allows us to integrate closer to the singularity. We show the results for  $\eta = 1$ . The space derivatives are calculated using Fourier transforms. The domain is periodic and we use 128 grid points. At first, we added a spatial derivative term in the amplitude equation of the form  $\zeta \nabla^2 A$ . The coefficient  $\zeta$  can be normalized after a redefinition of  $\lambda_{1S}$ , and of the space and time scales. However the limit  $\zeta \rightarrow 0$  is not singular and the observed behavior is the same in this limit as for a finite value of  $\zeta$ . Therefore, we chose  $\zeta = 0$ . We varied the value of  $\lambda_{1S}$  by varying  $g = \frac{\lambda_{1S}}{2\mu^2}$  in (C.10). (In the case of the complex Swift-Hohenberg equation,  $g$  is a constant equal to 1). An obvious result is that the time of formation of the singularity is larger for smaller values of  $\lambda_{1S}$ . In other words, the more the amplitude is slaved, the quicker the singularity is reached. Also the size of the core varies inversely proportional to  $\lambda_{1S}$  and becomes small as the distance between the local wavenumber  $k$  and  $k_r$  increases. Our definition of the dislocation core is the size of the spatial domain where the amplitude  $A$  deviates from  $\mu(k)$  by more than 5%. It is then verified that for larger values of  $\lambda_{1S}$  (or equivalently for smaller  $\epsilon$  since the spatial and temporal scalings can be absorbed in  $\lambda_{1S}$ ), the amplitude remains slaved to the wavenumber closer to the defect

center. In Figs. 14a,b,c we show results for the cases  $g = 0.1$ ,  $g = 1$ . and  $g = 10$ . and graph the wavenumber  $k$  as a function of space on the left picture, and the amplitude  $A$  (in plain) on the right picture. The dotted line represents the quantity  $\sqrt{|\mu^2(u)|} \equiv \mu$  where  $\mu^2(u) = R - (1 - u^2)^2$ . This last quantity is negative when  $k$  is bigger than  $k_r$  and that is the reason why we observe a discontinuity in the derivative of  $\mu$  in the defect core. The time value on each picture corresponds to the time of the last output before blow-up of the numerics. We observe on each picture that the amplitude tends to zero in the core while the wavenumber tends to infinity. The influence of  $\lambda_{1S}$  is both apparent on the time of formation of the defect and also on the size of the core region where  $A$  and  $\mu$  cease to be close. These simulations, and others (not shown) where we modified the shape of the function  $\mu^2(k)$  near  $k_r$  (leaving  $\tau$  and  $B$  unchanged) show that, once  $\epsilon$  is fixed by the size of the domain, it is important that the regularization equation gives the correct value of  $\lambda_{1S}$  in order to obtain the correct time of formation of defects and the sizes of their cores.

## References

- [1] J. Swift and P.C. Hohenberg, Hydrodynamic fluctuations at the convective instability, *Phys. Rev. A* 15 (1977) 319.
- [2] H.S. Greenside and W.M. Coughran Jr., Nonlinear pattern formation near the onset of Rayleigh-Bénard convection, *Phys. Rev. A* 30 (1984) 398.
- [3] P. Manneville, A two-dimensional model for three-dimensional convective patterns in wide containers, *Physique* 44 (1983) 759.
- [4] H.S. Greenside, M.C. Cross and W.M. Coughran, Jr., Mean flows and the onset of chaos in large-cell convection, *Phys. Rev. Lett.* 60 (1988) 2269.
- [5] A.C. Newell and J.A. Whitehead, Finite bandwidth, finite amplitude convection, *J. Fluid Mech.* 38 (1969) 279; Review of the finite bandwidth concept, *Proc. IUTAM 1969 Symp. on Instability in Continuous Systems*, Herrenalb, H. Leipholz, ed. (Springer, Berlin, 1969) pp. 284–289.
- [6] L.A. Segel, Distant sidewalls cause slow amplitude of modulation of cellular convection, *J. Fluid Mech.* 38 (1969) 203.
- [7] A. Zippelius and E.D. Siggia, Stability of finite-amplitude convection, *Phys. Fluids* 26 (1983) 2905.
- [8] W. Pesch and L. Kramer, Nonlinear analysis of spatial structure in two-dimensional anisotropic pattern forming systems, *Z. Phys. B* 63 (1986) 121.
- [9] M.C. Cross and A.C. Newell, Convection patterns in large aspect ratio systems, *Physica D* 10 (1984) 299.
- [10] Y. Pomeau and P. Manneville, Stability and fluctuations of a spatially periodic convective flow, *J. Phys. Lett.* 23 (1979) L609.
- [11] A.C. Newell, T. Passot and M. Souli, Convection at finite Rayleigh numbers in large-aspect-ratio containers, *Phys. Rev. Lett.* 64 (1990) 2378.
- [12] A.C. Newell, T. Passot and M. Souli, The phase diffusion and mean drift equations for convection at finite Rayleigh numbers in large containers, *J. Fluid. Mech.* 220 (1990) 187–252.
- [13] F.H. Busse, Non-linear properties of thermal convection, *Rep. Prog. Phys.* 41 (1978) 29–67.
- [14] M. Bestehorn and H. Haken, Traveling waves and pulses in a two-dimensional large-aspect-ratio system, *Phys. Rev. A* 42 (1990) 195–203.
- [15] A.C. Newell, T. Passot and J. Lega, Order parameter equations for patterns, *Ann. Rev. Fluid Mech.* 25 (1993) 399–653.
- [16] N. Ercolani, R. Indik, A.C. Newell and T. Passot, The geometry of the Cross–Newell equation (1994), preprint.
- [17] G.B. Whitham, *Linear and Nonlinear Waves* (Wiley, New York, 1974).
- [18] A. Pocheau and V. Croquette, Dislocation motion: a wavenumber selection mechanism in Rayleigh Bénard convection, *J. Phys. (Paris)* 45 (1984) 35.
- [19] H.S. Greenside and M.C. Cross, Stability analysis of two-dimensional models of three-dimensional convection, *Phys. Rev. A* 31 (1985) 2492–2501.
- [20] L. Tuckerman and D. Barkley, Bifurcation analysis of the Eckhaus instability, *Physica D* 46 (1990) 57–86.
- [21] A.C. Newell and T. Passot, Instabilities of dislocations in fluid patterns, *Phys. Rev. Lett.* 68 (1992) 1846–49.
- [22] V. Croquette, M. Mory and F. Schosseler, Rayleigh Bénard convective structures in a cylindrical container, *J. Phys.* 44 (1983) 293–301.
- [23] M. Assenheimer and V. Steinberg, Rayleigh-Bénard convection near the gas-liquid contact point (1993), Preprint.
- [24] G. Toulouse and M. Kleman, Principles of a classification of defects in ordered media, *J. Phys. Lett. (Paris)* 37 (1976) L149.

- [25] G.E. Volovik and V.P. Mineyev, Investigation of singularities in super fluid He<sup>3</sup> in liquid crystals by the homotopic topology methods, *Sov. Phys. JETP* 45 (1977) 1186.
- [26] N.D. Mermin, The topological theory of defects in ordered media, *Rev. Mod. Phys.* 51 (1979) 591.
- [27] Y. Pomeau and P. Manneville, Wavelength selection in axisymmetric cellular structures, *J. Phys. (Paris)* 42 (1981) 1067–1074.
- [28] Y. Pomeau, S. Zaleski and P. Manneville, Axisymmetric cellular structures revisited, *Z. Angew. Math. Phys.* 36 (1985) 367.
- [29] Y. Pomeau, Caustics of Nonlinear Waves and related questions, *Europhys. Lett.* 11 (1990) 713–718.
- [30] A.A. Nepomanyashchy and L.M. Pismen, Singular solutions of the nonlinear phase equation in pattern-forming systems, *Phys. Lett. A* 153 (1991) 427–430.
- [31] A.C. Newell, Two dimensional convection patterns in large aspect ratio systems, *Lecture Notes in Num. Appl. Anal.* 5 (1982) 202–231.
- [32] D. Meiron and A.C. Newell, The shape of stationary dislocations, *Phys. Lett. A* 113 (1985) 289–292.
- [33] Ph. Tchamitchian and B. Torrèsani, Ridge and skeleton extraction from the wavelet transform, Invited lecture given at the CBMS-NSF conference ‘Wavelets and their Application’, Lowell, June (1990).
- [34] N. Delprat, B. Escudé, P. Guillemain, R. Kronland-Martinet, Ph. Tchamitchian and B. Torrèsani, Asymptotic wavelet and Gabor analysis: extraction of instantaneous frequencies, preprint CPT, Luminy, France.
- [35] M.S. Heutmaker and J.P. Gollub, Wavevector field of convective flow patterns, *Phys. Rev. A* 35 (1987) 242–60.
- [36] M. Seul, L.R. Monar, L. O’Gorman and R. Wolf, Morphology and local structure in labyrinthine stripe domain phase, *Science* 254 (1991) 1557–1696.
- [37] J. Geddes, PhD Thesis 1994.